STRUCTURE/FUNCTION RELATIONSHIPS IN NICKEL-PEPTIDE COMPLEXES: IMPACT OF THE PRIMARY COORDINATION SPHERE ON SQUARE-PLANAR NICKEL CHEMISTRY

BY

Mary Elizabeth Krause

Submitted to the graduate degree program in Chemistry and the Graduate Faculty of the University of Kansas in partial fulfillment of the requirements for the degree of Doctor of Philosophy.

_____

Chairperson Jennifer S. Laurence

_____

Timothy A. Jackson

_____

Richard L. Schowen

_____

Emily E. Scott

_____

Teruna Siahaan

Date Defended: April 21, 2011

The Dissertation Committee for Mary Elizabeth Krause

certifies that this is the approved version of the following dissertation:

STRUCTURE/FUNCTION RELATIONSHIPS IN NICKEL-PEPTIDE COMPLEXES: IMPACT OF THE PRIMARY COORDINATION SPHERE ON SQUARE-PLANAR NICKEL CHEMISTRY

_____

Chairperson Jennifer S. Laurence

Date approved: April 21, 2011

Abstract

The novel metal-binding tripeptide asparagine-cysteine-cysteine (NCC) is capable of coordinating a metal ion, and we are exploring its use in several biological applications. Different metals may be incorporated into this tag, and when it is placed in line with a peptide or protein that has the potential to be used as a targeting agent, it has the potential to facilitate the diagnosis, treatment, and evaluation of cancers and other diseases. For example, platinum may be used as an anti-cancer therapeutic, whereas nickel generates a catalytic antioxidant. The advantage of this tag is that it is extremely small, is composed of naturally occurring amino acids, and binds metal with unique geometry. Metal binds irreversibly at physiological pH but is released upon modest acidification, as occurs with endocytosis.

In order to utilize the tripeptide as a metal-binding tag, it is important to understand the structure, reactivity, and stability of this novel system. Initial studies with nickel established that NCC binds metal with 2N:2S geometry. Electronic absorption, circular dichroism (CD), and magnetic CD (MCD) data collected for Ni-NCC are consistent with a diamagnetic Ni^{II} center bound in square planar geometry. This complex acts as a mimic of the enzyme nickel superoxide dismutase (Ni-SOD), which catalyzes the disproportionation of superoxide to hydrogen peroxide and molecular oxygen.

Changes in the CD signal of Ni-NCC indicate the optical activity of the complex changes over time, but mass spectrometry data show that the mass of the complex is unchanged, which suggests chiral rearrangement of the complex occurs. Performing the reaction in D_2O allows incorporation of deuterium into non-exchangeable positions, indicating chiral inversion occurs at two of the alpha carbon atoms in the peptide. Control peptides were also used to verify the

chirality of the final nickel-peptide complex is DLD-NCC. Characterization of the NCC sequence within a longer peptide shows that the geometry of metal coordination is maintained, though the electronic properties of the complex are varied to a small extent due to *bis*-amide coordination. Chiral inversion does not happen in the same two positions, though initial studies suggest inversion at a different location in the peptide may occur.

Acknowledgements

This work was supported by J.R. and Inez Jay Fund (Higuchi Biosciences Center) and the KU Cancer Center. I am grateful to have been funded by the Madison and Lila Self Graduate Fellowship, the KU Cancer Center, the Chemistry Department at the University of Kansas, and through a six-month Co-Op with Genentech, Inc. During her work on this project, collaborator Amanda Glass, was funded by the NIH Dynamic Aspects of Chemical Biology Training Grant (T2 GM GM08454) and the NSF GK-12 Fellowship (0742523).

This work would not have been possible without the collaborative participation of many different members of the research community at the University of Kansas. The initial discovery that led to this project, as well as early experiments on this project, were performed by A. Andrew Vartia, and Drs. Andria Skinner and Kevin Han, under the direction of Dr. Jennifer Laurence. We also thank Dr. Teruna Siahaan for his input on the initial peptide work. We thank Drs. Christian Schöneich and Victor Sharov for input on the xanthine oxidase assay, Drs. Susan Lunte, Matthew Hulvey, and Courtney Kuhnline for assistance with electrochemical studies, Drs. Christian Schöneich and Olivier Mozziconacci for input on cysteinyl radicals and insight into chiral peptide studies, and Dr. Kevin Frankowski for assistance with IR. Most importantly, the participation of our collaborators Dr. Timothy A. Jackson and Amanda Glass was vital to the completion of this work. Dr. Jackson's expertise in spectroscopy and bioinorganic chemistry in general made this project possible. He generously offered both his knowledge and spectrometers to help us answer our research questions. The collaboration that we have with Dr. Jackson and Amanda is a perfect collaboration, where both groups have learned tremendous amounts from the other. I would like to thank the members of the Laurence lab, past and current, especially

Natalie, Talia, Brittney, and Andi, for their support, assistance, and friendship; they have made this experience not only one of learning but one of enjoyment.

I have been fortunate to have been guided and trained by some wonderful scientists and mentors. First, I would like to thank the late Dr. Julian Limburg for his instruction and advisement during the first three years of my doctoral studies. He was a brilliant scientist who introduced me to my interest in bioinorganic chemistry. His impact on the field of enzymology will be missed. I also am thankful for the support of former members of his lab, with whom I worked for more than three years, especially Megen Culpepper, Matt Culpepper, Robyn Moore, and Tim Reed. Our friendship and support of one another helped all of us through a very difficult time and allowed us to move into the next phases of our individual lives. I would like to thank Dr. Emily Scott and Dr. Richard Schowen, who aside from serving as members of my committee, provided much guidance during a difficult transition within my graduate career and helped me get where I am today. I am very grateful for all of the members of my committee, who have played significant roles in my graduate career and have helped me in so many ways. I would also like to thank Dr. Ankit Patel and the entire Late State Processing and Pharmaceutical Development Department at Genentech, Inc., for all that they taught me during my six-month co-op at Genentech. I also thank the Directors of the Madison and Lila Self Graduate Fellowship for their hard work to provide an exceptional professional development program to accompany the specific objectives that come with a Ph.D. program. Additionally, I appreciate their support and interest in the progression of my success as a graduate student.

Most importantly, I would like to thank my advisor, Dr. Jennifer Laurence. She took me into her lab late in my graduate career under unusual circumstances; when I was looking for a new lab in my fourth year, Jen immediately made me feel comfortable, supported, and made the transition an easy one. I have learned so much from her, not only about chemistry, but about

what it means to be a mentor. In addition to all she has taught me, and making sure I have the skills and knowledge I will need to accomplish my future goals, she has given me confidence in my abilities as a scientist and an academic. Jen has gone above and beyond what is expected of a graduate advisor; she has not only inspired me to be a better scientist, but has truly impacted my life both professionally and personally. I couldn't be more excited to continue my development as a scientist as a post-doctoral fellow in her lab, and I could not ask for a better advisor, mentor, and friend.

Finally, on a personal note, I want to thank my amazing family and friends. My parents, Larry and Marie Krause, and my brother, Eric Krause, are wonderful, loving supports who have shaped who I am throughout my life and have supported and encouraged me without question through the last six years. My aunt, Dr. Sharon Baack, who shares my love of teaching and academia, has provided endless encouragement and understanding to the academic process. My Grandma and late Grandpa, Jean Baack and Rev. Ed Baack, always showed interest in what I have been doing and were also incredibly encouraging. I thank all of my family members for being proud of me and loving me wherever I was throughout this process, helping me to persevere and accomplish my goals. Additionally, I could not even begin to express my gratitude to my all of my wonderful friends, both those I made since moving to Lawrence, especially Krista and Kevin, Rachel and Jimmie, Melissa, Darla, Amber, Amanda, and Sarah, who were patient with my sometimes-unplanned work schedules and spend time with me and love me anyway, and those I have back at home, especially Katie and Rich, Karie and Dan, Ashley, Karen, and Liz, who always remind me that living life and being content where you are is still important in the middle of a graduate education. I cannot thank them enough for their love and support.

Table of Contents

List of Schemes and Figures

List of Tables

Chapter 1: Chemistry of nickel complexes in biological systems: Metalloproteins, metalloenzymes, and peptide-metal complexes

Bioinorganic chemistry is a broad field that examines the role of transition metals in a variety of biological systems. One major segment of this field involves studies focused on metalloproteins; metalloproteins utilize different transition metals for various structural and functional purposes. Metalloproteins comprise one-third of all structurally characterized proteins, where, in the cell, their purpose is to not only sequester metal ions from undesired reactivity but to participate in intercellular metal trafficking.[1,2] Metalloproteins also participate in such roles as maintaining structure, dioxygen transport, electron transfer, and specific catalytic purposes (metalloenzymes).[3] Much diversity is observed among the structure and function of these metalloproteins, depending not only on the identity of the metal ion but also on how the metal is coordinated, nearby structural features, and the overall structure of the protein.

1.1. Transition metals in biological systems

The side chains of a subset of amino acid residues are involved in the coordination of metal ions, particularly histidine, cysteine, aspartic acid, and glutamic acid. Ligands coordinating metal ions often include nitrogen, oxygen, or sulfur. As such, the backbone of polypeptides can also participate in metal coordination. The hard and soft acids and bases (HSAB) principle applies to metal binding to peptides and proteins; the HSAB nature of the set of ligands can drive specificity for coordination of certain metals. Specifically, large, more polarizable (soft) ligands prefer to coordinate with larger, softer metals, while small, less polarizable (hard) charged metal cations prefer to coordinate with oxygen or nitrogen ligands.[3]

The HSAB properties of a metal determine how it binds, but transition metals also have very distinctive properties based on their d-shell electron count and charge. For example, zinc, with a filled d shell, frequently plays a structural role in proteins, such as is the case in zinc finger proteins and superoxide dismutase. In these cases, zinc does not participate in a catalytic reaction but simply plays a structural role; however, in other zinc proteins, such as carbonic anhydrase, carboxypeptidase, zinc can act as a Lewis acid to promote catalysis. Other first row transition metals, such as iron, nickel, and copper, lack a full d shell and therefore can move between different oxidation states to facilitate electron transfer reactions and promote catalysis. The research in this dissertation pertains to nickel chemistry and, as such, this chapter will focus on nickel-containing proteins.

1.2 Coordination of nickel in proteins: basic principles

Nickel is a redox-active metal that is found in various metalloproteins and metalloenzymes. Divalent nickel cations are borderline hard-soft acids (metals) and can therefore be coordinated by many of the common ligating residues. It is often bound to sulfur ligands from cysteine or occasionally methionine, nitrogen ligands from the peptide backbone, histidine residues, and/or oxygen ligands from aspartic or glutamic acid.[3] The identity of the ligands determine the functionality of the nickel complex; while some ligands bind more loosely and are used for metal transport, others bind tightly, almost irreversibly, in order to promote catalysis. The coordination number, geometry, bond lengths, and type(s) of ligating atoms about the metal determines how easily it is released, as is the case with nickel trafficking proteins.[1]

The differences in the structure of nickel binding sites impacts their function.[4] Specifically, the octahedral, lower affinity sites can more easily release metal; high spin

nickel(II) centers are more likely to exchange their ligands via a dissociative mechanism, while ligand exchange in planar complexes utilizes an associative one that depends on the nucleophilicity of the incoming ligand. For this reason, it is more difficult to exchange the four coordinate, planar ligands, and they are less likely to release nickel. The octahedral, six coordination Ni^{II} sites can release metal when nickel concentrations are lower.[4] This selectivity of metal release is useful for these proteins that are involved in metalloregulation. Additionally, it can be concluded that complexes with cysteinyl ligands have higher affinity for nickel than those that do not. Many metallochaperones, where nickel binding needs to be reversible, coordinate the metal through the lower-affinity nitrogen ligands,[5] though this trend is not universal. Those proteins that utilize cysteine ligands often require a binding event, such as ATP hydrolysis or complexation with another nickel-binding protein, to release their metal.[6,7] Finally, it has been suggested that thiolate ligation is necessary for enzymatic activity, as this ligation helps tune the redox potential to one appropriate for catalysis;[5,8] however, the simple presence of a thiolate ligand is not enough to designate a protein as a catalytic enzyme. Several metallochaperones that have up to three sulfur ligands have been reported to lack catalytic activity.

Among catalytic nickel enzymes, the redox potential of transition metal complexes is tuned by its ligands, where the characteristics of the ligands impact the redox potential of the metal and its binding mode.[3] Nickel is commonly found in the +2 and +3 redox states, though it can also cycle through the +1 state, making it versatile in both its coordination geometry and reactivity.[9] Nickel(II) is a d^8 metal ion, making it energetically favorably to utilize a mononuclear square planar or square pyramidal geometry; however, it is not uncommon for nickel to be oxidized and ligated in an octahedral or tetrahedral geometry.[9]

1.3. Catalysis in nickel enzymes

Nickel cofactors in enzymes vary in their structure and function; nickel can coordinate in different geometries and has a wide potential for redox chemistry, as +1, +2, +3 states are all possible, and it can catalyze reactions over a range of 1.5 V. With this variety of reactivities, the coordination environment about the metal center plays a large role in defining the reactivity of the enzyme. In known nickel enzymes, nickel coordination may be mononuclear, part of a pyrrole cofactor, or part of a metal cluster.[9]

The ability of enzymes to promote catalytic processes is often driven by the primary coordination sphere and nearby structural components. The secondary environment around the metal center, however, often promotes the more subtle differences in redox potential that also drive differences in reactivity. Additionally, this proximal structure often drives substrate binding. For this reason, the structure/function relationship of nickel enzymes is not only dependent on the direct metal ligation but also on the nearby substrate binding cavities. These secondary structural effects are not present in peptide-metal complexes, and therefore, the use of peptide mimics permits direct study of first sphere effects, including differences in coordinating residues and metal geometry.

1.4. Metal abstraction peptide (MAP)

The metal abstraction peptide (MAP) is a tripeptide with the sequence asparagine-cysteine-cysteine (NCC) that is capable of coordinating a variety of metal ions, including nickel. Upon incubation with immobilized metal affinity chromatography (IMAC) resin, metal is transferred to the peptide to generate a unique metal-tripeptide complex. Initial studies on the

tripeptide complex performed with nickel revealed that NCC binds metal with a 2N:2S geometry (Chapter 2). Electronic absorption, circular dichroism, and magnetic CD (MCD) data collected for Ni-NCC are consistent with a diamagnetic Ni^{II} center bound in square planar geometry. The metal complex formed is extraordinarily tightly bound such that extreme temperature, saturating amounts of denaturants and enormous excesses of the chelator EDTA fail to disrupt binding. The metal is incorporated more rapidly with increasing pH and is released specifically by acidification. These properties are highly compatible with use of the peptide as a tag for targeted delivery and controlled release in biological systems. This sequence can be placed in line with a protein or peptide that has the potential to be used as a targeting agent. When paired with an appropriate metal or isotope, the tag can be used to facilitate the diagnosis, treatment, and evaluation of cancers and other diseases. While platinum may be used as an anti-cancer therapeutic, nickel generates a catalytic antioxidant complex. In order to utilize the tripeptide as a metal-binding tag, however, it is important to understand the structure, reactivity, and stability of the novel system, which is the focus of this dissertation.

1.4.1. MAP has superoxide dismutase activity

Ni-NCC acts as a mimic of the enzyme nickel superoxide dismutase (Ni-SOD), which catalyzes the disproportionation of superoxide to hydrogen peroxide and molecular oxygen (Chapter 2). While peptide mimics of Ni-SOD have been explored in the past,[10,11,12] the MAP sequence differs in that it is not derived from the sequence of the parent enzyme yet acts as a functional mimic of the enzyme. The MAP complex and Ni-SOD both have 2N:2S coordination; while Ni-NCC is much less efficient than Ni-SOD, it shows activity and maintains a redox potential in the appropriate range (*vide infra*) to disproportionate superoxide. It has

exceptional stability, resisting degradation during long-term storage, elevated temperature, and exposure to light and oxygen, making it compatible for use as a therapeutic agent.

1.4.2. MAP undergoes nickel dependent, site-specific chiral inversion

Unlike Ni-SOD and unlike any metal-polypeptide complex known, Ni-NCC undergoes rapid chiral rearrangement under ambient conditions (Chapter 3). CD aging profiles, H/D exchange mass spectrometry, and studies on peptides synthesized to contain D amino acids indicate chiral inversion occurs at the alpha carbon atoms at the first and third position within the tripeptide. To our knowledge, this is the first example of site-specific chiral inversion of amino acids within polypeptides that depends on metal binding.

1.4.3. NCC embedded in longer sequences

The effect of including NCC within longer peptides is conversion of the N-terminal amine to an amide, which alters the first coordinating ligand to the metal center. The incorporation remains rapid, nickel binding results in the same structure, and SOD activity is observed for all NCC-containing peptides (Chapter 4). The redox potential is altered somewhat, as expected by the nitrogen ligand being an amine in a tripeptide and an amide in the case of a longer sequence, but both facilitate superoxide disproportionation. While the chiral transformation of the tripeptide Ni-NCC can be detected by CD, no change is observed for the pentapeptide, suggesting either a chiral inversion is not necessary for SOD activity of the *bis*-amide form or inversion occurs even more quickly and concomitant with metal incorporation.

Studies to examine the differences between the tripeptide and the sequence embedded in longer peptides suggest chiral inversion may occur, but in a different position than in the tripeptide.

1.5. Catalytic, mononuclear nickel centers: Nickel superoxide dismutase (Ni-SOD)

The Ni-NCC complex acts as a structural and functional mimic of Ni-SOD. Superoxide dismutases catalyze the disproportionation of the toxic anion superoxide to molecular oxygen and hydrogen peroxide. Ni-SOD is the most recently discovered superoxide dismutase.[13-15] This enzyme contains a mononuclear Ni site, specifically where the metal is bound in a 2N:2S, square planar nickel(II) geometry, utilizing two nonadjacent cysteine side chains, a backbone amide nitrogen, and the N-terminal amine as ligands. In isolated samples of oxidized Ni-SOD, a fifth, axial histidine ligand is coordinated to the nickel(III) ion, and oxidation of the metal center to nickel(III) during catalysis may be concomitant with coordination of this axial ligand.[16] The metal binding site is found in the terminal end of the enzyme, comprising a nickel hook (Figure 1.1).[8,16-19]

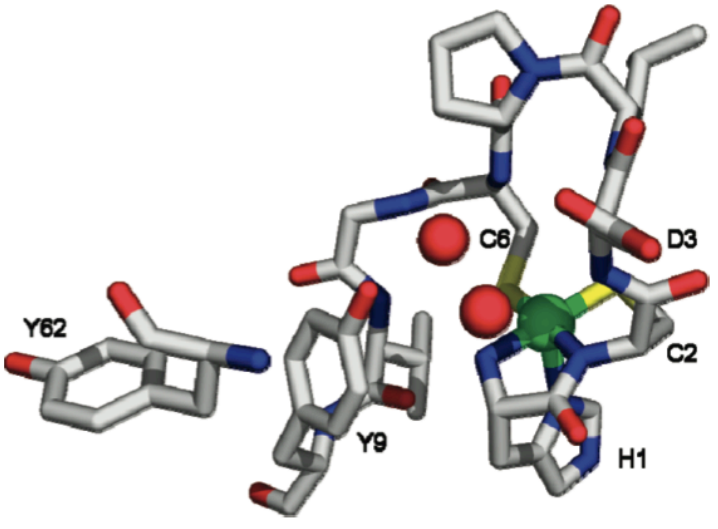

Figure 1.1. Active site of Ni-SOD, showing the directly coordinating metal ligands (H1, C2, C6) and nearby, catalytically important residues (H1 side chain, Y9, Y62, and E11 (not shown)). Reproduced with permission from Herbst, R. *et al.*[19]

The presence of two cysteine ligands helps maintain the Ni^{II}/Ni^{III} redox couple that is necessary to catalyze the disproportionation reaction, and without both cysteine residues, catalysis is not possible because nickel coordination becomes octahedral and binding affinity is decreased.[20,21] Ni-SOD has to maintain a redox potential that is somewhere between that necessary for each of the half reactions of superoxide disproportionation (-160 mV vs. NHE for the $O_2/O_2^{\cdot-}$ redox couple and 870 mV vs. NHE for the $O_2^{2-}/O_2^{\cdot-}$ redox couple).[22,23] During catalysis of Ni-SOD, an axial histidine ligand is critical, stabilizing the nickel(III) oxidized state and tuning the nickel redox potential for superoxide disproportionation,[18,19] where the Ni^{II}/Ni^{III} redox potential is higher for a four-coordinate nickel center versus a five-coordinate nickel center.[19] Without the axial histidine, the nickel is mostly reduced, and because the reduced form promotes one of the superoxide half-reactions and the oxidized form catalyzes the other, an approximately 100-fold reduction in the rate of disproportionation is observed.[16]

While the active site itself is tuned for superoxide disproportionation, outside of the primary coordination sphere, other factors influence the reactivity of Ni-SOD. Ni-SOD is a homohexamer, and interaction between the subunits appears to promote enzymatic activity.[17-19] Interestingly, the fully oxidized form of the enzyme maintains 50:50 Ni^{II}/Ni^{III}, supporting this cooperativity and communication between adjacent monomers.[19] Mutagenesis of residues His1, Asp3, Glu17, Arg39 and Arg47 impacted or completely prevented the reactivity of the protein.[17] Glu17 likely interacts with the axial histidine ligand and impacts reactivity.[17] Some of these residues are important for stabilizing the nickel-hook motif that allows metal binding,[18] while others are involved in stabilizing substrate binding during catalysis and still others act as proton donors during catalysis.[19] For example, if Pro5 is *trans* instead of *cis*, Cys6 is misaligned for metal binding.[18] Tyr9 is thought to be important in gating access to the nickel ion, preventing other, undesired anions from entering. Without gating, other anions would repulsively prevent

anionic superoxide from entering, impacting activity of the enzyme.[17,19,24] Additionally, mutagenesis of Tyr9 leads to differences in the Ni-S bond, although mutation of Tyr9 did not change the redox potential of the metal.[19] Asp3 impacts the position of Tyr9, also affecting reactivity.[19] The primary coordination of the metal is what drives the redox potential, directly impacting reactivity, yet, interestingly, larger structural differences and the secondary coordination sphere impact reactivity without changing the redox potential.

1.6. Models of metalloenzyme active sites: peptide-based mimics of Ni-SOD

Studies on metalloenzymes can be complex. While identifying residues involved in the metal binding can be accomplished using site directed mutagenesis and structural studies, probing the geometry and redox states of the metal throughout a catalytic process can be more difficult, especially due to synergistic effects that result from the unique environment within a folded protein. In addition to the impact of primary ligands to the metal center on both structure and reactivity, nearby residues can alter the reduction potential of the metal, residues direct substrate access and provide pockets for substrate binding, and the overall protein fold can direct access of the substrate or co-substrates to the active site. The secondary coordination sphere and other, more distant structural features can also impact the reactivity of the complex. Understanding this type of convoluted system can be difficult, especially without structural data. To mitigate this problem, the use of either truncated peptide complexes or synthetic compounds has aided in the understanding of the immediate reactivity of these complex systems. While the activity of enzymes as a whole is impacted by secondary coordination sphere and overall protein fold, the use of synthetic complexes and peptide mimics provides insight into the immediate coordination and reactivity of the enzymes. The literature is rich in nickel complexes, both

synthetic and peptide-based, that mimic the activity of various nickel enzymes. The focus of this work is on peptide complexes that accommodate nickel in square planar and square pyramidal geometry, especially those with nitrogen and sulfur coordination. The primary examples of such coordination and geometry typically mimic Ni-SOD and have been examined to better understand inner-sphere effects on this enzyme's function.

1.6.1. Peptide maquettes of Ni-SOD

Ni-SOD lends itself nicely to peptide mimic work, as all of the ligands required for metal binding are present in the N-terminus of the enzyme, which is referred to as the metal hook.[17,18] Only a few known synthetic mimics of Ni-SOD exhibit a midpoint potential in the range appropriate for SOD activity;[25,26] alternatively, peptide mimics of Ni-SOD derived from the parent enzyme, known as peptide maquettes, have been able to successfully reproduce the activity of the enzyme, albeit with less efficiency. Designing various, systematic differences into these maquettes has proved useful in the understanding of how the enzyme works as a whole.

The first maquette of Ni-SOD was composed of the 12 N-terminal residues (HCDLPCGVYDPA) from the Ni-SOD of *Streptomyces coelicolor* and is referred to as [Ni(SOD)^{M1}].[10] This maquette binds nickel in a 1:1 ratio, as does Ni-SOD, and while only the Ni^{II} form can be isolated, this maquette exhibits superoxide dismutase activity and has an appropriate redox potential for superoxide dismutation (Table 1.1).[10] In addition to the direct coordination sphere, this maquette includes both the His1 and Tyr9 residues that are known to affect activity of the intact Ni-SOD enzyme. Nonetheless, this maquette's activity is greatly diminished with respect to the parent enzyme.

Table 1.1. Comparison of peptide maquettes to Ni-SOD.

Complex	Thiol arrangement	Type of N coordination	Redox potential (vs. Ag/AgCl)	SOD activity (IC_{50})
Ni-SOD	*Cis*	Amine/amide	0.09 V [19,27]	4 x 10^{-8} M
$[Ni^{II}(SOD)^{M1}]$	*Cis*	Amine/amide	0.70 V [10,11]	2.1 x 10^{-7} M
$[Ni^{II}(SOD^{M1}\text{-Ac})]$	*Cis*	*Bis* amide	0.49 V [11]	3 x 10^{-5} M
$[Ni^{II}(SOD)^{M2}]$	*Cis*	Amine/amide	0.52 V [12]	1 x 10^{-6} M
$[Ni^{II}(SOD)^{M2}\text{-(D)}]$	*Cis*	Amine/amide	0.48 V [12]	5 x 10^{-6} M
$[Ni^{II}(SOD^{M2}\text{-(A)}]$	*Cis*	Amine/amide	0.67 V [12]	3 x 10^{-5} M

Ni-SOD is one of few proteins that coordinates nickel using its N-terminus. This allows the 2N:2S coordination to utilize one amine ligand and one amide ligand, where the amine is provided by the N-terminal end of the enzyme. For this reason, it was of interest to force the amine to become an amide to determine how this would impact the reactivity of the peptide maquette. $[Ni^{II}(SOD^{M1}\text{-Ac})]$ maintains the same sequence as the first maquette, but the N-terminus is acetylated, which provides *bis*-amide nickel coordination. The *bis*-amide form of the peptide displays a lower redox potential (0.49 vs 0.70) yet has catalytic activity that is two orders of magnitude lower than the mixed amine/amide maquette. This acetylated maquette maintains the same sequence as the original 12mer and therefore retains His1 and Tyr9, which are relevant for activity. The comparison shows that the difference between amine/amide and *bis*-amide coordination alters both the redox potential and activity. Interestingly, the lower activity of the *bis*-amide is not predicted by theory. The electrochemical data suggests that the activity should

be higher in the *bis*-amide than the mixed amine/amide maquette because the potential is closer to that of the native enzyme. Therefore, other properties of the metallopeptide complex may modulate reactivity, such as the increased anionic character of the bis-amide shell being more repulsive to approach of the anionic superoxide substrate, and investigation into these factors continues.[11]

An axial histidine ligand is involved in the catalysis of Ni-SOD.[16] With the maquettes, the peak separation in electrochemical studies is wide enough to suggest a change in coordination environment upon nickel oxidation, supporting involvement of a histidine ligand throughout catalysis.[11] To selectively probe the importance of this axial ligand and to help determine if the axial histidine remains coordinated throughout catalysis, maquettes with alternative N-terminal residues were synthesized and examined. Here, only seven residues were used in the maquette to represent what is minimally necessary for metal binding (XCDLPCG, where X is histidine, aspartic acid, or alanine) and to look specifically at the impact of the histidine on reactivity. In Table 1.1, [$Ni^{II}(SOD)^{M2}$] is the 7mer with the native sequence, but [$Ni^{II}(SOD)^{M2}$-(D)] and [$Ni^{II}(SOD)^{M2}$-(A)] are the aspartic acid and alanine substituted sequences. This study suggests that once the histidine is axially bound, it remains coordinated and catalysis follows an outer sphere mechanism. Regardless, the substitution of the histidine with alanine or aspartic acid reduces its efficiency by 100 fold and alters its redox potential. These results show that the axial histidine may play several roles in the mechanism, including structural rearrangement, making the redox potential more negative, and ensuring nickel-based oxidation rather than thiolate oxidation.[12] One study suggested that a proline (Pro5) isomerization to the *trans* form was the reason for the reduced activity in biomimics of Ni-SOD, acting as the fifth ligand in the absence of histidine,[24] but more recent studies on sequences where the *cis*-conformation was forced did not have improved activity over the previous mimics.[28]

Cyanide can be used to mimic substrate binding to the peptide sequence; reaction of cyanide with a 9mer maquette showed that this anion can bind to the metal, as demonstrated by IR. This suggests again the possibility of an inner sphere mechanism, where the substrate binds in an axial position to oxidize the enzyme, and histidine displaces the oxidized, hydrogen peroxide product.[29] While the discussion of an inner sphere or outer sphere mechanism is still underway, the use of peptide maquettes that maintain similar primary coordination and mimic the reactivity of the whole enzyme may inform this debate.[23,24]

1.7. Catalytic nickel enzymes

Comparison of Ni-SOD to other nickel-containing enzymes promotes fundamental understanding of the factors that drive nickel-based catalysis. A recent review describes six major known nickel enzymes,[9] including urease, hydrogenase, carbon monoxide dehydrogenase, methyl coenzyme M reductase, acetyl-coenzyme A synthase, and the more recently discovered nickel superoxide dismutase,[9,30,31] as well as two lesser studied enzymes, glyoxalase I and acireductone dioxygenase. These two are less commonly recognized as nickel enzymes because they often bind other metals in the same active site.[32,33] The major nickel enzymes employ very different nickel coordination environments, including a dinuclear Ni-Fe complex, a dinuclear Ni-Ni complex, nickel in a tetrapyrrole complex, an iron sulfur cluster also containing nickel,[31] and a mononuclear nickel center (Table 1.2). The context of nickel is highly varied, promoting distinct chemistries and reactivities.

Table 1.2. Brief descriptive summary of major Ni-containing enzymes by classification. Non-redox active enzymes are shaded green, iron-sulfur cluster containing enzymes are shaded blue, and enzymes with mononuclear nickel sites are shaded pink. N_{im} indicates the coordinating nitrogen is from an imidazole.

Nickel enzyme	Nickel coordination	Nickel redox states	Reaction type
Urease	Ni1: $2N_{im}$:3O Ni2: $2N_{im}$:4O (Binuclear Ni-center with bridging water and carbamylated lysine)	Ni^{II} throughout	Hydrolysis of urea
Ni-Fe Hydrogenase	Ni-(μ_2Cys)$_2$-Fe (Active Ni: 4S)	Ni^{I} to Ni^{III}	2 electron redox chemistry of H_2
Carbon monoxide dehydrogenase	[FeS]-Ni (Ni: 4S)	Ni^{II} to $Ni^{"0"}$	Reversible oxidation of CO to CO_2
Acetyl coenzyme A synthase	[FeS]-Ni-(μ_2Cys)$_2$-Ni (active Ni: 4S)	Ni^{II}/Ni^{I} (possibility of Ni^0)	Acetylation of coenzyme A
Methyl coenzyme M reductase	Ni-tetrapyrrole (4N)	Ni^{I} to Ni^{III}	Reduction of methyl coenzyme M
Nickel superoxide dismutase	2N:2S; axial N_{im}	Ni^{II}/Ni^{III}	Disproportionation of superoxide

1.7.1. Catalytic nickel centers with no redox activity

The enzymes glyoxalase I,[9,32] acireductone dioxygenase,[9,33] and urease[9,34,35] all have mononuclear or dinuclear nickel centers, but in these particular enzymes, the nickel remains in the nickel(II) redox state throughout catalysis.

1.7.1.1. Glyoxalase I. Glyoxalase I is part of a series of enzymatic reactions that catalyze the conversion of methylglyoxal to lactate. Specifically, glyoxalase I utilizes an octahedral nickel ion that remains in the +2 redox state throughout an isomerization reaction. Three

histidine residues, one glutamic acid residue, and two water molecules coordinate the metal. The metal ion acts as a Lewis acid; one of the water ligands is displaced upon substrate binding, allowing the coordinated glutamate to abstract a proton from the substrate before the substrate is reprotonated to generate an *S*-D-lactoylglutathione, which continues to be processed in reactions catalyzed by other enzymes.[9,32] Interestingly, while the eukaroytic forms of this enzyme utilize zinc in their active site, the *E. coli* form is only fully active when bound to nickel and is inactive with zinc. Studies suggest the coordination of the metal, rather than the properties of the metal itself, drive the differences in reactivity.[32]

1.7.1.2. Acireductone dioxygenase. Acireductone dioxygenase is another enzyme that can bind different metals with different geometries to promote alternate reactivities. When nickel is bound, the enzyme cleaves acireductone into formate, carbon monoxide, and methylthiopropionate.[33] Here, nickel is high spin Ni^{II} and is bound in an octahedral geometry with three histidine ligands, one aspartic acid ligand, and two water molecules. Like in glyoxalase I, nickel remains in the +2 redox state through catalysis, acting as a Lewis acid. In this reaction, the acireductone substrate displaces a water molecule, where oxygen then reacts with the substrate, but oxygen itself does not interact directly with the metal.[9,33] Interestingly, this enzyme can also utilize iron in its active site, breaking acireductone into formate and methylthiobutyrate. The metal-different isoforms have significant structural differences, which therefore changes the function of the enzyme.[33]

1.7.1.3. Urease. Urease breaks down urea into ammonia and carbamic acid, which then hydrolyzes into carbon dioxide.[34-36] The crystal structure of urease from *Klebsiella aerogenes* revealed a binuclear nickel center in each active site.[37,38] The nickel ions are 3.5 Å apart; both utilize nitrogen and oxygen ligands and a bridging, bidentate carboxylate ligand from a carbamylated lysine, which is critical for appropriate metal binding. One of the nickel ions is

held in a square pyramidal environment, where two histidines, one water molecule, a bridging lysine carbamate, and one bridging water/hydroxyl molecule participate in its coordination (2N:3O coordination). The other nickel, along with the shared bridging carbamylated lysine and bridging water, has an additional water ligand, two histidine residues, and one aspartic acid residue (2N:4O coordination).[9,37] Once again, in urease, the nickel ions remain in the +2 redox state throughout catalysis; the metal simply acts as a Lewis acid. The differences in the coordination of the two nickel ions drive their participation in the enzymatic activity.[35] The urea bridges the two nickel ions; the carbonyl oxygen binds to the first nickel ion, while one amine group coordinates to the other nickel ion and the second amine group interacts with hydrogen bond acceptors in the active site pocket. Binding of the carbonyl to the first nickel ion polarizes the substrate, while the second nickel increases the nucleophilicity of a bound water or hydroxide for its attack on the carbonyl group of the urea. This attack forms ammonia and carbamate; water binds and displaces the bound ammonia and carbamate for further catalysis, and the carbamate spontaneously hydrolyzes to bicarbonate and another ammonia molecule. [9,34,35]

1.7.2. Redox active nickel enzymes with additional cofactors

Other nickel enzymes undergo redox activity throughout their catalytic processes. In these enzymes, nickel is coordinated either in metal cluster cofactors or by complex nitrogen ligated tetrapyrrole systems that bind the nickel and are tightly coordinated to the enzyme.

1.7.2.1. Carbon monoxide dehyrodgenase/ Acetyl-Coenzyme A synthase. Carbon monoxide dehydrogenase (CODH) catalyzes the reversible oxidation of CO to CO_2.[9,39,40] CODH is sometimes found as a monofunctional enzyme, but it is often tightly bound to the enzyme acetyl-coenzyme A synthase (ACS).[9,31,40]ACS catalyzes the synthesis of acetyl coenzyme A from

CO (often generated by CODH), coenzyme A, and a methyl group of methylated corrinoid iron-sulfur protein (CoFeSP).[9,40] The bifunctional, coordinated form of these two enzymes, CODH/ACS, is an $\alpha_2\beta_2$ heterotetramer (CODH, containing the C cluster, is the β subunit, and ACS, containing the A cluster, is the α subunit) that catalyzes two different reactions of carbon monoxide.[31,41] In some cases, the CO that is generated by CODH acts as one of the substrates for the acetyl-coenzyme A synthesis, as CO is transported through a tunnel from the active site of CODH to that of ACS; the enzyme switches from an open to a closed conformation throughout catalysis, delivering CO at a specific time during the reaction.[39,40,42]

CODH catalyzes the reversible interconversion between CO and CO_2.[9,39,40] Structures of the CODH subunit from *Rhodospirillum rubrum*[43] and *Carboxydothermus hydrogenformans*[44] have been solved to reveal [Ni_1-Fe_4-S_4] cluster for the former and [Ni_1-Fe_4-S_5] for the latter. In the *C. hydrogenformans* structure, the nickel is ligated in 4S geometry with three labile sulfurs from the iron-sulfur cluster and a fourth sulfur ligand from a cysteine residue. Three of the iron atoms are coordinated via cysteine ligands and sulfurs from the iron sulfur cluster, but one iron is coordinated with a histidine residue.[31,44] In the structure from *R. rubrum*, the nickel is part of the cluster, but the fourth iron is mononuclear and not part of the cluster.[43] The nickel ion has been described as a nickel(II) bound in 4S, square planar geometry with the substrate CO binding in the axial position,[42,45] though more recent crystallographic studies on an isoform from *Morella thermoacetica* argue that no bridging sulfur ligand is present and it does not participate in catalysis (though it may play a pre-catalytic stabilizing role), so the catalytic cluster of CODH should be described as a [Ni-Fe_4-S_4] cluster (Figure 1.2).[46] In this case, nickel is initially bound with 3S coordination, but during catalysis, the fourth site is filled to complete the four-coordinate, square planar geometry.[46,47] Catalysis begins with CO binding to the nickel in the fourth position of a square planar arrangement. The iron-bound hydroxide then attacks the

nickel-bound CO to form a bound carboxylate that bridges both metal ions. A nearby histidine acts as a catalytic base and deprotonates the bound carboxylic acid group. CO_2 is released, leaving a potential $Ni^{"0"}$ center; these two electrons are transferred first to the C cluster internally from the metal center to bring nickel back to the Ni^{II} state before being transferred on to other iron-sulfur clusters within the CODH subunit.[46]

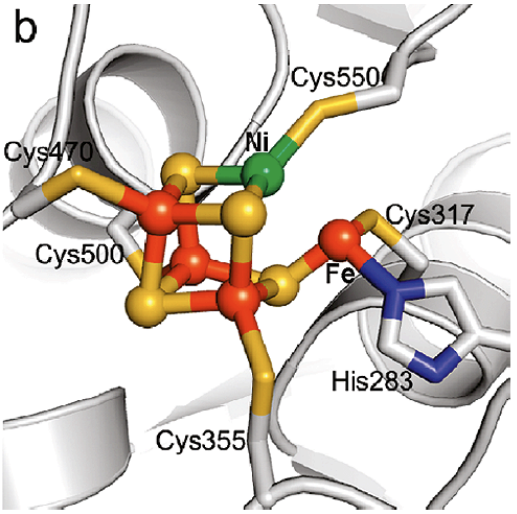

Figure 1.2. Active site of CODH, showing the [Ni-Fe_4-S_4] coordination.

Reproduced with permission from Kung, Y. *et al*.[46]

ACS catalyzes the synthesis of acetyl coenzyme A from CO (often generated by CODH), coenzyme A, and a methyl group of methylated corrinoid iron-sulfur protein (CoFeSP).[9,40] The crystal structure of CODH/ACS from *Moorella thermoacetica* has recently been solved by two different groups.[42,48] An iron-sulfur cluster with nickel comprises the catalytic metallocenter of the enzyme, called the A cluster, specifically a [Fe_4-S_4] cluster adjacent to a binuclear nickel-metal cluster, where different metals, including iron, copper, and zinc have been postulated to be in the second position of the binuclear cluster.[9,42,48] It is likely that only the bi-nickel form is active.[42] This site is coordinated with cysteine ligands, where the four iron atoms are coordinated to cysteine residues, as well as the proximal nickel. The proximal nickel maintains 4S

coordination using one sulfur ligand from the cluster, one cysteinyl side chain, and two cysteinyl side chains which bridge to another, distal nickel.[9] The bridging cysteine between the [Fe_4-S_4] and the proximal nickel is important for communication between the cofactors.[49] The distal nickel is bound in a *cis*-2N:2S geometry by Cys-Gly-Cys sequence from the protein, using the two sulfur side chains and two backbone nitrogens for metal coordination.[50] The proximal nickel ion is the active species, where the 2N:2S, *bis*-amide coordinated distal nickel remains as a bystander during catalysis. The proximal nickel can likely stabilize two different redox states; the resting state of the enzyme maintains a Ni^{II} center, but in the presence of substrates, methylated CoFeSP and CO, the active nickel moves to either a Ni^{I} or potentially a Ni^{0} state.[51] The presence of the adjacent iron sulfur cluster and the distal nickel ion may allow the proximal nickel to reach this highly reduced state by neutralizing its cysteine ligands.[42,52] Studies on the mechanism are still underway to probe the more likely of the nickel states.[53] While early studies demonstrated that the CO and CH_3 groups bind before CoA enters, it later became evident that the order of substrate binding drives the different possibilities for the nickel redox states, where if the methyl group binds first, a $Ni^{II/}Ni^{0}$ redox couple (diamagnetic cycle) can be used, whereas if the CO group binds first, $Ni^{II/}Ni^{I}$ is used (paramagnetic cycle).[54] It is now thought that methylation occurs before CO binds, allowing control over CO binding, yet preventing formation of a Ni^{0} species that could be inactive. ACS changes from an open to a closed conformation throughout catalysis.[42,48,55] This conformational change allows the order of substrate binding to be appropriate, where after methylation, the smaller CO substrate binds. This conformational change closes a tunnel, keeping CO bound and also allowing the larger CoA substrate to enter. More specifically, in this proposed mechanism, the methyl group binds in the fourth planar position to complete the planar coordination of Ni, followed by CO binding in the axial position,

before CO inserts into the Ni-CH_3 bond to generate the acetyl group. This acetyl group is then attached to coenzyme A, generating acetyl coenzyme A.[55]

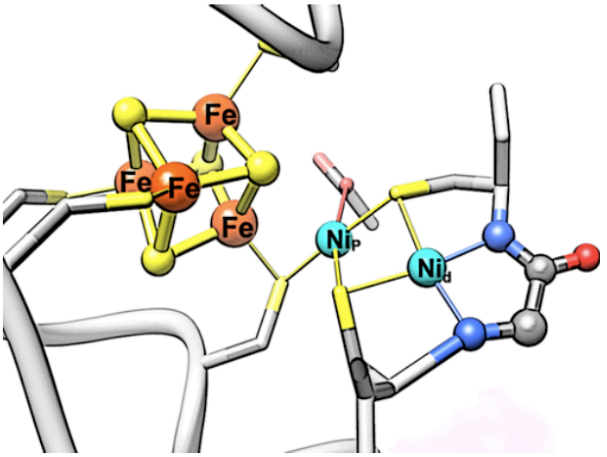

Figure 1.3. Active site of acetyl coenzyme A, showing the iron-sulfur cluster, the active proximal nickel (Ni_p), and the distal nickel (Ni_d). Reproduced with permission from Ragsdale, S.W.[9]

1.7.2.2. Hydrogenase. [Ni-Fe] hydrogenases catalyze the reversible reduction of protons to form hydrogen gas.[9] The enzymes are heterodimers; the smaller subunit contains one or more iron-sulfur clusters, but the larger subunit contains an active site with a nickel ion and an iron ion, where the metal ions are connected by bridging thiolate ligands.[9,38] Hydrogenases have two conserved CXXC motifs that are involved in metal binding,[56] where the nickel ion is coordinated by four cysteine ligands (Figure 1.4).[57] Iron is bound by the two bridging cysteine ligands, as well as CO and two CN groups.[9] A hydrophobic channel is involved in hydrogen gas transport through the enzyme, ending at the nickel site.[58,59] In the case of H_2 oxidation, an activation step is necessary; the enzyme must sit with H_2 for a period of time before heterolytic H-H bond cleavage occurs, resulting in a bridging metal hydride and a proton binding to sulfur in the active site. The autocatalytic mechanism begins with proton coupled electron transfer (PCET) to an active site base that results in a nickel(III) center. From here, hydride transfer to the attached

cysteinyl sulfur generates a nickel(I) center. Oxidative addition of H_2 to the nickel center allows heterolytic cleavage, where one hydrogen ends up as a bridging hydride and the other as a proton on the adjacent cysteine residue. In total, the enzyme undergoes three PCET events to regenerate the catalytic resting state.[9,59]

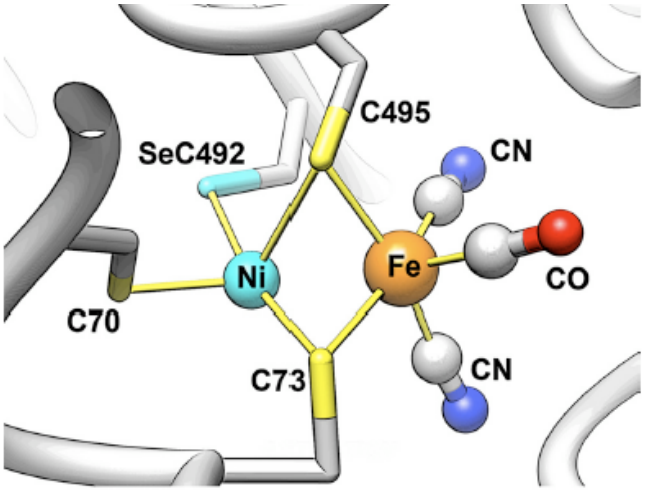

Figure 1.4. Active site of Ni-Fe hydrogenase. Reproduced with permission from Ragsdale, S.W.[9]

1.7.2.3. Methyl coenzyme M reductase. Methyl-coenzyme M reductase (MCR) is involved in methane formation in archea.[60-62] It catalyzes the reduction of methyl-coenzyme M to methane and a disulfide bound form of coenzyme M (CoM) and coenzyme B (CoB). One of the substrates, methyl-coenzyme B, binds and creates a channel in which methyl coenzyme M can enter and approach the active site. Methyl coenzyme M interacts with several residues to appropriately align itself in a binding pocket above the catalytic metal cofactor, including tyrosine, phenylalanine, histidine, and arginine. MCR contains a tightly bound coenzyme F430 nickel catalytic center, which is a nickel hydrocorphin where nickel is coordinated in an octahedral geometry. Four nitrogen atoms from the pyrrole ring provide the planar ligands, while one axial ligand is provided by the side-chain oxygen of glutamine and the other axial position is occupied by the substrate methyl CoM (Figure 1.5).[63] Many of the residues forming the active site pocket are chemically modified; these modifications are likely required for activity

of the enzyme, even among phylogenetically different organisms that utilize this type of enzyme.[64] The F430 cofactor in MCR cycles from Ni^{I} to Ni^{III}, where catalysis can only be initiated by the Ni^{I} resting state of the enzyme.[9,63] Different mechanisms that describe binding to the free axial position during catalysis and hydrogen transfer to the methyl group have been proposed.[63,65] In the first, it is suggested that the methyl group on methyl CoM nucleophilically reacts with Ni^{I} to generate methyl-Ni^{III} and coenzyme M. The methyl-Ni^{III} becomes methyl-Ni^{II} with a thiyl radical, where methyl-Ni^{II} then reacts with a proton to produce methane and Ni^{II}.[63-65] Alternatively, the methyl-thioether bond on CoM is homolyzed, generating a methyl radical that then reacts with CoB. This produces methane and a CoB thiyl radical that is available for reaction with the CoM radical to form a disulfide bond.[65] It has been proposed that MCR may also be involved in the anaerobic oxidation of methane to carbon dioxide.[65-67] Although studies on this enzyme are still underway, more recent studies using analogues of CoB suggest that methyl-CoM is the key coenzyme triggering the necessary conformational changes in MCR and therefore catalysis.[68] The highly reduced nickel(I) species required for activity is achieved only by the presence of the F430 cofactor; this tetrapyrrole cofactor allows the unique nickel behavior and therefore activity of this enzyme.

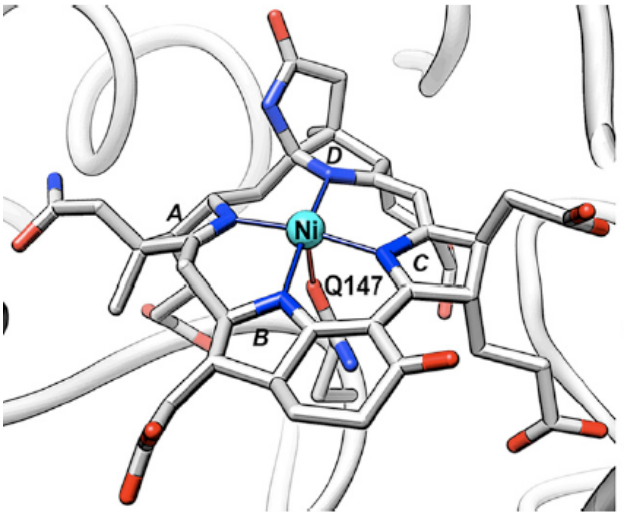

Figure 1.5. Active site of methyl coenzyme M reductase, showing the F430 tetrapyrrole cofactor. Reproduced with permission from Ragsdale, S.W.[9]

1.7.3. Comparison of nickel enzymes

Of the eight nickel enzymes described above, each has a unique active site, where nickel performs a wide variety of chemistry. Three of the nickel enzymes bind with strictly nitrogen and oxygen ligands, but these three enzymes (glyoxalase I, acireductone dioxygenase, and urease) utilize nickel simply as a Lewis acid where the metal remains in the Ni^{II} state throughout catalysis. Methyl coenzyme M reductase is unique in that it cycles between nickel(I) and nickel(III) throughout its catalytic mechanism, but it is coordinated with four nitrogen ligands and an axial glutamine ligand; however, the source of the nitrogen ligands is an F430 cofactor, which provides very different electronic properties than 4N coordination from all protein-based ligands.

The other four Ni-enzymes are redox active and cycle between various nickel states, from a possible Ni^{0} state all the way to Ni^{III}. For each of these four enzymes, sulfur ligation is critical for tuning the redox potential into a biologically relevant range.[10,11] Three of the remaining enzymes contain iron-sulfur cofactors (hydrogenase, CODH, ACS). Each of these enzymes reacts with a gaseous substrate and has a long hydrophobic tunnel leading to the catalytic nickel ion. In each of these enzymes, the catalytic nickel has two available *cis* coordination sites to interact with substrate and all of the coordinated ligands are sulfur based. Additionally, all three of these proteins utilize a catalytic mechanism that involves more than a one-electron process.[69] Ni-SOD is a Ni-enzyme that contains a mononuclear metal center with no other source of potential electrons to facilitate catalysis. Likely for this reason, it only cycles between nickel(II) and nickel(III) during its catalytic mechanism. All of its ligands are protein based, maintaining a 2N:2S coordination, or 3N:2S in the oxidized form. This mixture of nitrogen and sulfur ligands differs from the coordination of the other nickel enzymes, which utilize either 4S or 4-6N/O

ligation. Perhaps these differences explain why Ni-SOD is capable of catalyzing a one-electron process; the ligands to a metal tune its reduction potential, in this case impacting the reactivity of Ni-SOD.

Monodentate ligands can also interact with the nickel(III) species that forms, particularly imidazole; even in simple peptide complexes, solvent (water) can act as an axial, transient ligand and impact the potential of the Ni^{II}/Ni^{III} redox couple.[70,71] This is the case in Ni-SOD, where an axial histidine ligand coordinates to Ni^{III} during catalysis. This helps tune the redox potential for superoxide dismutase activity; Ni-SOD catalyzes a disproportionation reaction, and its redox potential must be between those of the two different half reactions. The addition of the axial histidine ligand makes the potential more negative and appropriate to catalyze both reactions.

1.8. Peptide-nickel complexes

Many of the nickel binding proteins described above have nickel-peptide analogues, the examination of which has greatly aided in understanding the chemistry and coordination of the metal binding sites in these proteins.[10,72] A review of key nickel-binding reveals common themes important to understanding fundamental properties of nickel-based chemistry. Unrelated peptides to the aforementioned enzymes have also been shown to perform chemistry and are described here, as they supplement understanding about nickel-based catalysis.

1.8.1. Nickel-binding by Cys-X-Cys motif

Cys-X-Cys is a common metal binding motif found in proteins. Cys-Gly-Cys is found in the enzyme ACS, and this sequence has been examined as an isolated peptide to characterize its nickel binding properties. Studies on the peptides CGC and CPCP, used in their acetylated and native forms, have shown that CXC peptides typically dimerize around nickel with 4S ligation. When glycine is present in the X position, this peptide is able to utilize amide coordination and form a monomeric 2N:2S complex with nickel. While acetylated CPCP forms dimeric complexes using all sulfur ligands, the amine groups on the free CPCP formed 2N:2S complexes, but still used two peptides per metal ion.[73] Comparison of this sequence to sequences with adjacent cysteines implies that an interceding glycine is small enough to allow the side chains of cysteine to still bind metal in adjacent coordination spheres of a planar complex. Although the CGC within the sequence of ACS binds to nickel in a 2N:2S geometry, it does not have electron transfer properties and therefore catalytic activity.[50,73]

1.8.2. Cleavage of DNA with an ATCUN motif

A number of proteins have an N-terminal GGH motif. Histidine in this third position allows the protein to bind metal in a square planar, 4N arrangement with the N-terminus, the histidine side chain, and two amide backbone nitrogens acting as ligands. This motif, termed amino terminal Cu^{II}, Ni^{II}-binding (ATCUN) motif, was first discovered in the protein human serum albumin.[74-76] The simple peptide GGH is sufficient for metal binding in this geometry,[77] though different residues can be substituted for one or both of the glycines to modulate the binding and reactivity of the complex. The metal binds specifically and tightly, but upon interaction with the appropriate ligands, the sequence can release its metal, which is important

for its role in metal transport in albumins.[76] The sequence may also bind metal and play a structural role when it is found within the sequence of a protein rather than at a terminus.[78] Additionally, this sequence can be engineered into proteins for various purposes.[76] Both the copper and nickel forms of this peptide are capable of catalyzing various chemistries. Specifically, copper is known for its ability to cleave DNA and even to be an anticancer agent. Nickel can mediate specific, oxidative protein cross linking to a tyrosine residue within the protein or with nearby proteins.[79,80,81] Ni-ATCUN can also perform DNA cleavage.[82] The cleavage is dependent on nickel-mediated oxidation, which can be activated with several different oxidants.[83] The nickel is likely oxidized to nickel(III) and in the presence of hydrogen peroxide, produces hydroxyl radicals and superoxide.[76] The reactivity is driven by involvement of metal-associated reactive oxygen species, generated by the Ni^{II}/Ni^{III} redox couple. Like Ni-SOD, this 4N coordinated Ni-peptide allows for cycling between Ni^{II} and Ni^{III}, but the result is generation of ROS rather than antioxidant activity. The coordinated ROS then acts to cleave the DNA bond. When a lysine is placed in the first position, KGH, the reactivity towards DNA is increased, likely due to the increased sigma donor character of lysine versus glycine; the ability of the oxygen species to be coordinated to the nickel and for it to be in position to react with DNA drives its reactivity.[84] Additionally, Ni-GGH can react with other compounds, such as sulfate, in solution to promote radical chemistry. In the presence of Ni-GGH, sulfur(IV) in the presence of air oxidizes the nickel(II) to nickel(III). Nickel(III) then oxidizes sulfate in solution to $SO_3^{\cdot-}$, which reacts with dioxygen and propagates a radical reaction that is damaging to DNA in solution.[85]

When cysteine is present in the first position of an ATCUN motif (CXH) in sequences where an N-terminus is not available, the nickel binds with 3N:1S coordination, utilizing the cysteine side chain as a ligand. If the thiolate group is blocked, it still binds nickel, and utilizes

the N-terminus as a ligand to accomplish 4N, square planar geometry with nickel(II). Interestingly, this peptide-metal complex with 4N coordination exhibits quasi-reversible redox behavior with a potential of 791 mV vs. Ag/AgCl. When nickel is bound via sulfur ligation, only irreversible oxidation is observed. When neither the thiol side chain nor the N-terminus is protected, pH drives the metal coordination. At neutral pH and anaerobic conditions, the thiolate coordination was allowed, but in the presence of air, the complex formed disulfide-linked nickel-peptide species. At higher pH, nitrogen replaces the sulfur ligand, and the deprotonated thiol is free to form a disulfide bond, generating disulfide-linked nickel-peptide complexes. When the nickel is bound with 4N geometry, a nickel(III) intermediate forms, followed by formation of a thiol radical. The thiol radical reacts with oxygen to form a thiol peroxyl radical and rearranges to a sulfonyl radical, propagating the radical reaction and leading eventually to sulfinic acid formation.[86] Preferential oxidation of the sulfur ligand rather than nickel is common, and understanding what drives thiol oxidation instead of metal oxidation is still of great interest.[87]

In general, when a cysteine precedes a histidine residue within a polypeptide, metal coordination depends on neighboring residues. In most cases, the resulting nickel complex is square planar, 3N:1S, where the cysteine side chain, the imidazole side chain of the histidine, and adjacent backbone nitrogens act as ligands. In cases where the CH sequence is near the N-terminus, metal preferentially binds in an all-nitrogen, ATCUN-like arrangement and forgoes use of the cysteine side chain.[88]

1.8.3. Intramolecular cleavage of nickel-bound peptides

One nickel-peptide complex, bound in 4N, square planar geometry, has been shown to promote hydrolysis of the peptide backbone at neutral/basic pH. Histone H2A containing the

sequence –TETHHK– was shown to promote backbone hydrolysis before the second Thr residue, though it was less than 50% complete over 140 hours.[89] Peptides with the embedded sequence (S/T)XHZ (where X and Z are bulky, hydrophobic residues, specifically SRHW) undergo hydrolysis in the presence of nickel selectively at the Ser/Thr backbone position over the course of hours, showing that differences in the sequence can modulate the rate of the reaction.[90] Nickel is coordinated by the histidine side chain and the three preceding backbone nitrogens, forming a 4N, square planar complex. It is thought that the binding of nickel in this position destabilizes the peptide bond between serine and the residue on its N-terminal side, promoting an N-O acyl shift with the OH group on the serine to form an intermediate ester, which hydrolyzes to generate the cleaved peptide. This reaction emanates from metal-induced steric cleavage rather than redox chemistry, as bulkier residues enhance the rate of cleavage of the peptide backbone.[91] Cysteine can also anchor the metal binding site, generating a square planar, 3N:1S complex where nickel is bound with the cysteine side chain and the preceding three backbone nitrogens. The SRCW-containing peptide can also perform the reaction, though with reduced efficiency.[92]

1.9. Structure/function relationship of nickel systems and comparison to MAP

1.9.1. Differences in coordination environment drive reactivity

Like the nickel enzymes, nickel chaperones and proteins involved in the biosynthesis of nickel enzymes utilize a wide variety of approaches to coordinate nickel, including deprotonated backbone nitrogens.[93] While it was previously believed that sulfur ligation was reserved for catalytic nickel centers,[5] the discovery and characterization of so many nickel metallochaperones

has altered thinking. The nickel-binding proteins UreE,[38,94-97] CooJ, [38,98-100] and RcnR[4] all utilize nitrogen and oxygen ligands to coordinate the metal. CooC binds with a CXC motif, where two monomers come together to provide 4S ligation of the nickel center, and this 4S configuration confers tight binding. The protein transfer process is therefore necessarily aided by ATP, which upon binding enables separation of the two monomers, facilitating release of the nickel.[7,101]

Three nickel-binding proteins are involved in hydrogenase biosynthesis, HypA, HypB, and SlyD. HypA binds nickel with micromolar affinity with four nitrogen ligands in a square planar geometry.[38,102-104] HypB binds nickel much more tightly with 3S:1N coordination and only releases its metal upon interaction with SlyD.[103,104] SlyD has a tail containing several Cys-Cys pairs and histidine residues, which accomplish binding to seven nickel ions, the structure of which has yet to be determined. In the absence of HypB, nickel cannot bind in all seven sites, suggesting that transfer is required for proper incorporation.[105,6] Moreover, despite the use of sulfur ligation, catalysis has not been reported. In general, in the pathway of nickel insertion, the affinity for nickel successively increases with each protein.

Studies reported to date do not explain why sulfur ligation sometimes allows catalysis and other times does not. For example, it is not clear what makes Ni-SOD catalytically active when it is analogous in structure to nickel proteins that do not catalyze reactions. Ni-SOD and the distal nickel of Ni-ACS have the same *cis*, 2N:2S coordination geometries, but while Ni-SOD is able to transfer electrons, the distal nickel of ACS is not. The distal nickel of ACS is present only to tune the reactivity of the proximal active site. This again emphasizes the importance of the overall protein structure and nearby structural motifs that impact reactivity. HspA also binds nickel with 2N:2S geometry, using a CC sequence; despite similarities to the active site structure of Ni-SOD, SOD activity has not been reported.[38,106,107] Differences among these proteins provide evidence that the coordinating ligands, binding geometry, as well as

overall protein structure all contribute toward the promotion of electron transfer and control of reactivity.

Though proteins with cysteine residues have been reported to bind metal, the geometry and chemistry of the Ni-NCC motif is unique. Of previously reported Ni-binding sequences that contain geminal Cys,[105,107,108] no SOD activity and only minimal structural characterization have been reported. The Ni-SOD maquettes do not contain contiguous Cys, yet MAP recapitulates the coordination and activity using adjacent Cys residues. Another tripeptide, the ATCUN motif, has the same geometry but carries out electron transfer in the absence of sulfur ligands, which leads to the generation of reactive oxygen species. The NCC tripeptide neutralizes rather than generates ROS, providing an additional tool for characterizing inner sphere effects. Additionally, in this work, we have noted the significance of the method of metal insertion, which requires transfer from a weak chelator to incorporate metal into the arrangement that is capable of productive electron transfer. Such a metal transfer reaction has not previously been described in the formation of other metal-peptide complexes. As such, this reaction may aid in understanding the mechanism of transfer within metallochaperone pathways, such as the transfer of nickel between HypB and SlyD.

1.10. References

(1) Finney, L. A.; O'Halloran, T. V. *Science* **2003**, *300*, 931-936.

(2) Rosenzweig, A. C. *Chemistry & Biology* **2002**, *9*, 673-677.

(3) Lippard, S. J.; Berg, J. M. *Principles of Bioinorganic Chemistry*; University Science Books: Mill Valley, CA, 1994.

(4) Iwig, J. S.; Leitch, S.; Herbst, R. W.; Maroney, M. J.; Chivers, P. T. *J. Am. Chem. Soc.* **2008**, *130*, 7592-7606.

(5) Maroney, M. J. *Curr. Opin. Chem. Biol.* **1999**, *3*, 188-199.

(6) Leach, M. R.; Zhang, J. W.; Zamble, D. B. *J. Biol. Chem.* **2007**, *282*, 16177 -16186.

(7) Jeoung, J.-H.; Giese, T.; Gruenwald, M.; Dobbek, H. *J. Mol. Biol.* **2010**, *396*, 1165-1179.

(8) Choudhury, S. B.; Lee, J.-W.; Davidson, G.; Yim, Y.-I.; Bose, K.; Sharma, M. L.; Kang, S.-O.; Cabelli, D. E.; Maroney, M. J. *Biochemistry* **1999**, *38*, 3744-3752.

(9) Ragsdale, S. W. *J. Biol. Chem.* **2009**, *284*, 18571-18575.

(10) Shearer, J.; Long, L. M. *Inorg. Chem.* **2006**, *45*, 2358-2360.

(11) Neupane, K. P.; Shearer, J. *Inorg. Chem.* **2006**, *45*, 10552-10566.

(12) Neupane, K. P.; Gearty, K.; Francis, A.; Shearer, J. *J. Am. Chem. Soc.* **2007**, *129*, 14605-14618.

(13) Miller, A.-F. *Curr. Opin. Chem. Biol.* **2004**, *8*, 162-168.

(14) Youn, H.-D.; Kim, E.-J.; Roe, J.-H.; Hah, Y. C.; Kang, S.-O. *Biochem. J.* **1996**, *318*, 889-896.

(15) Youn, H.-D.; Youn, H.; Lee, J.-W.; Yim, Y.-I.; Lee, J. K.; Hah, Y. C.; Kang, S.-O. *Arch. Biochem. Biophys.* **1996**, *334*, 341-348.

(16) Bryngelson, P. A.; Arobo, S. E.; Pinkham, J. L.; Cabelli, D. E.; Maroney, M. J. *J. Am. Chem. Soc.* **2004**, *126*, 460-461.

(17) Wuerges, J.; Lee, J.-W.; Yim, Y.-I.; Yim, H.-S.; Kang, S.-O.; Carugo, K. D. *Proc. Natl. Acad. Sci. U.S.A.* **2004**, *101*, 8569-8574.

(18) Barondeau, D. P.; Kassmann, C. J.; Bruns, C. K.; Tainer, J. A.; Getzoff, E. D. *Biochemistry* **2004**, *43*, 8038-8047.

(19) Herbst, R. W.; Guce, A.; Bryngelson, P. A.; Higgins, K. A.; Ryan, K. C.; Cabelli, D. E.; Garman, S. C.; Maroney, M. J. *Biochemistry* **2009**, *48*, 3354-3369.

(20) Johnson, O. E.; Ryan, K. C.; Maroney, M. J.; Brunold, T. C. *J. Biol. Inorg. Chem.* **2010**, *15*, 777-93.

(21) Ryan, K. C.; Johnson, O. E.; Cabelli, D. E.; Brunold, T. C.; Maroney, M. J. *J. Biol. Inorg. Chem.* **2010**, *15*, 795-807.

(22) Bryngelson, P. A.; Maroney, M. J. *Met. Ions Life Sci.* **2007**, *2*, 417-443.

(23) Fiedler, A. T.; Bryngelson, P. A.; Maroney, M. J.; Brunold, T. C. *J. Am. Chem. Soc.* **2005**, *127*, 5449-5462.

(24) Schmidt, M.; Zahn, S.; Carella, M.; Ohlenschlaeger, O.; Goerlach, M.; Kothe, E.; Weston, J. *ChemBioChem* **2008**, *9*, 2135-2146.

(25) Mathrubootham, V.; Thomas, J.; Staples, R.; McCraken, J.; Shearer, J.; Hegg, E. L. *Inorg. Chem.* **2010**, *49*, 5393-5406.

(26) Shearer, J.; Zhao, N. *Inorg. Chem.* **2006**, *45*, 9637-9639.

(27) Tabbi, G.; Driessen, W. L.; Reedijk, J.; Bonomo, R. P.; Veldman, N.; Spek, A. L. *Inorg. Chem.* **1997**, *36*, 1168-1175.

(28) Tietze, D.; Tischler, M.; Voigt, S.; Imhof, D.; Ohlenschlaeger, O.; Goerlach, M.; Buntkowsky, G. *Chem.--Eur. J.* **2010**, *16*, 7572-7578.

(29) Tietze, D.; Breitzke, H.; Imhof, D.; Koeth, E.; Weston, J.; Buntkowsky, G. *Chem.--Eur. J.* **2009**, *15*, 517-523.

(30) Walsh, C. T.; Orme-Johnson, W. H. *Biochemistry* **1987**, *26*, 4901-6.

(31) Thauer, R. K. *Science* **2001**, *293*, 1264-1265.

(32) He, M. M.; Clugston, S. L.; Honek, J. F.; Matthews, B. W. *Biochemistry* **2000**, *39*, 8719-878727.

(33) Ju, T.; Goldsmith, R. B.; Chai, S. C.; Maroney, M. J.; Pochapsky, S. S.; Pochapsky, T. C. *J. Mol. Biol.* **2006**, *393*, 823-834.

(34) Walsh, C. T.; Orme-Johnson, W. H. *Biochemistry* **1987**, *26*, 4901-4906.

(35) Blakeley, R. L.; Zerner, B. *J. Mol. Catal.* **1984**, *23*, 263-92.

(36) Sumner, J. B. *J. Biol. Chem.* **1926**, *69*, 435-441.

(37) Jabri, E.; Carr, M. B.; Hausinger, R. P.; Karplus, P. A. *Science* **1995**, *268*, 998-1004.

(38) Kaluarachchi, H.; Chan-Chung, K. C.; Zamble, D. B. *Nat. Prod. Rep.* **2010**, *27*, 681-694.

(39) Maynard, E. L.; Sewell, C.; Lindahl, P. A. *J. Am. Chem. Soc.* **2001**, *123*, 4697-4703.

(40) Tan, X.; Volbeda, A.; Fontecilla-Camps, J. C.; Lindahl, P. A. *JBIC, J. Biol. Inorg. Chem.* **2006**, *11*, 371-378.

(41) Ralston, C. Y.; Wang, H.; Ragsdale, S. W.; Kumar, M.; Spangler, N. J.; Ludden, P. W.; Gu, W.; Jones, R. M.; Patil, D. S.; Cramer, S. P. *J. Am. Chem. Soc.* **2000**, *122*, 10553-10560.

(42) Darnault, C.; Volbeda, A.; Kim, E. J.; Legrand, P.; Vernede, X.; Lindahl, P. A.; Fontecilla-Camps, J. C. *Nat. Struct. Biol.* **2003**, *10*, 271-279.

(43) Drennan, C. L.; Heo, J.; Sintchak, M. D.; Schreiter, E.; Ludden, P. W. *PNAS* **2001**, *98*, 11973-11978.

(44) Dobbek, H.; Svetlitchnyi, V.; Gremer, L.; Huber, R.; Meyer, O. *Science* **2001**, *293*, 1281-1285.

(45) Ha, S.-W.; Korbas, M.; Klepsch, M.; Meyer-Klaucke, W.; Meyer, O.; Svetlitchnyi, V. *J. Biol. Chem.* **2007**, *282*, 10639-10646.

(46) Kung, Y.; Doukov, T. I.; Seravalli, J.; Ragsdale, S. W.; Drennan, C. L. *Biochemistry* **2009**, *48*, 7432-7440.

(47) Jeoung, J.-H.; Dobbek, H. *J. Am. Chem. Soc.* **2009**, *131*, 9922-9923.

(48) Doukov, T. I.; Iverson, T. M.; Seravalli, J.; Ragsdale, S. W.; Drennan, C. L. *Science* **2002**, *298*, 567-572.

(49) Liu, Y.; Zhu, X.; Wang, F.; Ying, T.; Li, P.; Huang, Z.-X.; Tan, X. *Chem. Commun. (Cambridge, U. K.)* **2011**, *47*, 1291-1293.

(50) Evans, D. J. *Coord. Chem. Rev.* **2005**, *249*, 1582-1595.

(51) Lindahl, P. A. *J. Biol. Inorg. Chem.* **2004**, *9*, 516-524.

(52) Hausinger, R. P. *Nat. Struct. Biol.* **2003**, *10*, 234-236.

(53) Hegg, E. L. *Acc. Chem. Res.* **2004**, *37*, 775-783.

(54) Seravalli, J.; Ragsdale, S. W. *J. Biol. Chem.* **2008**, *283*, 8384-8394.

(55) Gencic, S.; Duin, E. C.; Grahame, D. A. *J. Biol. Chem.* **2010**, *285*, 15450-15463.

(56) Vignais, P. M.; Billoud, B. *Chem. Rev.* **2007**, *107*, 4206-4272.

(57) Kuchar, J.; Hausinger, R. P. *Chem. Rev.* **2004**, *104*, 509-525.

(58) Montet, Y.; Amara, P.; Volbeda, A.; Vernede, X.; Hatchikian, E. C.; Field, M. J.; Frey, M.; Fontecilla-Camps, J. C. *Nat. Struct. Biol.* **1997**, *4*, 523-526.

(59) Lill, S. O. N.; Siegbahn, P. E. M. *Biochemistry* **2009**, *48*, 1056-1066.

(60) Gunsalus, R. P.; Wolfe, R. S. *J. Biol. Chem.* **1980**, *255*, 1891-1895.

(61) Scheller, S.; Goenrich, M.; Boecher, R.; Thauer, R. K.; Jaun, B. *Nature* **2010**, *465*, 606-608.

(62) Ellefson, W. L.; Wolfe, R. S. *J. Biol. Chem.* **1981**, *256*, 4259-4262.

(63) Ermler, U.; Grabarse, W.; Shima, S.; Goubeaud, M.; Thauer, R. K. *Science* **1997**, *278*, 1457-1462.

(64) Grabarse, W.; Mahlert, F.; Shima, S.; Thauer, R. K.; Ermler, U. *J. Mol. Biol.* **2000**, *303*, 329-344.

(65) Shima, S.; Thauer, R. K. *Curr. Opin. Microbiol.* **2005**, *8*, 643-648.

(66) Krueger, M.; Meyerdierks, A.; Gloeckner, F. O.; Amann, R.; Widdel, F.; Kube, M.; Reinhardt, R.; Kahnt, J.; Boecher, R.; Thauer, R. K.; Shima, S. *Nature* **2003**, *426*, 878-881.

(67) Thauer, R. K.; Shima, S. *Ann. N. Y. Acad. Sci.* **2008**, *1125*, 158-170.

(68) Cedervall, P. E.; Dey, M.; Pearson, A. R.; Ragsdale, S. W.; Wilmot, C. M. *Biochemistry* **2010**, *49*, 7683-7693.

(69) Volbeda, A.; Fontecilla-Camps, J. C. *Coor. Chem. Rev.* **2005**, *249*, 1609-1619.

(70) Youngblood, M. P.; Margerum, D. W. *Inorg. Chem.* **1980**, *19*, 3068-3072.

(71) Murray, C. K.; Margerum, D. W. *Inorg. Chem.* **1982**, *21*, 3501-3506.

(72) Chung, K. C. C.; Cao, L.; Dias, A. V.; Pickering, I. J.; George, G. N.; Zamble, D. B. *J. Am. Chem. Soc.* **2008**, *130*, 14056-14057.

(73) Kulon, K.; Wozniak, D.; Wegner, K.; Grzonka, Z.; Kozlowski, H. *J. Inorg. Biochem.* **2007**, *101*, 1699-1706.

(74) Laussac, J.-P.; Sarkar, B. *Biochemistry* **1984**, *23*, 2832-2838.

(75) Harford, C.; Sarkar, B. *Biochhem. and Biophys. Res. Comm.* **1995**, *209*, 877-882.

(76) Harford, C.; Sarkar, B. *Acc. Chem. Res.* **1997**, *30*, 123-130.

(77) Sakurai, T.; Nakahara, A. *Inorg. Chem.* **1980**, *19*, 847-853.

(78) Sankararamakrishnan, R.; Verma, S.; Kumar, S. *Proteins: Structure, Function, and Bioinformatics* **2005**, *58*, 211-221.

(79) Person, M.; Brown, K. C.; Mahrus, S.; Craik, C. S.; Burlingame, A. L. *Protein Sci.* **2001**, *10*, 1549-1562.

(80) Brown, K. C.; Yu, Z.; Burlingame, A. L.; Craik, C. S. *Biochemistry* **1998**, *37*, 4397-4406.

(81) Endrizzi, B. J.; Huang, G.; Kiser, P. F.; Stewart, R. J. *Langmuir* **2006**, *22*, 11305-11310.

(82) Footer, M.; Egholm, M.; Kron, S.; Coull, J. M.; Matsudaira, P. *Biochemistry* **1996**, *35*, 10673-9.

(83) Mack, D. P.; Dervan, P. B. *Biochemistry* **1992**, *31*, 9399-9405.

(84) Jin, Y.; Lewis, M. A.; Gokhale, N. H.; Long, E. C.; Cowan, J. A. *J. Am. Chem. Soc.* **2007**, *129*, 8353-8361.

(85) Alipzazga, M. V.; Moreno, R. G. M.; Linares, E.; Medeiros , M. H. G.; Coichev, N. *Dalton Trans.* **2005**.

(86) Van Hort, J. D.; Bulaj, G.; Goldenberg, D. P.; Burrows, C. J. *J. Biol. Inorg. Chem.* **2003**, *8*, 601-610.

(87) Maroney, M. J.; Choudhury, S. B.; Bryngelson, P. A.; Mirza, S. A.; Sherrod, M. J. *Inorg. Chem.* **1996**, *35*, 1073-6.

(88) Kulon, K.; Valensin, D.; Kamysz, W.; Nadolny, R.; Gaggelli, E.; Valensin, G.; Kozlowski, H. *Dalton Trans.* **2008**, 5323-5330.

(89) Bal, W.; Liang, R.; Lukszo, J.; Lee, S.-H.; Dizdaroglu, M.; Kasprzak, K. S. *Chem Res Toxicol* **2000**, *13*, 616-624.

(90) Krezel, A.; Kopera, E.; Protas, A. M.; Poznanski, J.; Wyslouch-Cieszynska, A.; Bal, W. *J. Am. Chem. Soc.* **2010**, *132*, 3355-3366.

(91) Kopera, E.; Krezel, A.; Protas, A. M.; Belczyk, A.; Bonna, A.; Wyslouch-Cieszynska, A.; Poznanski, J.; Bal, W. *Inorg. Chem.* **2010**, *49*, 6636-6645.

(92) Protas, A. M.; Bonna, A.; Kopera, E.; Bal, W. *J. Inorg. Biochem.* **2011**, *105*, 10-16.

(93) Cherifi, K.; Decock-Le Reverend, B.; Varnagy, K.; Kiss, T.; Sovago, I.; Loucheux, C.; Kozlowski, H. *J. Inor.g Biochem.* **1990**, *38*, 69-80.

(94) Soriano, A.; Colpas, G. J.; Hausinger, R. P. *Biochemistry* **2000**, *39*, 12435-12440.

(95) Grossoehme, N. E.; Mulrooney, S. B.; Hausinger, R. P.; Wilcox, D. E. *Biochemistry* **2007**, *46*, 1050-10516.

(96) Colpas, G. J.; Hausinger, R. P. *J. Biol. Chem.* **2000**, *275*, 10731-10737.

(97) Stola, M.; Musiani, F.; Mangani, S.; Turano, P.; Safarov, N.; Zambelli, B.; Ciurli, S. *Biochemistry.* **2006**, *45*, 6495-6509.

(98) Jeon, W. B.; Cheng, J.; Ludden, P. W. *J. Biol. Chem.* **2001**, *276*, 38602-38609.

(99) Watt, R. K.; Ludden, P. W. *J. Biol. Chem.* **1998**, *273*, 10019-10025.

(100) Kerby, R. L.; Ludden, P. W.; Roberts, G. P. *J. Bacteriol.* **1997**, *179*, 2259-2266.

(101) Jeoung, J.-H.; Giese, T.; Gruenwald, M.; Dobbek, H. *Biochemistry* **2009**, *48*, 11505-11513.

(102) Atanassova, A.; Zamble, D. B. *J. Bacteriol*. **2005**, *187*, 4689-4697.

(103) Mehta, N.; Olson, J. W.; Maier, R. J. *J Bacteriol*. **2003**, *185*, 726-734.

(104) Xia, W.; Li, h.; Sze, K.-H.; Sun, H. *J. Am. Chem. Soc*. **2009**, *131*, 10031-10040.

(105) Kaluarachichi, H.; Sutherland, D. E. K.; Young, A.; Pickering, I. J.; Stillman, M. J.; Zamble, D. B. *J. Am. Chem. Soc*. **2009**, *131*.

(106) Schauer, K.; Muller, C.; Carriere, M.; Labigne, A.; Cavazza, C.; De Reuse, H. *J. Bacteriol*. **2010**, *192*, 1231-1237.

(107) Rowinska-Zyrek, M.; Witkowska, D.; Valensin, D.; Kamysz, W.; Kozlowski, H. *Dalton Trans*. **2010**, *39*, 5814-5826.

(108) Heaton, D. N.; George, G. N.; Garrison, G.; Winge, D. R. *Biochemistry* **2001**, *40*, 743-451.

Chapter 2: A Novel Tripeptide Model of Nickel Superoxide Dismutase

The radical species superoxide ($O_2^{\cdot-}$) and its reactive downstream products are known to cause oxidative damage to biological molecules, and the presence of superoxide in the body has been linked to many different diseases.[1] Superoxide dismutases (SODs) are oxidoreductases that catalyze the disproportionation of superoxide to hydrogen peroxide and molecular oxygen, therefore helping to protect biological systems from oxidative damage. These enzymes, classified by their metal center, include Cu/Zn-SODs, Fe- and Mn-SODs, and Ni-SODs.[2]

Ni-SOD is the most recently discovered form of the enzyme.[3,4] Its active site contains a mononuclear nickel center[5] coordinated in square planar geometry at the N-terminus of the enzyme via two cysteine sulfurs (Cys-2 and Cys-6), an amine nitrogen from the N-terminus, and a deprotonated, anionic amide nitrogen from the peptide backbone (Cys-2).[6,7] Ni-SOD reacts with superoxide in a two-step reaction, involving oxidized and reduced forms of the enzyme (Scheme 2.1).[3,6-8]

Scheme 2.1. Reaction catalyzed by Ni-SOD.

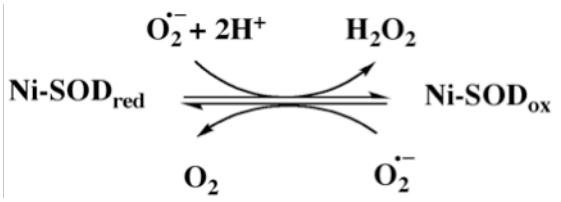

As part of the redox reaction, the geometry of the bound nickel switches from square planar Ni^{II} to square pyramidal Ni^{III}. An additional ligand, an axial nitrogen donor, coordinates

Ni^{III} in the resting state,[3] and the X-ray crystal structure revealed this species to be the imidazole nitrogen of His1. Upon reduction of the enzyme, the histidine imidazole rotates away from the active site, leaving Ni^{II} coordinated in 2N:2S, square planar geometry.[6,7,9]

While much has been learned about the structure of the enzyme, only recently have studies begun to reveal more about the influence of the secondary coordination sphere.[10,11] While recent studies support an inner sphere mechanism,[12,13] the catalytic mechanism is not yet fully elucidated. In order to further explore these issues, it has been of interest to develop model systems that mimic the activity of this enzyme. Within Ni-SOD, the metal is coordinated by ligands found within the first six residues of the N-terminus.[6,7] Synthetic models with square planar 2N:2S geometries have appropriate redox potentials to act as SOD mimics, yet these do not exhibit SOD activity.[14-16] Peptide models based on the terminal sequence of the enzyme, however, have been shown to mimic SOD activity.[12,13,17-19] Here we present a novel tripeptide mimic, asparagine-cysteine-cysteine (NCC), that exhibits both quasi-reversible Ni^{II}/Ni^{III} transitions and SOD activity. (Jennifer Ann Stowell Laurence, Anthony Andrew Vartia, Mary Elizabeth Krause. METAL ABSTRACTION PEPTIDE (MAP) TAG AND ASSOCIATED METHODS. Provisional Patent Application USPTO 61/052,918. Filed May 13, 2008. International Patent Application PCT/US2009/43821. Filed May 13, 2009. Published September 10, 2010.) NCC is unique because it is not derived from the sequence of the parent enzyme. Because of its small size, this tripeptide is likely to have better stability and lower cost of production than larger peptide alternatives. Importantly, using an alternative simple model also has the potential to shed insight into the minimal geometric/electronic features necessary for SOD activity using Ni.

2.1. Experimental

2.1.1. Generation of Ni-NCC complex: The NCC peptide was purchased from Genscript Corporation (Piscatway, NJ, USA). The Ni-NCC complex was generated using a transmetallation reaction performed in aqueous solution at neutral to basic pH. Incubation of the peptide for approximately 30 minutes with immobilized metal affinity chromatography (IMAC) resin (GE Healthcare) charged with nickel ensures a clean reaction with no undesired side products and no free metal ions in solution, yielding a reddish-brown complex.

2.1.2. ESI-MS: Samples were diluted 100x in methanol and analyzed on an LCT Premier (Waters Corporation) operating in negative ion mode. In order to verify that no changes were made to the peptide upon release of the metal, samples were acidified to approximately pH 5 by addition of 1 M hydrochloric acid (HCl) and analyzed using the same technique.

2.1.3. CD and absorption studies: A 1.5 mM solution of Ni-NCC was prepared in 50 mM sodium phosphate, pH 7.4, sparged with argon. Immediately after incubation, samples were placed in a cuvette with a 1-cm path length and scanned from 900-300 nm using both absorption and CD spectroscopy. Background scans of buffer alone were subtracted from each scan. Absorption studies were performed on an Agilent 8453 UV/Visible spectrophotometer. Circular dichroism analysis was performed on a J-815 (Jasco Corporation). The data presented are the average of five scans.

2.1.4. Deconvolution: Deconvolution of CD and absorption data was performed using Igor Pro (Wavemetrics). Iterative Gaussian deconvolutions were performed with a constant peak width of 1650 cm^{-1}. Absorption band energies were kept within 10% of the corresponding CD bands due to the broad nature of the absorption spectrum.

2.1.5. DFT: DFT calculations were performed by A. Glass. The *ORCA* 2.7 software package designed by Neese and coworkers was used for all DFT computations.[20]Spin restricted geometry optimizations were converged to the $S = 0$ spin state and employed the Becke-Perdew (BP86) functional,[21,22] and the aug-TZVP (Dunning diffuse functions added to Ahlrichs triple-x valence polarized) basis in conjunction with the TZV/J auxiliary basis for all atoms.[23,24] These calculations employed the resolution of identity (RI) approximation developed by Neese.[25] Solvation effects associated with water ($\varepsilon = 80$) were incorporated using COSMO, as implemented in *ORCA*.[26] Subsequent single-point energy calculations on the geometry-optimized structures employed the B3LYP functional,[27,28] the aug-TZVP basis,[29] and the COSMO solvation model.

2.1.6. pH titration: The absorption of the complex was monitored over a pH range of 7.4 to 10 to confirm that no structural changes result from pH adjustment. As observed with similar systems,[30] the peaks observed at pH 7.4 increase in intensity with increasing pH. To monitor the dependence of absorption intensity on pH, a sample containing 1.5 mM Ni-NCC was prepared in 50 mM borate at pH 10, sparged with argon. After incubation, the pH was adjusted back to 10 and the CD and absorption spectra were measured as described above. pH was lowered in half-

log increments (pH 9.5, 9.0, 8.5, 8.0, and 7.4) using 1 M HCl, and CD and absorption spectra were collected at each pH point.

2.1.7. MCD: Samples containing 6 mM Ni-NCC were prepared in 50 mM borate at pH 10, sparged with argon. Solid sucrose was added as a glassing agent and the mixture was heated to form a saturated solution. The dilution resulted in a final Ni-NCC concentration of 2 mM. The sample was placed in an MCD cell and flash frozen. Spectra were collected by A. Glass on a J-815 (Jasco Corporation) interfaced with an Oxford Spectromag 4000. Spectra were collected at +7 and -7 Tesla and the difference was found via subtraction in order to remove any CD signal. Spectra were collected at 15 K, 8 K, 4.5 K, and 2 K and analyzed to identify any changes in the spectra that indicate paramagnetic character. The feasibility of correlating these low temperature data with the structure of Ni-NCC at room temperature is demonstrated by the lack of apparent changes in the corresponding CD spectra collected at 298 and 4.5 K.

2.1.8. Solid phase peptide synthesis: The peptides GCC, GGGCC, and GGNCC were synthesized in house using solid phase peptide synthesis on Wang resin using Fmoc protected amino acids and HBTU/DIPEA coupling techniques. Wang resin and Fmoc-protected amino acids were purchased from Novabiochem and used as received. The peptide was cleaved from the resin using Reagent R (90% TFA/5% thioanisole/3% EDT/2% anisole). The resulting solution was added dropwise to cold diethyl ether to precipitate the peptide. The cleavage solution was washed several times with cold ether and the resulting crude peptide was purified by preparative reverse phase HPLC (Shimadzu) with a C18 column (Varian Microsorb 300 C18; 8 μM, 250 x 21.4) and guard column (Varian Microsorb 300 C18; 8 μM, 50 x 21.4). The

fractions containing the purified peptide were lyophilized and the mass was verified by ESI-MS.

2.1.9. Electrochemical studies: A 3-mL, 3-mM Ni-NCC sample was prepared in 50 mM borate at pH 10. Cyclic voltammetry (CV) data were collected with a CHI812C Electrochemical Analyzer potentiostat (CH Instruments) with a three-electrode setup (platinum working electrode, Bioanalytical Systems Inc.; Pt auxiliary electrode; Ag/AgCl reference electrode) in a glass CV cell. Potential was applied from zero to 1.2 V with a scan rate of 0.2 V per second, and current was measured. Bulk electrolysis was performed on a 3-mL, 3-mM Ni-NCC sample prepared in the same manner. Using the same setup as the CV measurements, potential was applied at 0.95 V while stirring to fully oxidize the sample, and current was monitored until no further change was observed. ESI-MS operating in negative ion mode was performed on the sample following bulk electrolysis to confirm the peptide was unaltered.

2.1.10. Xanthine/xanthine oxidase SOD activity assay: An assay using xanthine/xanthine oxidase was performed as described by Crapo *et al*.[32] with minor modifications. The assay was performed in 50 mM potassium phosphate with 100 μM EDTA at pH 7.8. In this assay, 600 μM cytochrome c from bovine heart (Sigma), 300 μM xanthine (Sigma), and enough xanthine oxidase (from buttermilk; Sigma) to cause a change in absorbance at 550 nm of 0.02 AU to 0.04 AU per minute were added to a final volume of 300 μL, and the change in absorbance at 550 nm was monitored on a Cary 100 UV-visible spectrophotometer (Varian). The assay was performed with several concentrations (0, 10, 15, 20, 25, 30, 35, 40, 50 μM and beyond as necessary) of Ni-NCC to measure an IC_{50} value.

2.2. Results and Discussion

NCC binds nickel, apparently with extremely high affinity at physiological pH, and this system is thought to be a potential mimic of Ni-SOD based on similarities in coordination. To show the extent of incorporation of metal into the complex and assess changes in protonation of the free versus bound peptide, electrospray ionization mass spectrometry (ESI-MS) operating in negative ion mode was used. The data show full incorporation of the metal in a 1:1 ratio and suggest that no irreversible modifications to the peptide occur upon incorporation or release of the metal via acidification. These data further indicate a tetra-deprotonated species binds the metal ion (Ni-NCC = 392.98).

To probe the Ni^{II} geometry in more detail, electronic absorption, circular dichroism (CD), and variable-temperature magnetic CD (MCD) data were collected for Ni-NCC. Supporting the mass spectrometry data, absorption spectra collected over a broad range of concentrations of the complex resulted in an increase in band intensity, indicating that there is one primary species present in solution (data not shown). Signal intensity also varies with pH, where the low energy bands corresponding to the *d-d* transitions are less intense at lower pH (Figure 2.1).

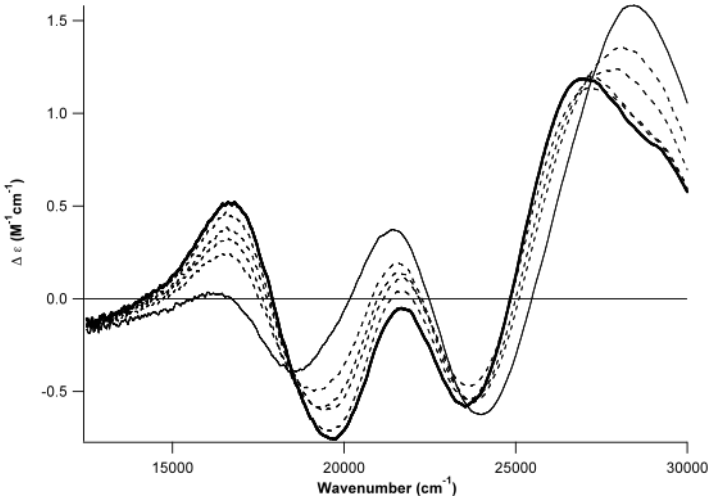

Figure 2.2. CD of a pH titration of Ni-NCC in 50 mM borate. The bold line represents the highest pH (10.0) and the solid line represents the lowest pH (7.4). Dashed lines represent other pH values measured (pH 9.5 – 8.0), in which the peaks are reduced in intensity with each half-log decrease in pH.

An iterative deconvolution of the absorption and CD spectra reveal seven electronic transitions between 14 000 and 29 000 cm^{-1} (Table 2.1 and Figure 2.2). With the exception of band 1, the energies of these transitions are within ~1000 to 2000 cm^{-1} of those reported for Ni-SOD (Table 2.2), which is indicative of structural similarities between the Ni^{II} centers in these two systems. Bands 1 – 4 of Ni-NCC, which are relatively intense in the CD spectrum but carry only moderate absorption intensities, are assigned as the four *d-d* transitions expected for a square planar Ni^{II} center. By analogy to Ni-SOD, we assign the higher-energy bands 5 – 7 as thiolate-to-nickel(II) charge transfer (CT) transitions.

Table 2.1. Deconvolution of peaks in absorption and CD spectra of Ni-NCC.

Band	Absorption		CD	
	Energy (cm^{-1})	ε ($M^{-1}cm^{-1}$)	Energy (cm^{-1})	Δε ($M^{-1}cm^{-1}$)
1	14 500	20	14 200	-0.1
2	17 300	60	16 270	-0.21
3	19 650	160	18 900	0.22
4	21 850	205	22 170	0.64
5	24 300	275	23 900	-0.44
6	26 850	575	26 520	0.71
7	28 850	1080	28 475	1.1

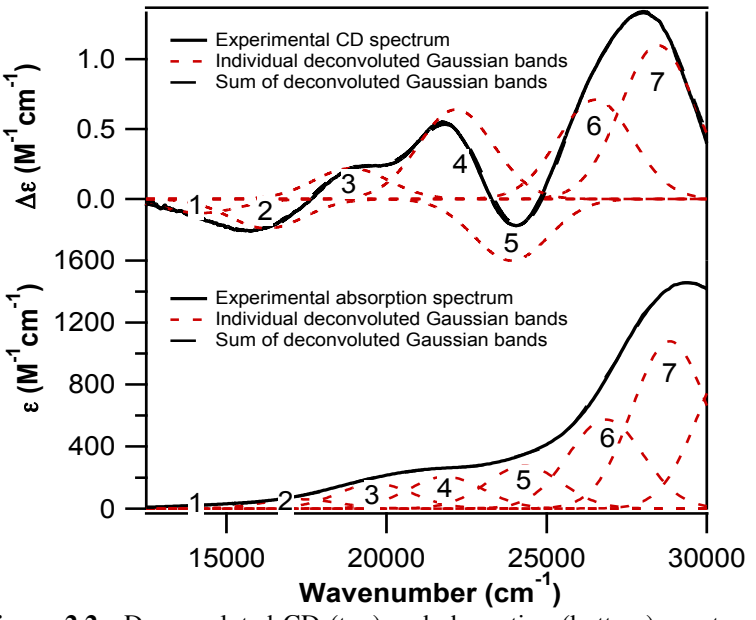

Figure 2.2. Deconvoluted CD (top) and absorption (bottom) spectra of 1.5 mM Ni-NCC in 50 mM phosphate buffer, pH 7.4. Spectra were deconvoluted with Igor Pro (Wavemetrics). The sum of the deconvoluted bands overlays exactly with the measured values.

Table 2.2. Comparison of Ni-NCC and Ni-SOD CD transition energies and assignments.

(Ni-SOD values were measured by Fiedler *et al*.[33])

Band	Transition Assignment	Ni-NCC (cm^{-1})	Ni-SOD (cm^{-1})
1	Ni^{II} *d-d*	14 200	17 110
2	Ni^{II} *d-d*	16 270	18 430
3	Ni^{II} *d-d*	18 900	20 500
4	Ni^{II} *d-d*	22 170	22 240
5	S^{-} - Ni^{II} CT	23 900	24 970
6	S^{-} - Ni^{II} CT	26 520	27 650
7	S^{-} - Ni^{II} CT	28 475	29 220

Further support for the presence of a square planar Ni^{II} center in Ni-NCC comes from the temperature independence of MCD signals observed for Ni-NCC over the temperature range 2 – 15 K (Figure 2.3). This behavior is indicative of a diamagnetic (S = 0) species, which is best

rationalized in terms of a square planar Ni^{II} center.[34] Room temperature and low temperature CD spectra are parallel (Figure 2.4). The only changes between these two spectra are the expected blue-shifts and sharpening of the bands in the spectrum collected at 4.5 K. The percentage of paramagnetic species was determined by comparing the MCD intensity of the most intense feature in our spectrum to a purely paramagnetic tetrahedral Ni^{II} species (Ni^{II}-substituted rubredoxin) at comparable field (5T) and temperature (4.5K) in $\Delta\varepsilon$ ($M^{-1}cm^{-1}$). Qualitatively, our most intense feature occurs at 26 000 cm^{-1} with an intensity of ~1 $M^{-1}cm^{-1}$. In comparison, in the tetrahedral Ni^{II}-substituted rubredoxin MCD spectrum, the most intense feature at 23 000 cm^{-1} has an intensity of > 100 $M^{-1}cm^{-1}$.[31] Therefore, under the assumption that the paramagnetic species observed for Ni-NCC has a similar $\Delta\varepsilon$ value, this species represents approximately less than 1% of the overall sample.

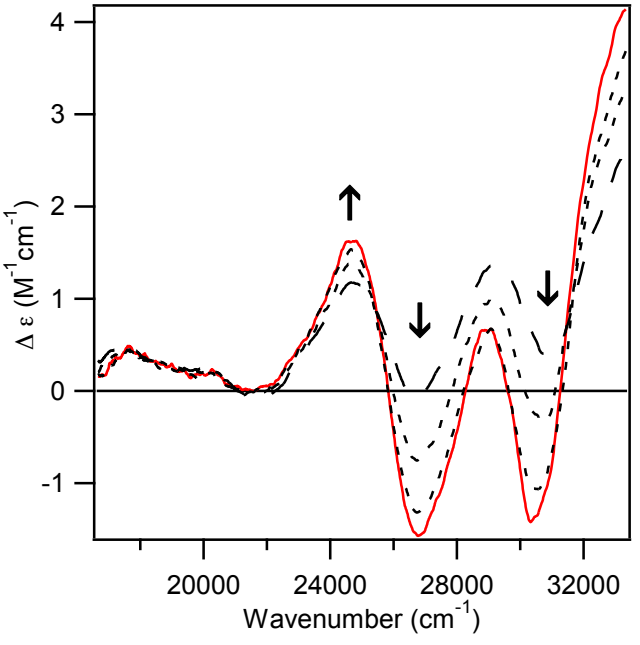

Figure 2.3. Variable temperature, 7 T MCD difference of Ni-NCC in a 34:66 solution of 50 mM borate:sucrose. Spectra show very little temperature dependence. (The solid red line represents data collected at 2 K, the dotted spectra were collected at 4.5 K and 8 K and the dashed line represents data collected at 15 K.)

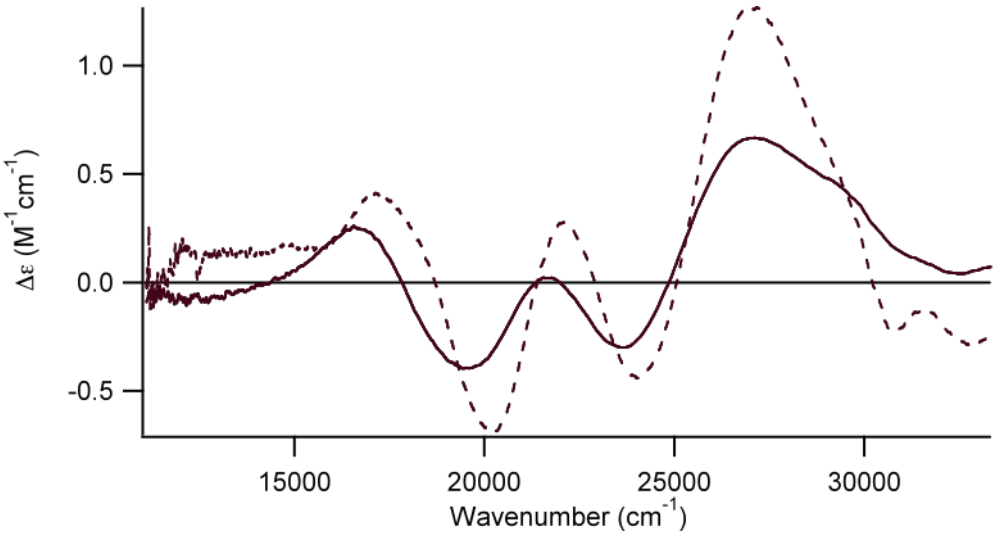

Figure 2.4. Room- and low-temperature CD spectra. The 4.5 K and 298 K spectra are represented as dashed and solid lines, respectively.

Based on the data presented above, nickel is coordinated in a square planar 2N:2S geometry. In Ni-SOD, the thiolate ligands are *cis* and the nitrogen ligands include one amide and one amine.[33] Our current studies support a possible arrangement that parallels the coordination by Ni-SOD in which the two sulfur ligands are arranged *cis* and one nitrogen is derived from a backbone amide while the second is from the N-terminal amine (Figure 2.5). DFT computations[20] show that this proposed structure has the lowest total energy when compared with other potential structures with different nitrogen coordination environments and other *cis* and *trans* configurations (Table 2.3).

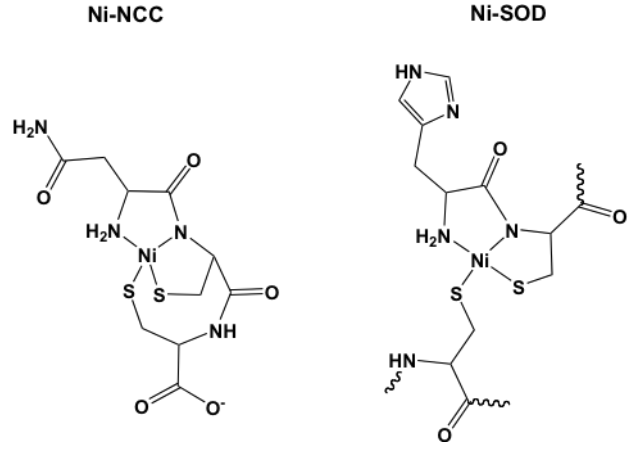

Figure 2.5. Metal coordination in Ni-SOD (right) and the proposed coordination in Ni-NCC (left). Wavy lines indicate the connection to the rest of the protein.

Table 2.3. Energies of converged structures of Ni-NCC in various conformations. The lowest energy conformation corresponds to Ni-NCC with *cis*-thiolates and the backbone amide and N-terminal amine nitrogens involved in coordination. Relative energies versus the lowest energy model (*cis*-proximal) are listed in kcal/mol. Nitrogen atoms are color coded to be consistent between models.

cis-proximal (0 kcal/mol) 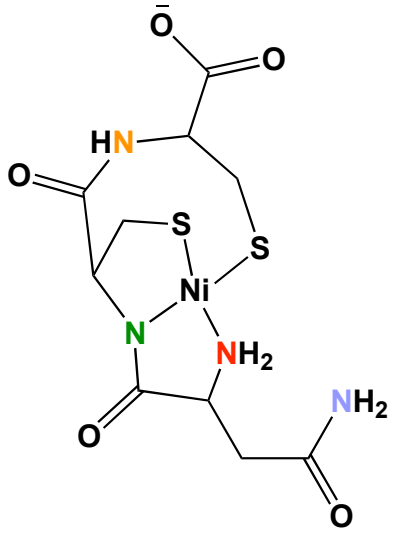	*trans*-mixed (+9.4 kcal/mol) 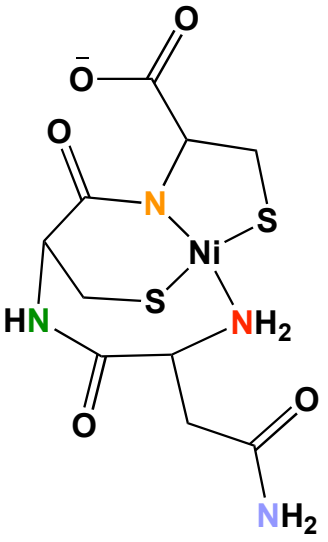
cis-distal (+23.6 kcal/mol) 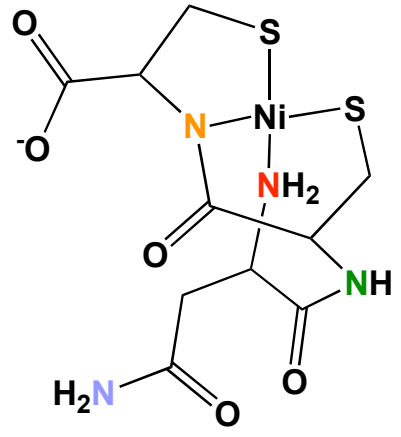	*trans-bis*-amide (+33.7 kcal/mol) 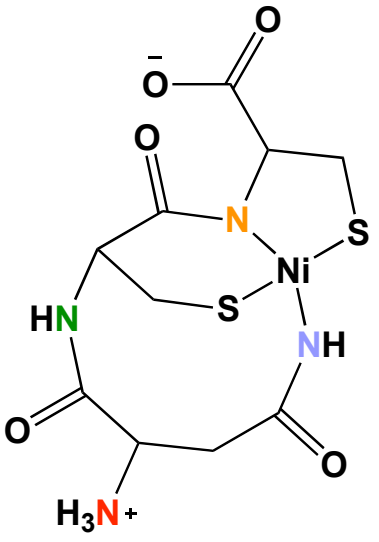

To probe whether or not the Asn side chain is involved in Ni^{II} coordination, the tripeptide GCC was synthesized and transmetallated. The observation that the Ni-GCC spectra parallel those of Ni-NCC supports the structure proposed above, where the Asn side chain is not ligated to the Ni^{II} center. GGNCC and GGGCC peptides were also synthesized to further examine the identity of the nitrogen ligands in Ni-NCC. The spectral features of the pentapeptides are similar to each other but differ from the tripeptides (Figure 2.6).

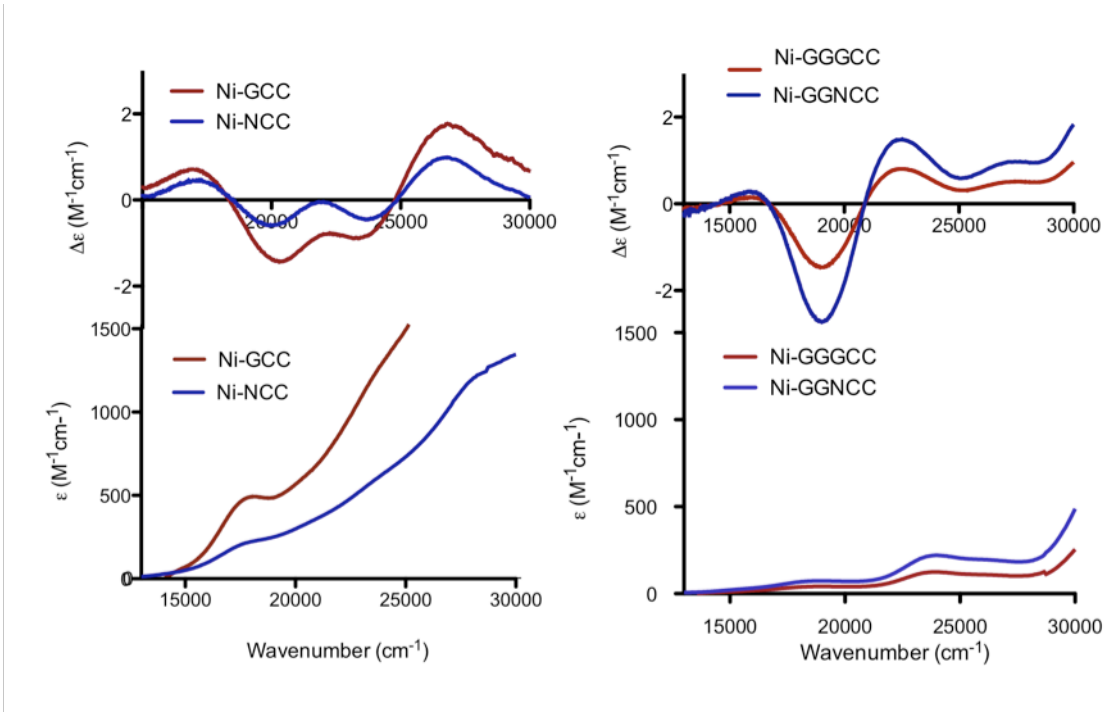

Figure 2.6. CD and absorption spectra of Ni-NCC, Ni-GCC, Ni-GGNCC, and Ni-GGGCC in 50 mM borate, pH 9.3. Differences in intensity reflect different abilities of the peptides to pick up metal, consequently altering concentrations of the overall metal-peptide species.

This suggests the N-terminal amine participates in metal coordination in the tripeptides. Presumably, the N-terminal amine in the pentapeptides is too far removed from the Ni^{II} center to act as a ligand and the backbone amide nitrogen from the Asn substitutes for the terminal amine nitrogen to accomplish metal binding. Additionally, it is thought that mixed amine/amide coordination species are more stable to oxygenation than *bis*-amide species,[15] and the observation

that Ni-NCC does not experience oxidation of the S ligands is further evidence for the proposed mixed amine/amide coordination. Similarities in the chemistry (*vide infra*) support the use of Ni-NCC as a model system for understanding the catalytic mechanism of Ni-SOD.

Because the studies above demonstrate that Ni-NCC serves as a reasonable structural mimic of Ni-SOD, the midpoint potential of Ni-NCC was measured using cyclic voltammetry (CV). CV data show electron transfer is quasi-reversible, with a midpoint potential of 0.72(2) V versus Ag/AgCl (Figure 2.7), which is similar to the 0.70(2) V measured for a peptide mimic based on the sequence of the parent enzyme with mixed amine/amide coordination and *cis* ligation [Ni(SOD)^{M1}].[17] Ni-SOD has a midpoint potential of 0.290 V (NHE, 0.093 versus Ag/AgCl).[10] The quasi-reversibility of the CV data indicate structural changes upon oxidation/reduction, which is rationalized in terms of the different geometries preferred by Ni^{II} and Ni^{III} centers.

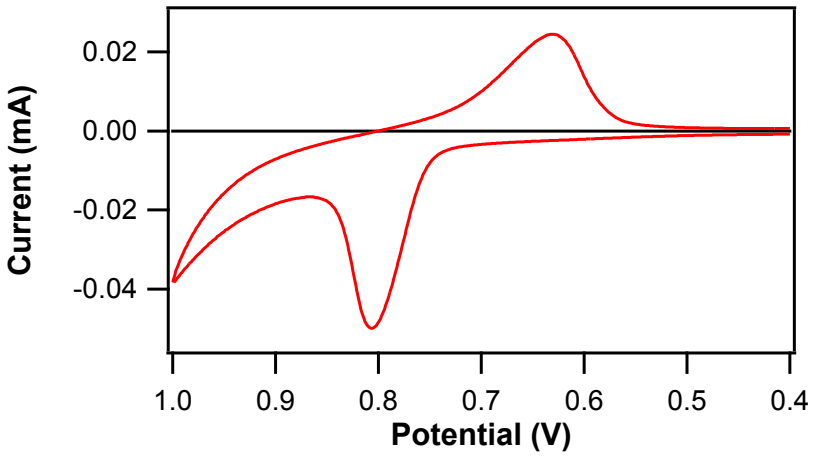

Figure 2.7. CV of Ni-NCC in 50 mM borate, pH 9.3, with a scan rate of 0.2 V per second. Electrochemically, the system is quasi-reversible (E_m= 0.72(2) versus Ag/AgCl.)

To confirm that electron transfer does not alter the peptide and that the measured potential specifically reflects a change at the nickel ion, ESI-MS was collected after performing bulk electrolysis. The mass is the same before and after undergoing oxidation, implying the

peptide is unaltered. Therefore, the redox potential measured corresponds to the Ni^{II}/Ni^{III} redox couple. Because the midpoint potential of the Ni-NCC complex falls between the reduction and oxidation potentials for superoxide, the ability of Ni-NCC to dismutate the reactive superoxide species was examined.

A standard SOD activity assay using xanthine oxidase was performed.[32,35] The data show that Ni-NCC does exhibit SOD activity, but it is slower than Ni-SOD. The IC_{50} for Ni-NCC (4.1 ± 0.8 x 10^{-5} M; Figure 2.8) is comparable to those values reported for other peptide mimics, particularly the maquette with *bis*-amide nitrogen coordination (3 x 10^{-5} M).[18]

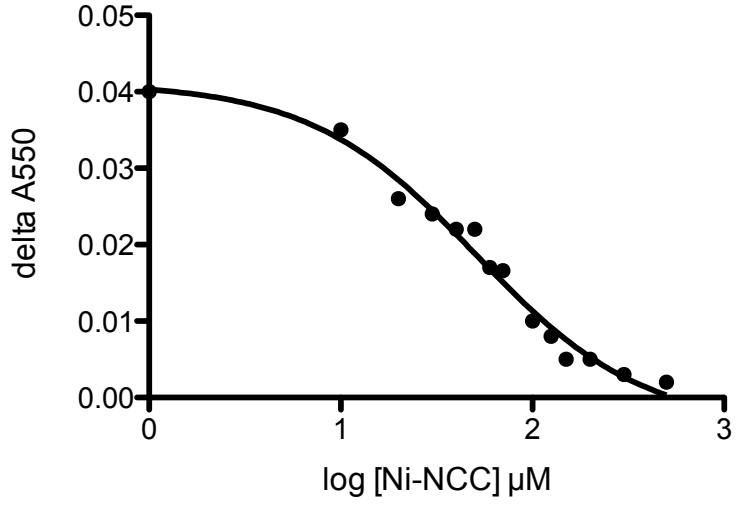

Figure 2.8. Representative IC_{50} plot for Ni-NCC in the xanthine/xanthine oxidase SOD activity assay.

Because the reduction potential of Ni-NCC is similar to that of [$Ni(SOD^{M1}$], but the activity of Ni-NCC is lower than this amine/amide maquette (2.1 x 10^{-7} M),[18] the rate may be decreased by the absence of a fifth ligand in the Ni-NCC complex. For Ni-SOD, it has been suggested that the axial imidazole ligand tunes the redox properties of the Ni^{III} species to be appropriate for superoxide dismutation.[19,33] In follow-up studies to be presented elsewhere, examination of the system in the presence of anions showed that Ni-NCC coordinates a transient, anionic fifth ligand, further supporting its similarity to Ni-SOD.

Ni-NCC exhibits similar features to Ni-SOD, and its midpoint potential and ability to break down superoxide support its use as a mimic of the enzyme. The sequence of this novel peptide mimic is unrelated to that of Ni-SOD and provides a complementary system for understanding how the identity and geometry of the supporting ligands influence not only the reduction potential but functional electron transport.

2.3. References

(1) Bryngelson, P. A.; Maroney, M. J. *Met. Ions Life Sci.* **2007**, *2*, 417-443.

(2) Miller, A.-F. *Curr. Opin. Chem. Biol.* **2004**, *8*, 162-168.

(3) Youn, H.-D.; Kim, E.-J.; Roe, J.-H.; Hah, Y. C.; Kang, S.-O. *Biochem. J.* **1996**, *318*, 889-896.

(4) Youn, H.-D.; Youn, H.; Lee, J.-W.; Yim, Y.-I.; Lee, J. K.; Hah, Y. C.; Kang, S.-O. *Arch. Biochem. Biophys.* **1996**, *334*, 341-348.

(5) Szilagyi, R. K.; Bryngelson, P. A.; Maroney, M. J.; Hedman, B.; Hodgson, K. O.; Solomon, E. I. *J. Am. Chem. Soc.* **2004**, *126*, 3018-3019.

(6) Wuerges, J.; Lee, J.-W.; Yim, Y.-I.; Yim, H.-S.; Kang, S.-O.; Carugo, K. D. *Proc. Natl. Acad. Sci. U.S.A.* **2004**, *101*, 8569-8574.

(7) Barondeau, D. P.; Kassmann, C. J.; Bruns, C. K.; Tainer, J. A.; Getzoff, E. D. *Biochemistry* **2004**, *43*, 8038-8047.

(8) Choudhury, S. B.; Lee, J.-W.; Davidson, G.; Yim, Y.-I.; Bose, K.; Sharma, M. L.; Kang, S.-O.;Cabelli, D. E.; Maroney, M. J. *Biochemistry* **1999**, *38*, 3744-3752.

(9) Bryngelson, P. A.; Arobo, S. E.; Pinkham, J. L.; Cabelli, D. E.; Maroney, M. J. *J. Am. Chem. Soc.* **2004**, *126*, 460-461.

(10) Herbst, R. W.; Guce, A.; Bryngelson, P. A.; Higgins, K. A.; Ryan, K. C.; Cabelli, D. E.; Garman, S. C.; Maroney, M. J. *Biochemistry* **2009**, *48*, 3354-3369.

(11) Gale, E. M.; Patra, A. K.; Harrop, T. C. *Inorg. Chem.* **2009**, *48*, 5620-5622.

(12) Schmidt, M.; Zahn, S.; Carella, M.; Ohlenschlaeger, O.; Goerlach, M.; Kothe, E.; Weston, J. *ChemBioChem* **2008**, *9*, 2135-2146.

(13) Tietze, D.; Breitzke, H.; Imhof, D.; Koeth, E.; Weston, J.; Buntkowsky, G. *Chem.--Eur. J.* **2009**, *15*, 517-523.

(14) Ma, H.; Chattopadhyay, S.; Petersen, J. L.; Jensen, M. P. *Inorg. Chem.* **2008**, *47*, 7966-7968.

(15) Shearer, J.; Zhao, N. *Inorg. Chem.* **2006**, *45*, 9637-9639.

(16) Stibrany, R. T.; Fox, S.; Bharadwaj, P. K.; Schugar, H. J.; Potenza, J. A. *Inorg. Chem.* **2005**, *44*, 8234-8242.

(17) Shearer, J.; Long, L. M. *Inorg. Chem.* **2006**, *45*, 2358-2360.

(18) Neupane, K. P.; Shearer, J. *Inorg. Chem.* **2006**, *45*, 10552-10566.

(19) Neupane, K. P.; Gearty, K.; Francis, A.; Shearer, J. *J. Am. Chem. Soc.* **2007**, *129*, 14605-14618.

(20) Neese, F. University of Bonn, **2009**.

(21) Becke, A. D. *J. Chem. Phys.* **1986**, *84*, 4524-4529.

(22) Perdew, J. P. *Physical Review B* **1986**, *33*, 8822-8824.

(23) Schäfer, A.; Horn, H.; Ahlrichs, R. *J. Chem. Phys.* **1992**, *97*, 2571-2577.

(24) Schäfer, G.; Huber, C.; Ahlrichs, R. *J. Chem. Phys.* **1994**, *100*, 5829-5835.

(25) Neese, F. *J. Comput. Chem.* **2003**, *24*, 1740-1747.

(26) Sinnecker, S.; Rajendran, A.; Klamt, A.; M., D.; Neese, F. *J. Phys. Chem. A* **2006**, *110*, 2235-2245.

(27) Becke, A. D. *J. Chem. Phys.* **1993**, *98*, 5648-5652.

(28) Becke, A. D. *J. Chem. Phys.* **1993**, *98*, 1372-1377.

(29) Dunning, T. H., Jr. *J. Chem. Phys.* **1989**, *90*, 1007-1023.

(30) Zoroddu, M. A.; Schinocca, L.; Kowalik-Jankowska, T.; Kozlowski, H.; Salnikow, K.; Costa, M. *Environ Health Perspect* **2002**, *110*, 719-723.

(31) Kowal, A. T.; Zambrano, I. C.; Moura, I.; Moura, J. J. G.; LeGall, J.; Johnson, M. K.*Inorg. Chem.* **1987**, *27*, 1162-1166.

(32) Crapo, J. D.; McCord, J. M.; Fridovich, I. *Methods Enzymol.* **1978**, *53*, 382-393.

(33) Fiedler, A. T.; Bryngelson, P. A.; Maroney, M. J.; Brunold, T. C. *J. Am. Chem. Soc.* **2005**, *127*, 5449-5462.

(34) A minor paramagnetic component is observed that represents less than 1% of the sample. The presence of this component has complicated 1H-NMR experiments.

(35) Tabbi, G.; Driessen, W. L.; Reedijk, J.; Bonomo, R. P.; Veldman, N.; Spek, A. L. *Inorg. Chem.* **1997**, *36*, 1168-1175.

Chapter 3: MAPping the Chiral Inversion and Structural Transformation of a Metal-Tripeptide Complex having Ni-SOD Activity

Reproduced with permission from:

Krause, M.E.; Glass, A.M.; Jackson, T.A.; Laurence, J.S. MAPping the Chiral Inversion and Structural Transformation of a Metal-Tripeptide Complex Having Ni-Superoxide Dismutase Activity, *Inorg. Chem.* **2011**, *50*, 2479-2487.

The metal abstraction peptide (MAP) is a tripeptide, here with the sequence Asn-Cys-Cys (NCC).[1] A reaction with IMAC resin-chelated nickel allows this NCC peptide to react with and abstract the metal, resulting in a high affinity Ni-peptide complex at neutral pH. The nickel-bound peptide, Ni-NCC, contains a diamagnetic Ni^{II} center bound in square planar geometry (Figure 3.1) with 2N:2S coordination.[1] Computational analysis determined the structure of Ni-NCC has mixed amine/amide nitrogen coordination and *cis* deprotonated thiolates. This coordination is very similar to that of Ni in the enzyme nickel superoxide dismutase (Ni-SOD), which consists of two cysteinate sulfurs (Cys2 and Cys6) arranged *cis* to one another, the N-terminal amine, and the deprotonated amide nitrogen from the peptide backbone of Cys2.[2-4] When bound to nickel, the tripeptide acts a functional mimic of the enzyme nickel superoxide dismutase.[1] The reaction catalyzed by Ni-SOD is unusual as it employs oxidation-prone thiolate ligands to bind the redox-active Ni ion. Metal-centered redox cycling between the Ni^{II} and Ni^{III} states is necessary to afford Ni-SOD activity. Coordination of the metal ion in the protein shifts between square planar (Ni^{II}) and square pyramidal (Ni^{III}) and leaves one face of the Ni ion open to solvent or substrate binding and enzymatic turnover. Complementary studies of the spectroscopic properties and reactivities of maquettes derived from a sequence of Ni-SOD have provided additional insights into the structure and mechanism of Ni-SOD.[5-9]

Our previous studies allowed the determination of ligands to the metal and the overall geometry of the Ni-NCC complex; however, a stability study has further revealed that the metal-tripeptide complex undergoes chiral inversion in a site-specific manner. (Jennifer Ann Stowell Laurence, Mary Elizabeth Krause, Timothy A. Jackson. SITE-SPECIFIC CHIRAL INVERSION OF THE AMINO ACIDS.Provisional Patent Application USPTO 61/432,231. Filed January 13, 2011.) This modification is distinctive, as chiral inversion is not often observed in proteins, and the structural change that occurs in this complex is both site and structurally specific. This chiral change has not been reported to occur in Ni-SOD or in small peptide maquettes derived from the N-terminal sequence, which contains the metal-binding loop. Amino acids and dipeptides are known to undergo base-catalyzed racemization at the chiral α-carbon as a result of metal chelation, but inversion is typically accomplished over several hours at highly elevated temperature (>90 °C) and basic pH (>9).[10-14] Studies performed on metal-amino acid chelates in deuterated solvent reveal that approximately an equal proportion of L and D isomers are generated during such reflux reactions in the absence of strong conformational influences. Because of the need for such extreme conditions, this type of reaction is not relevant to proteins expressed and purified using the typical range of conditions.

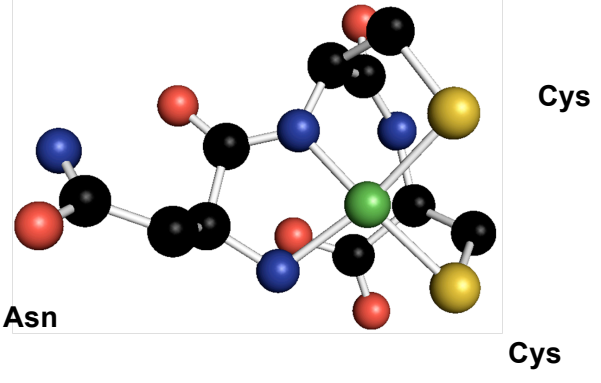

Figure 3.1. Chemical structure of Ni-NCC showing the square planar arrangement of 2N:2S coordination around the nickel ion.

The D amino acids that have been observed in proteins and peptides often impart significant differences in biological function to the chiral peptide and protein variants; while some act as inhibitors, others act as activators.[15] The introduction of a D amino acid alters the structure of the peptide or protein,[16] which can in turn influence the biological activity of the parent peptide.[17,18] Conversely, chiral mutagenesis of proteins has been shown to stabilize certain proteins, including insulin.[19] All naturally occurring, biosynthetic peptides and proteins that contain D amino acids are first generated entirely from L amino acids, and the inversion occurs as a post-translational modification.

Three major methods of incorporation of D amino acids have been reported, and the majority of D amino acids are found within three amino acids of the N- or C-terminus. First, if the placement of the D amino acid is intentional, it is enzyme catalyzed by amino acid racemases.[15] While most of these racemases employ a pyridoxalphosphate cofactor and proceed through a Schiff-base intermediate, some are thought to follow a different mechanism that does not require this cofactor. Reported examples of known enzyme-catalyzed epimerization include an enzyme from the venom of the funnel web spider that catalyzes the conversion of Ser-46 to D-Ser 46 within a 48 residue peptide (ω-agatoxin IV),[15,18] an enzyme isolated from the skin of a frog (*Bombina*) that incorporates a D-amino acid into the second position of the substrate,[15,20] and a mammalian enzyme from platypus venom that has specific, but not completely known, substrate requirements.[21]

The only other reports of D amino acids in mammalian proteins are in aged tissues, and these aging proteins have been shown to contain D amino acids, largely at aspartic acid residues, which are prone to racemization.[15,22] Examples of proteins and peptides containing D-Asp from this type of reaction include human lens alpha A-crystallin,[23] human lens alpha B-crystallin,[24] and beta-amyloid protein in the brain.[25] The presence of the D-Asp influences the behavior of the

peptide and its effect on neurodegeneration in Alzheimer's patients.[26] These spontaneous inversions of chirality arise from a mechanism involving cyclization and hydrolysis reactions, where the nearby environment of the protein helps initiate and drive the conversion.[22]

The mechanisms described above are reversible reactions, but conversion of an amino acid from L to D chirality within proteins has also been reported to proceed via a free radical reaction, in which cysteine residues are involved in the electron transfer.[27] These reactions are light-driven and unidirectional. The cysteinyl radical is generated by intense UV light and subsequently abstracts hydrogen from a surrounding amino acid, leading to epimerization.[27-30] The selectivity determining where the reaction occurs is controlled by the secondary structure of the peptide or protein, leading to a variety of different products, depending on the context.[28]

Despite the limited number of examples of site-specific L to D conversions that have been reported, the literature reveals that diverse mechanisms are used to accomplish chiral inversion. To our knowledge, we report here the first site-specific chiral inversion of amino acids that depends on metal binding. The reaction proceeds at room temperature and near neutral pH in aqueous solution over the course of hours. While NCC was synthesized to contain all L amino acids, conversion to the D-containing form occurs after complexation with nickel, and the reaction results in inversion at two positions to produce the stable DLD-NCC-metal complex. The resulting DLD-peptide-metal complex is very stable in aqueous solution, and DFT calculations indicate that the change in chirality produces a large increase in thermodynamic stability.

3.1. Experimental

3.1.1. Generation of metal-peptide complexes: The peptides NCC, GCC, and NCC with a D-cysteine in the middle position [LDL-NCC] were purchased from Genscript Corporation

(Piscatway, NJ, USA). The NCC peptides with a D-cysteine in the third position [LLD-NCC] and with both D-asparagine in the first position and D-cysteine in the third position [DLD-NCC] were purchased from Neo-Peptide (Cambridge, MA, USA). Nickel-peptide complexes were generated in aqueous, argon-sparged solutions at neutral to basic pH. Incubation of the peptide for approximately 30 minutes with immobilized metal affinity chromatography (IMAC) resin (GE Healthcare) charged with nickel ensures a clean reaction with no undesired side products and no free metal ions in solution, yielding a reddish-brown complex, varying slightly by the identity of the peptide. Aged Ni-NCC samples were allowed to age for >40 days.

3.1.2. CD and absorption studies: A 1.5 mM solution of Ni-NCC was prepared in 50 mM potassium phosphate, pH 7.4. Immediately after incubation, samples were placed in a cuvette with a 1-cm path length and scanned from 800-300 nm using both absorption and CD spectroscopy. Samples were aged and monitored at various time points over the course of several days. Background scans of buffer alone were subtracted from each scan. Absorption studies were performed on an Agilent 8453 UV/Visible spectrophotometer. Circular dichroism analysis was performed on a J-815 (Jasco Corporation) spectropolarimeter. The CD data presented represent the average of at least five scans. To accurately control the time frame of Ni-NCC aging for activity assays, the complex also was formed in solution upon addition of one equivalent of $NiSO_4$.

3.1.3. MCD experiments: Samples of Ni-NCC were prepared in 50 mM potassium phosphate buffer at pH 7.4 sparged with argon. Solid sucrose was added as a glassing agent and the mixture was heated to form a saturated solution. CD spectra of sucrose-saturated samples demonstrated

no significant changes in features compared with samples lacking sucrose, indicating that this procedure did not perturb the structures of the Ni-NCC complex. The samples were placed in an MCD cell and flash frozen in liquid N_2. Spectra were collected by A. Glass on a J-815 (Jasco Corporation) spectropolarimeter interfaced with a magnetocryostat (Oxford Spectromag 4000-8). To remove contributions from CD signals, MCD data reported herein represent difference spectra of accumulations at +7 and -7 T. Because the signal intensities from paramagnetic species display inverse temperature dependence, spectra were collected at several temperatures.

3.1.4. Deconvolution of CD and absorption data: Deconvolution of CD and absorption data was performed using Igor Pro (Wavemetrics). Iterative Gaussian deconvolutions were performed with a constant peak width of 1650 cm^{-1}. Absorption band energies were kept within 10% of the corresponding CD bands due to the broad nature of the absorption spectrum.

3.1.5. ESI-MS: Samples were diluted 100x in a 1:1 mixture of methanol/water and analyzed on an LCT Premier (Waters Corporation) operating in negative ion mode, as described previously.[1]

3.1.6. Deuterium exchange: A solution of 50 mM potassium phosphate was prepared in D_2O and adjusted with NaOD and DCl to a pD of 7.4. Samples of 1.5 mM NCC and GCC were prepared in this solution. Metallation was performed as described above. After removal of the solid resin, 10 μL of the sample was back-exchanged into one mL of a 1:1 water/methanol mixture and analyzed using ESI-MS operating in negative ion mode. The original samples were then incubated for 24 hours and analyzed in the same manner.

3.1.7.Electrochemistry: Electrochemical data were collected as previously described.[1] A 3-mL sample of 3 mM Ni-NCC was prepared in 50 mM sodium borate at pH 10. CV data were collected with a CH1812C Electrochemical Analyzer potentiostat (CH Instruments) with a three-electrode setup (platinum working electrode, Bioanalytical Systems, Inc.; Pt auxiliary electrode; Ag/AgCl reference electrode) in a glass CV cell. Potential was applied from zero to 1.2 V with a scan rate of 0.2 V per second, and current was measured. The same experiment was attempted on a 3 mM Ni-NCC sample in 50 mM potassium phosphate at the same pH. The sample was incubated for 24 hours and analyzed again.

3.1.8. Coordination of cyanide and IR analysis: Samples of Ni-NCC were prepared at a concentration of 3 mM in 50 mM sodium borate at pH 10 and 50 mM potassium phosphate at pH 7.4. A sample of Ni-NCC in phosphate buffer was incubated for 24 hours. One equivalent of potassium cyanide was added to each of the three Ni-NCC samples. Samples were flash frozen and lyophilized. IR analysis was performed to observe the cyanide peak in each sample. IR spectra were acquired from dry powder samples on a Perkin Elmer Spectrum 100 FT-IR spectrometer equipped with a universal ATR (Attenuated Total Reflection) sampling accessory. The spectrum of solid potassium cyanide was used to compare the shift of $\nu(C\equiv N)$ vibration from the free to the nickel-coordinated state.

3.1.9. Computations: Spin-restricted density functional theory (DFT) computations were performed by A. Glass using ORCA 2.8.0[31] and employed the conductor-like screening model (COSMO)[32] with an epsilon value of 80 to approximate water. Geometry optimizations used the BP86 functional[33,34] and the aug-TZVP basis set (a triple-zeta basis set with diffuse and polarization functions).[35,36] Because these computations employed the resolution of identity (RI)

approximation,[37] the TZV/J auxiliary basis set was also used. Single point and time-dependent DFT (TD-DFT) computations used the B3LYP[38-40] functional and the aug-TZVP basis set. In order to evaluate if the inclusion of explicit water molecules H-bonded to charged groups gave rise to geometries markedly different than those obtained using COSMO, a water molecule was added to hydrogen bond with the C-terminal carboxylate in the LLL, DLD, and DDL models of Ni-NCC. Because differences in bond lengths of less than 0.015 Å were observed, we reasonably conclude that the use of COSMO is sufficient to account for major solvation effects in this system.

3.1.10. Ni-SOD xanthine/xanthine oxidase coupled assay: Ni-SOD activity was determined as reported previously,[1] except Ni-NCC was generated *in situ* using one equivalent $NiSO_4$. Ni-NCC was aged for 0 – 120 minutes, and the Ni-SOD activity was determined using the standard xanthine/xanthine oxidase method developed by Crapo and coworkers.[41] All reagents were generated in 50 mM potassium phosphate, 100 μM EDTA reaction buffer at pH 7.8 except for Ni-NCC, which was generated in 50 mM potassium phosphate, pH 7.4. In this assay, 600 μM cytochrome c from bovine heart (Sigma), 300 μM xanthine (Sigma) and enough xanthine oxidase from buttermilk (Sigma) to cause a change in absorbance at 550 nm of 0.02 – 0.04 AU per minute were added to a final volume of 300 μL in reaction buffer. The change in absorbance at 550 nm was monitored on a Cary 100 UV-Visible spectrophotometer (Varian). The assay was performed with 100 μM Ni-NCC. Time points and assays on the D-containing peptide were performed by A. Glass.

3.2. Results

3.2.1. Preparation and spectroscopic characterization of Ni-NCC

As previously reported, metal incorporation into the described complex is most efficiently accomplished via metallation.[1] Peptides were incubated with IMAC resin in either 50 mM potassium phosphate buffer at pH 7.4 or in 50 mM sodium borate at pH 10. Absorption and CD spectroscopies were utilized to characterize the Ni-NCC complex. Studies have shown that pH, ionic strength, and concentration of the metal-peptide complex do not change the spectral features of the system;[1] however, these studies show that the initial spectra differ between buffer systems (Figure 3.2) but later converge to a common final state. pH is not a factor in the differences between spectra, as Ni-NCC samples analyzed in phosphate buffer at pH 10 directly after incubation exhibit the same spectral features as those in phosphate buffer at pH 7.4.

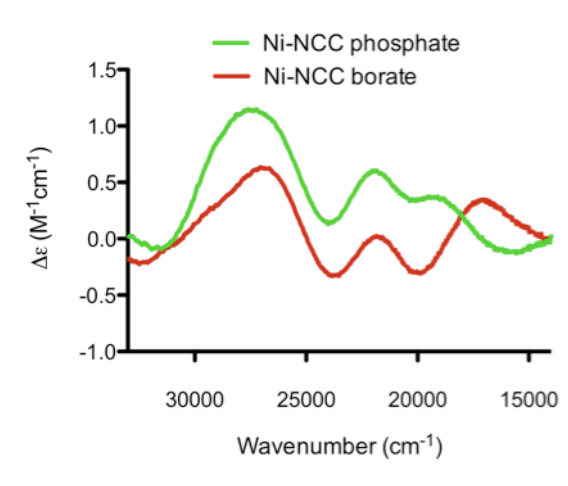

Figure 3.2. CD spectral features of Ni-NCC in different buffer systems. (Green=phosphate at pH 7.4, Red = borate at pH 10.0).

Over time, however, the spectral features of Ni-NCC in phosphate buffer change to resemble those in borate buffer, suggesting rearrangement to a more stable structure occurs. Although samples were prepared in sparged solutions, no further precautions were taken to avoid

oxygen dissolution during aging. To ensure complete conversion, a Ni-NCC sample in phosphate buffer was aged in air for up to 90 days and analyzed again (Figure 3.3). ESI-MS of the Ni-NCC complex in various conditions demonstrated that the peptide mass does not change with the changes in spectral features (m/z = 392.98), indicating a lack of oxidation of thiolate ligands. Varied pH did not affect the overall rate of the aging process (Figure 3.4). This suggests that the changes observed in the CD are due to more subtle changes about the metal center. A Ni-GCC sample was examined in the same manner to evaluate the influence of the chirality at the first position. Although the spectral changes for the two complexes are not identical, a similar perturbation of CD signals was observed for Ni-GCC over a comparable time frame (data not shown).

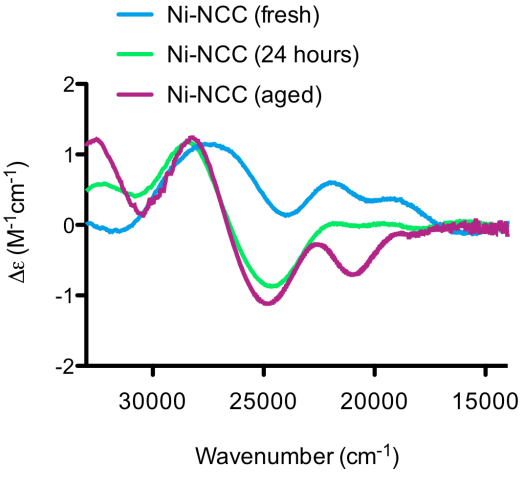

Figure 3.3. Aging progression of Ni-NCC in phosphate. (Blue = fresh, Green = 24 hours, Pink = aged).

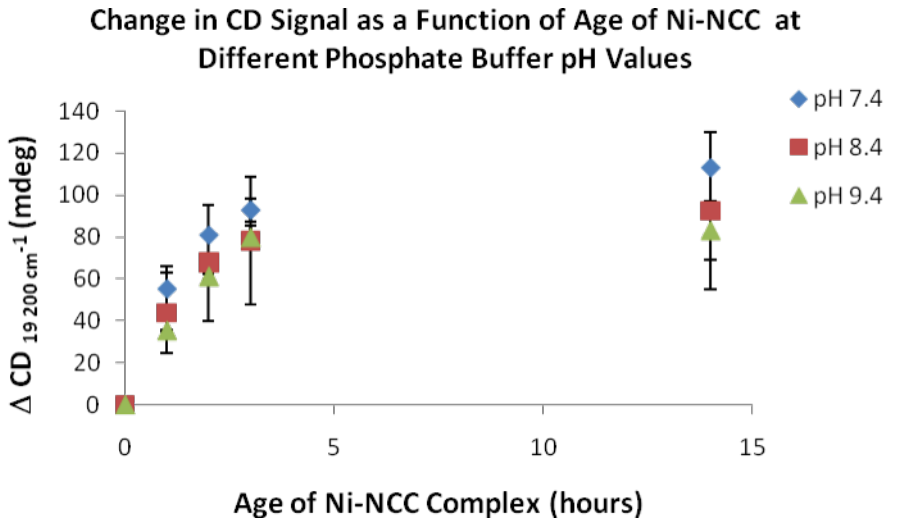

Figure 3.4. Change in CD spectrum at 19 200 cm^{-1} as Ni-NCC ages at pH 7.4, 8.4, and 9.4 in 50 mM phosphate buffer. Data represents the average of two experiments, and error bars are the standard deviation of those two experiments. *Data collected by A. Glass.*

3.2.2. Spectral deconvolutions

In contrast to the changes in the CD spectra of Ni-NCC, absorption spectra of Ni-NCC freshly prepared in phosphate buffer and that same sample aged for 40 days appear nearly identical (Figure 3.5a). Both feature a broad envelope centered at 21 000 cm^{-1}(ε = 210 $M^{-1}cm^{-1}$) with a higher energy feature at 29 000 cm^{-1} (ε = 1400 $M^{-1}cm^{-1}$). These data are consistent with both species having a four-coordinate Ni^{II} center in an 2N:2S square planar geometry.[1]To quantitatively evaluate the CD spectral changes, spectral deconvolutions of these data were performed to determine the energies and signs of the electronic transitions (Figure 3.5b). Whereas freshly prepared Ni-NCC displays signals with positive sign at 18 900, 22 170, and 26 520 cm^{-1}, the spectrum of the aged sample shows negative bands at similar energies (Table 3.1). These transitions shift to slightly lower energies (Δ~200 – 900 cm^{-1}) with age. Bands 1 – 4 of freshly prepared Ni-NCC were previously assigned as *d-d* transitions[1] and their energies should be very sensitive to changes in geometry about the Ni^{II} center. The observation that the energies of these bands shift by < 900 cm^{-1} upon aging demonstrates that fresh and aged Ni-NCC have

nearly identical coordination environments. The major spectral perturbations are predominately due to changes in sign and intensity of CD features. These minor changes in the *d-d* transition energies (Table 3.1) along with the virtually identical absorption spectra (Figure 3.5a) of fresh and aged Ni-NCC demonstrate that the geometry and ligands of the Ni^{II} center are unaltered and that neither dimerization of the complex nor oxidation of the thiolate ligand occurs.

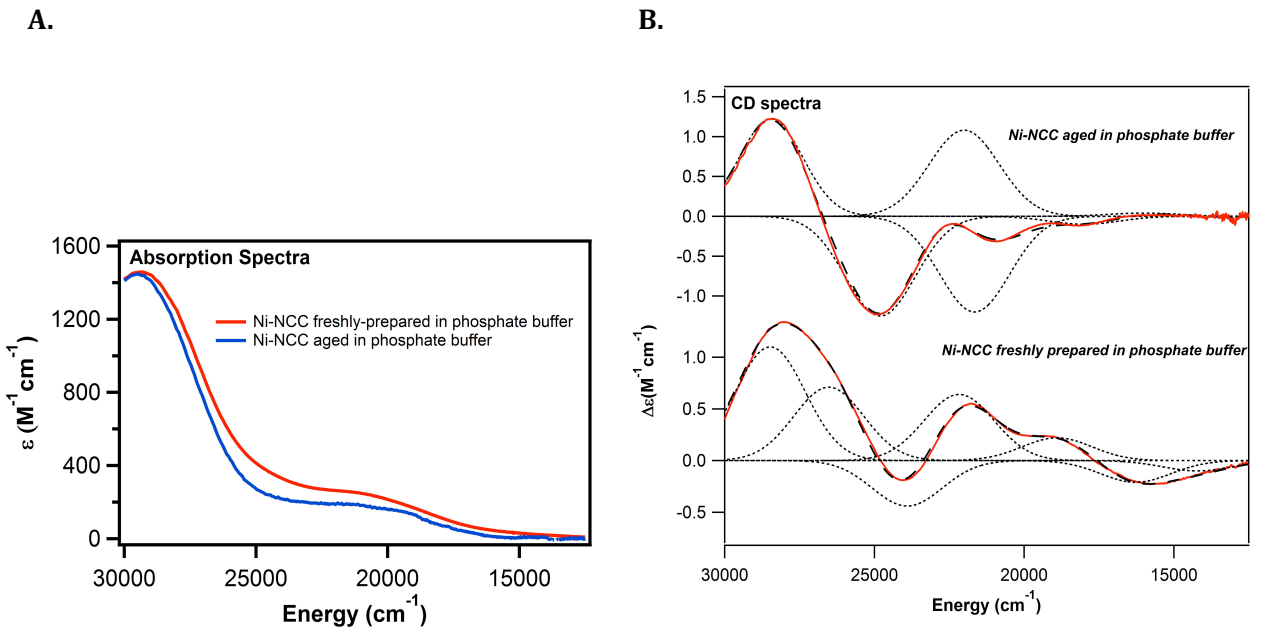

Figure 3. 5. **(a)** Electronic absorption spectra of freshly prepared (red) and aged (blue) Ni-NCC in 50 mM phosphate buffer at pH 7.4. **(b)** CD spectra of the same samples. Individual Gaussian curves (···) and their sums (---) obtained from fits of the CD data are displayed.

Table 3.1. Transition energies derived from Gaussian deconvoluted CD spectra of freshly prepared and aged Ni-NCC in phosphate buffer. Bands having opposite sign in the fresh and aged spectra are shown in bold.

Band	Freshly Prepared		Aged	
	$\Delta\varepsilon$ ($M^{-1}cm^{-1}$)	Energy (cm^{-1})	$\Delta\varepsilon$($M^{-1}cm^{-1}$)	Energy (cm^{-1})
1	-0.1	14200	[a]	[a]
2	**-0.21**	**16270**	**0.04**	**16000**
3	**0.22**	**18900**	**-0.1**	**18000**
4	**0.64**	**22170**	**-0.78**	**21600**
5	**-0.44**	**23900**	**0.7**	**22000**
6	**0.71**	**26520**	**-1.3**	**24800**
7	1.1	28475	1.22	28450

[a]The low signal-to-noise ratio between 11 000 and 14 000 cm^{-1} precludes reliable deconvolution within this spectral window.

3.2.3. Magnetic circular dichroism

To investigate whether a paramagnetic, tetrahedral intermediate is formed, magnetic CD (MCD) experiments were performed. Previous MCD experiments have shown that the primary Ni-NCC species in borate buffer at pH 10 is largely diamagnetic, although a minor paramagnetic (S=1) species was present.[1] Here, MCD experiments performed on a freshly prepared Ni-NCC sample demonstrated that the species initially present in phosphate buffer is also primarily diamagnetic; a minor paramagnetic component that accounts for less than 1% of the sample may reflect an intermediate state that does not accumulate (Figure 3.6). After aging, these temperature-dependent signals are no longer observed. Therefore, it can be concluded that aged Ni-NCC contains neither appreciable amounts of S = 1 Ni^{II} or S = 1/2 Ni^{III} centers. These data

collectively show that both fresh and aged Ni-NCC contain diamagnetic Ni^{II} centers in square planar geometries with nearly identical coordination spheres; the differences in spectral features and in reactivity between the freshly prepared and aged samples led to further investigation of the subtle changes in the Ni-NCC complex.

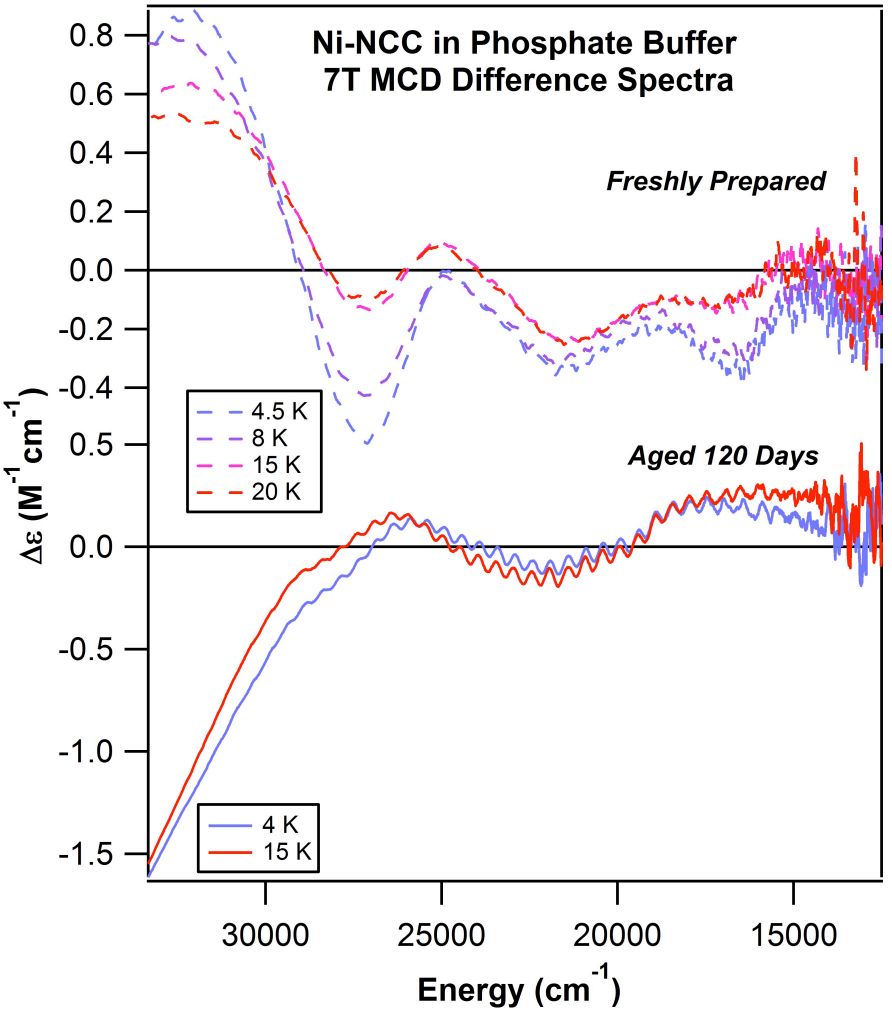

Figure 3.6. Low-temperature MCD spectra collected for freshly prepared Ni-NCC and aged Ni-NCC. (*Collected by A. Glass).*

3.2.4. Electrochemistry and reactivity of Ni-NCC

Previous electrochemical experiments have shown that Ni-NCC in borate buffer at pH 9.3 has a midpoint potential of 0.72 V (vs. Ag/AgCl).[1] When attempts to measure the midpoint potential of Ni-NCC in phosphate buffer at the same pH were made, the complex prepared in phosphate buffer did not exhibit a measurable potential; however, when the same sample was aged for 24 hours, the midpoint potential was comparable to that of the sample in borate buffer (0.71 V vs. Ag/Ag^{+}). Previous studies have shown that square planar geometries, for example peptide mimics of Ni-SOD, coordinate cyanide in an axial position, as determined by IR of the bound cyanide.[42] Similarly, IR experiments have demonstrated that Ni-NCC in borate buffer is capable of coordinating CN^- in the axial position, as a shift in the $\nu(C\equiv N)$ vibration occurs. The IR spectrum of Ni-NCC freshly prepared in phosphate buffer did not exhibit a peak corresponding to coordinated cyanide; however, addition of cyanide after aging the sample overnight generated the expected peak for the coordinated state (Table 3.2). These data lend support to a slow structural rearrangement that occurs over the course of hours, resulting in a structure that allows for the interaction of a fifth ligand with the Ni-NCC complex.

Table 3.2. IR data for cyanide coordinated to nickel.

Species	**$\nu(C\equiv N)$ (cm^{-1})**
NaCN	2088
$K_2[Ni(CN)_4]$[42]	2123
Ni(CN)-(mSOD)[42]	2108
Ni-NCC + CN^- borate	2109
Ni-NCC + CN^- phosphate (fresh)	N/A
Ni-NCC + CN^- phosphate (aged)	2107

3.2.5. Deuterium exchange

The flip in sign of CD signals suggests the structural change that allows for ligand binding may be due to chiral inversion. Because of this possibility, NCC was transmetallated with Ni-IMAC resin in buffers prepared in D_2O to determine if deuterium would be incorporated into the peptide at any non-exchangeable site. After back-exchanging the Ni-NCC into 1:1 water/methanol to preserve the integrity of the complex but remove any exchangeable deuterium atoms, ESI-MS demonstrated incorporation of deuterium into two non-exchangeable positions (392.98 vs. 394.99). ESI-MS of the same reaction performed in H_2O showed no difference in *m*/*z* over 24 hours. Because Ni-GCC shows a similar inversion of CD signals with time, but lacks chirality in the first position, Ni-GCC was also examined for deuterium exchange. Ni-GCC exhibited incorporation of deuterium into one non-exchangeable position, suggesting that the chirality of Asn in the first position and only one of the Cys is affected. This information was used to predict the possible location(s) of the incorporated deuterium atom(s).

3.2.6. Characterization of peptides containing D amino acids

The LDL-Ni-NCC, LLD-Ni-NCC, and DLD-Ni-NCC complexes were generated and each analyzed using absorption and CD spectroscopies and ESI-MS. All of the complexes exhibit the same mass profile (*m*/*z*=392.98) in ESI-MS, suggesting that each forms 1:1 complexes with the metal. To determine the chirality of the final, stable Ni-NCC arrangement, CD spectra of each D-containing peptide were compared to the data collected for the aged (>40 days) Ni-NCC sample in phosphate buffer. The DLD-Ni-NCC spectrum overlaid with the aged Ni-NCC spectrum shows parallel features (Figure 3.7). These data indicate chiral inversion occurs at the first and third position within Ni-NCC to generate the DLD-Ni-NCC complex.

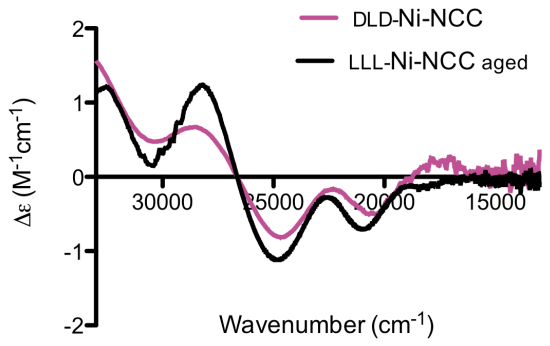

Figure 3.7. CD spectra of Ni-NCC aged in phosphate buffer (black) vs. DLD-Ni-NCC (purple).

Whereas the spectral features of DLD-Ni-NCC do not shift or lose intensity with time, the CD spectrum of LLD-Ni-NCC evolves over time to look like that of DLD-Ni-NCC (Figures 3.8 and 3.9). In contrast, the CD spectrum of aged LDL-Ni-NCC looks like the mirror image of that of DLD-Ni-NCC. When the freshly prepared peptides were reacted with cyanide, only DLD-Ni-NCC was able to immediately coordinate cyanide in the axial position, providing further evidence that the DLD-form is the arrangement that aged Ni-NCC reaches over time.

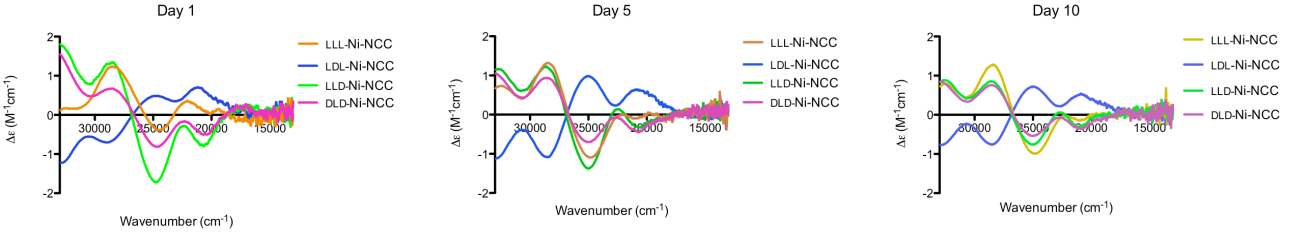

Figure 3.8. CD aging progression of various chiral versions of the Ni-NCC complex.
(Orange = LLL-NCC, Blue = LDL-Ni-NCC, Green = LLD-Ni-NCC, Pink = DLD-Ni-NCC.)

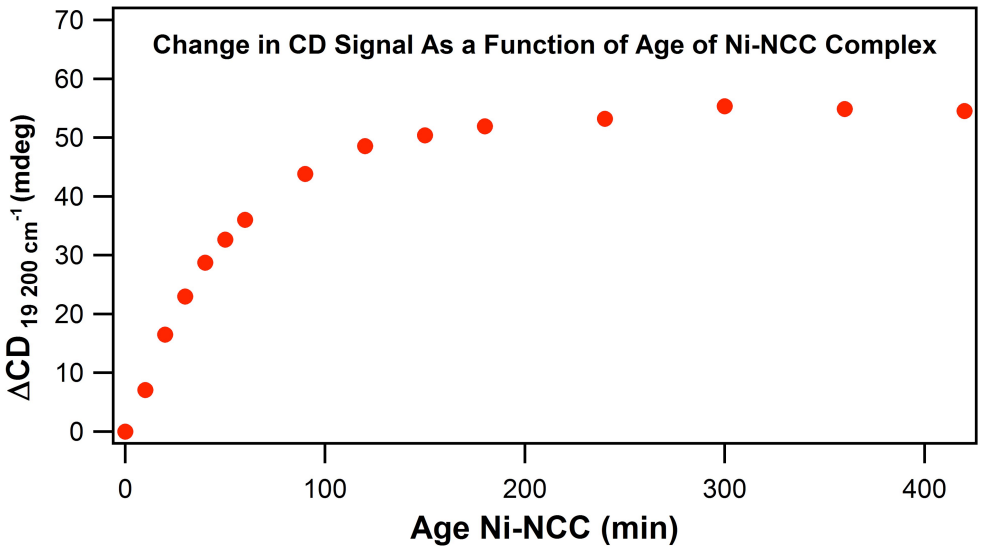

Figure 3.9. Change in CD signal at 19 200 cm^{-1} as Ni-NCC ages. *(Generated by A. Glass).*

3.2.7. DFT-Optimized Models and Computed Energies

Computations were performed on models of Ni-NCC to explore the structural and energetic changes associated with chiral inversion of the different amino acid residues in the tripeptide-Ni^{II} complex. These results are summarized in Table 3.3. In the optimized structure of LLL-Ni-NCC, the nickel(II) ion is bound in a near-square planar geometry (Figure 3.10). The coordination of the terminal amine, internal amide, and sulfur of Cys2 form two five-membered chelate rings that share a common edge. The sulfur of Cys3 coordinates *trans* to the amide nitrogen, which requires that the peptide wrap around the nickel center, thereby blocking one coordination site perpendicular to the square plane. The other open coordination site is partially blocked by the Asn side chain. These results suggest that the metal center may be sterically occluded in the LLL-peptide complex, explaining the lack of CN^- coordination observed in the freshly prepared samples described above.

The energies of Ni-NCC models with the chirality of different amino acids inverted show that inversion of Asn1 leads to a model (DLL-Ni-NCC) that is isoenergetic to that of LLL-Ni-NCC. In addition, the models in which Cys2 is inverted, LDL- and DDL-Ni-NCC, have an

energetic destabilization of ~5 kcal/mol when compared to LLL-Ni-NCC. In contrast, when Cys3 is inverted, as in LLD- and DLD-Ni-NCC, an energetic stabilization of ~11 kcal/mol is predicted. Investigation into the role of solvation on the total energy of the conformers shows that although DLD-Ni-NCC does have an overall stabilization with respect to LLL-Ni-NCC in solvation energy, the relief of steric strain of the loop containing Cys3 has a more pronounced effect on the total energy. These results for DLD-Ni-NCC agree with the experimental data described above (Figure 3.6). The inversion from LLL-Ni-NCC to DLD-Ni-NCC opens one face of the Ni^{II} ion to interact with exogenous ligands, consistent with the observation that aged Ni-NCC binds CN^-.

Table 3.3. Bond lengths (Å) and relative energies (kcal/mol) of DFT-optimized models of Ni^{II}-NCC with amino acids of differing chiralities.*Calculations performed by A. Glass.*

	LLL-Ni-NCC	DLL-Ni-NCC	LDL-Ni-NCC	LLD-Ni-NCC	DDL-Ni-NCC	DLD-Ni-NCC
$Ni\text{-}N_{amine}$	1.976	1.972	1.974	1.982	1.979	1.990
$Ni\text{-}N_{amide}$	1.890	1.856	1.867	1.866	1.866	1.887
$Ni\text{-}S_{cys2}$	2.222	2.184	2.165	2.179	2.164	2.196
$Ni\text{-}S_{cys3}$	2.161	2.199	2.199	2.221	2.199	2.238
Relative Energy	0.0	-0.3	4.7	-11.6	5.1	-11.1

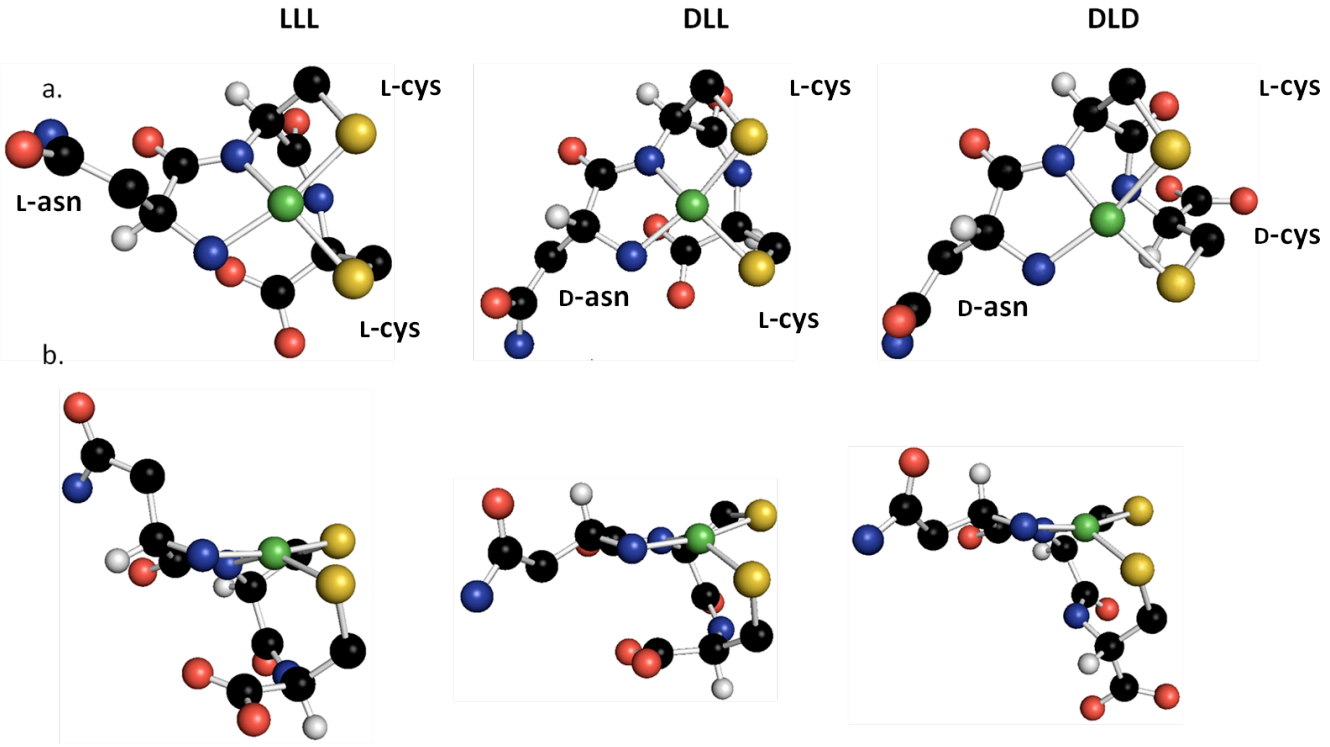

Figure 3.10. Energy-minimized structures of LLL-, DLL-, and DLD-Ni-NCC. The only hydrogen atoms shown are those attached to the C_α of the residues. Views perpendicular to the square plane (a) and in the plane (b) are shown. (*Figure generated by A. Glass)*

3.2.8. TD-DFT computations

TD-DFT computations were performed to determine if the structural differences between LLL-Ni-NCC and DLD-Ni-NCC can account for the experimentally observed red-shift in the Ni^{II}*d-d* transition energies upon aging of Ni-NCC. Because Ni-S bond lengths are frequently overestimated in DFT geometry-optimized models, it is expected that the predicted electronic transition energies for both Ni-NCC models will be computed at lower energy than experimentally observed. Nonetheless, this known shortcoming in DFT-computed Ni-S bond lengths[43] will not hinder the analysis performed here, as the focus is on reproducing the relative shift in Ni^{II} *d-d* transitions between LLL-Ni-NCC and DLD-Ni-NCC. For an $S = 0$, d^8 metal ion in a square planar geometry, four *d-d* transitions are expected from excitation from each of the four doubly-occupied d orbitals to the unoccupied d_{x2-y2} orbital. The computed energies of these

transitions are shown in Table 3.4; corresponding spectra are shown in Figure 3.11. Relative to LLL-Ni-NCC, all calculated *d-d* transitions for DLD-Ni-NCC are red-shifted, consistent with the experimental observation. This shift in transition energies is directly related to the energy of the d_{x2-y2} orbital. In an idealized square planar geometry (*e.g.*, D_{4h} symmetry), the d_{x2-y2} orbital is the dominant σ* orbital and is significantly destabilized relative to the remaining four d orbitals. As the geometry is perturbed from this limit, other d orbitals take on partial σ* character. This leads to the d_{x2-y2} orbital being at a relatively lower energy and a red shift in *d-d* transitions. The nickel(II) coordination sphere in DLD-Ni-NCC is more distorted from square planar geometry than that of LLL-Ni-NCC, which gives rise to a smaller splitting between the Ni^{II} d orbitals (Figure 3.12) and thus red shifted *d-d* transitions.

Table3. 4. TD-DFT computed *d-d* transition energies (cm^{-1}) for Ni-NCC models.

Band	LLL	DDL	DLD
1	14 500	15 500	12 400
2	15 600	16 600	14 300
3	17 000	17 300	15 600
4	19 300	18 800	18 500

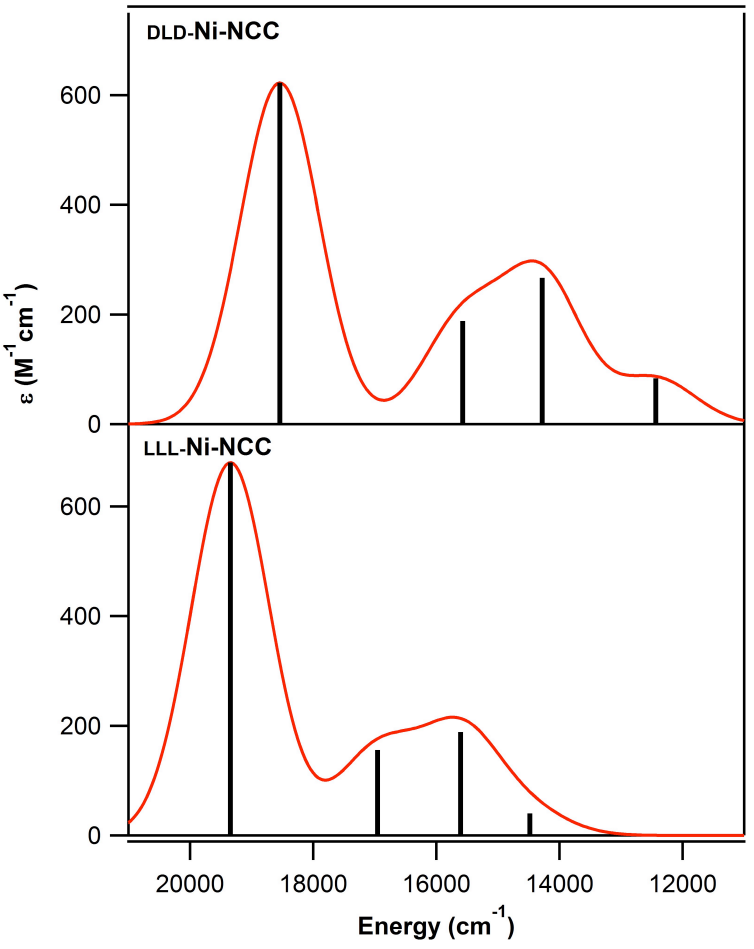

Figure 3.11. TD-DFT predicted absorption spectra of LLL-Ni-NCC (bottom) and DLD-Ni-NCC (top). Ni^{II} *d-d* transitions are marked with vertical lines. *Figure generated by A. Glass.*

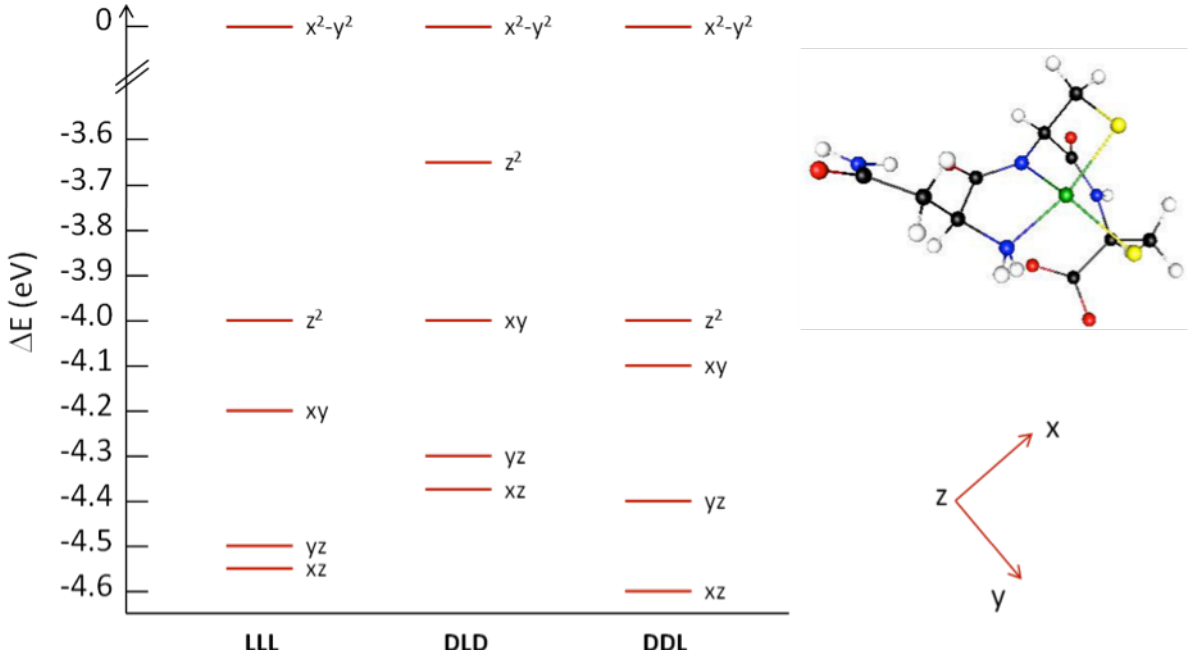

Figure 3.12. Ni^{II} *d* orbital energy level diagram for Ni-NCC models. A structural model of DLD-Ni-NCC and the coordinate system used for all models (where the z-axis is pointing into the plane of the page) are shown to the right. *Figure generated by A. Glass.*

TD-DFT computations performed for DDL-Ni-NCC predict the three lower-energy *d-d* transitions to shift to higher-energy relative to LLL-Ni-NCC, which is inconsistent with experimental data. Taken together, both the total energies of the Ni-NCC models and the results of these TD-DFT computations are consistent with aged Ni-NCC corresponding to DLD-Ni-NCC, where the chirality of Asn1 and Cys3 have been inverted.

3.2.9. Ni-SOD Activity

The Ni-SOD activity assay was performed in order to probe whether the structural rearrangement that Ni-NCC undergoes while aging has an effect on the ability of the complex to consume the toxic anion superoxide. We previously showed that Ni-NCC behaves as a functional mimic of Ni-SOD, with an IC_{50} value of 41 μM.[1]

As computational analysis revealed, the final low-energy conformation, DLD-Ni-NCC, results in a more exposed Ni ion for solvent accessibility and reactivity with exogenous ligands. This is supported experimentally by the observed increase in SOD activity over time, as well as the lack of cyanide binding to Ni-NCC initially, prior to chiral inversion.[1] Control experiments with $NiSO_4$ verify SOD activity is only detected when Ni-NCC is present in solution. SOD activity was measured at several time points while the Ni-NCC complex was aged. The activity change, as determined using the xanthine/xanthine oxidase assay, increased linearly with respect to time over the first several hours of the experiment. The initial activity was subtracted from the value measured for each aged sample, and these data were fit to a linear equation. Two replicates involving a total of 12 data points were analyzed to compare the change in SOD activity with the change in chirality of the aged Ni-NCC complex between 0 and 90 minutes. The data comparison shows a linear correlation between these two parameters with R^2 values of 0.9242 and 0.9543 (data not shown). In addition, the functional data were compared to the intensity

changes in the CD spectra at the same time points during the aging process. A linear relationship between SOD activity and chiral inversion was observed (R^2 = 0.9592), revealing a direct correlation between this structural change and SOD activity of the Ni-NCC complex (Figure 3.13).

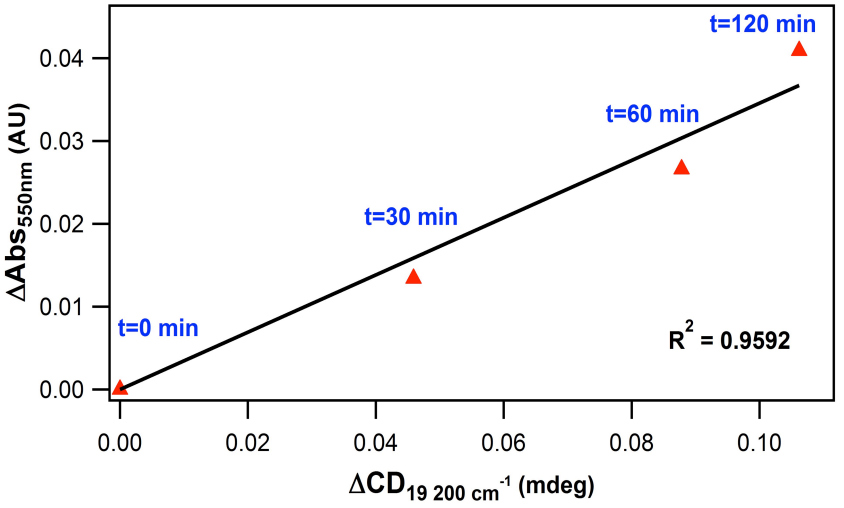

Figure 3.13. Change in SOD activity of Ni-NCC as a function of structural change over time, as measured by CD spectroscopy.

Finally, after examining the control DLD complex immediately following formation, the IC_{50} value was determined to be 39 μM, which is the same as the aged LLL-Ni-NCC species, indicating conversion to the DLD isoform confers activity.

3.3. Discussion

3.3.1. Structural rearrangement of Ni-NCC

Metal incorporation into the described Ni-NCC complex is accomplished rapidly (within seconds) via metallation.[1] The studies described here show that, following complex formation,

chiral inversion occurs over the course of hours to generate the DLD isoform, which correlates to SOD activity. The initial CD spectra acquired immediately following metal abstraction by the peptide differ among buffer systems but later converge to a common final state. The spectral differences observed between buffer systems are dramatic, whereas varying the pH (7 – 10) and sparging do not significantly impact the rate of aging. Samples prepared in borate buffer reach the rearranged, final state much faster than samples prepared in phosphate buffer. The Ni-NCC samples prepared in borate buffer also immediately coordinate cyanide in the axial position, while the Ni-NCC samples prepared in phosphate buffer must be aged overnight before cyanide coordination can be detected. As mentioned above, these data lend support to a slower structural rearrangement that occurs over the course of hours-days, resulting in a structural state that allows for the interaction of a fifth ligand with the Ni-NCC complex. Similarly, Ni-NCC prepared in borate buffer has a midpoint potential that can be measured immediately using CV, whereas samples prepared in phosphate buffer must be aged overnight before any electrochemical signal is observed. These studies demonstrate that there is a difference between the final and initial arrangements of Ni-NCC that are observed in different buffer systems. The initial state is likely the all L-coordinated square planar arrangement, which the DFT computations suggest would be sterically hindered from binding even small ligands (e.g. CN^- and superoxide) due to occlusion by the asparagine side chain. Furthermore, MCD experiments reveal that both the Ni-NCC species measured immediately after complexation and then after aging are predominantly S=0 square planar.

The differences in spectral features and in reactivity between the freshly prepared and aged samples of Ni-NCC prompted further investigation of the subtle changes in the Ni-NCC complex. Using spectroscopic and ESI-MS studies, including those involving deuterium exchange, it was proposed that a change in the chirality of specific residues within this metal-

peptide complex occurs as a result of metal binding. The incorporation of deuterium into non-exchangeable positions further supports chiral rearrangement.

Studies on the control peptides, GCC and those containing D-amino acids in various positions, helped elucidate the positions directly influenced by chiral inversion. A Ni-GCC sample was examined in the same manner to evaluate the influence of chirality at the first alpha carbon position. Although the spectra for these two complexes are not expected to be identical, a similar trend was observed for Ni-GCC in a similar time frame, suggesting that conversion occurs in the second and/or third positions. Recalling that NCC increased in mass by 2 amu during the deuterium exchange experiment, but GCC only increased by 1 amu and additionally taking into consideration that Gly is achiral, the data collectively indicate that only one of the Cys residues undergoes chiral inversion and that in NCC the first residue is also altered.

To determine which cysteine residue undergoes chiral inversion, the D-containing peptide complexes LDL-Ni-NCC, LLD-Ni-NCC, and DLD-Ni-NCC were characterized. All of the complexes exhibit the expected mass profile when examined using ESI-MS, suggesting that the same moieties from each of these peptides participate to accomplish metal binding using the same geometry. In general, inversion of the chirality at the metal center leads to CD spectra that are complete mirror images of one another;[44] however, changes in the CD spectra cannot be easily assigned to chiral inversions at individual positions in the peptide, and as such, the best indicator of the chirality of the final stable state is obtained through comparison to standards.

By overlaying the spectra of the D-containing peptides with the aged Ni-NCC spectra, it is evident that the DLD-Ni-NCC spectrum displays the same features as the aged Ni-NCC spectrum. These data further indicate chiral inversion occurs at the first and third position within Ni-NCC to generate the DLD-Ni-NCC complex. Moreover, it is obvious that the data for the aged all-L peptide does not correspond to inversion in the central position (Cys2), as the LDL peptide

yields a spectral mirror image of the aged complex. The changes observed in the aged LLL complex rather closely, but do not exactly, parallel those associated with D-Cys in the third position, as demonstrated by comparison to LLD-Ni-NCC. All of the possible permutations of chirality were tested with DFT, showing the DLD form to be thermodynamically favorable. Based on the DFT calculations, there is a very large difference in energy between the peptides containing an L or D amino acid in that third position, strongly corroborating that the DLD peptide-metal complex is highly favorable.

The Ni-NCC complex was previously shown to mimic the Ni-SOD reaction in which a single electron is transferred through the metal center.[1] Here we show that the SOD activity of Ni-NCC increases as the complex ages, and the activity is linearly and directly related to the structural rearrangement of the complex. Although the structural rearrangement was unknown at the time of our previous report,[1] the IC_{50} (data not shown) of the aged Ni-NCC sample is comparable with that value, indicating the original IC_{50} reflected a mostly chirally converted Ni-NCC species. The direct measurement of the DLD complex also has a comparable IC_{50}, indicating this is the species with SOD activity. Chiral inversion has not been observed in the Ni-SOD protein or small peptide maquettes that have been used to probe the mechanism and structure of this protein. Although metal binding is accomplished with the same geometry and direct coordinating atoms in both cases, the connectivity among these atoms is not analogous. As the data and computations indicate, structural rearrangement of Ni-NCC from LLL to DLD promotes SOD activity by overcoming the steric hindrance that blocks ligand access to the axial position. Chiral inversion results in a substantially more favorable energy for the complex and a structure in which one face of the square planar Ni^{II} ion becomes more available for interaction with solvent, exogenous ligand, or potential substrate.

3.4. Conclusion

Here we have described the first metal-catalyzed site-specific chiral inversion of amino acids within a peptide. While a previous study defined the ligands involved in metal coordination and the geometry by which the metal is bound,[1] this study has elaborated the organization of the peptide in the complex and specifically shown that chiral inversion occurs at the first and third Cα positions in the NCC sequence. An intramolecular hydrogen transfer occurs, likely through an intermediary carbon-centered radical, to generate the more thermodynamically stable DLD-Ni-NCC configuration. This stable isomer appears to be responsible for the majority of the SOD activity of Ni-NCC.

3.5. References

(1) Krause, M. E.; Glass, A. M.; Jackson, T. A.; Laurence, J. S. *Inorg. Chem.* **2010**, *49*, 362-364.

(2) Szilagyi, R. K.; Bryngelson, P. A.; Maroney, M. J.; Hedman, B.; Hodgson, K. O.; Solomon, E. I. *J. Am. Chem. Soc.* **2004**, *126*, 3018-3019.

(3) Wuerges, J.; Lee, J.-W.; Yim, Y.-I.; Yim, H.-S.; Kang, S.-O.; Carugo, K. D. *Proc. Natl. Acad. Sci. U.S.A.* **2004**, *101*, 8569-8574.

(4) Barondeau, D. P.; Kassmann, C. J.; Bruns, C. K.; Tainer, J. A.; Getzoff, E. D. *Biochemistry* **2004**, *43*, 8038-8047.

(5) Fiedler, A. T.; Brunold, T. C. *Inorg. Chem.* **2007**, *46*, 8511-8523.

(6) Fiedler, A. T.; Bryngelson, P. A.; Maroney, M. J.; Brunold, T. C. *J. Am. Chem. Soc.* **2005**, *127*, 5449-5462.

(7) Shearer, J.; Dehestani, A.; Abanda, F. *Inorg. Chem.* **2008**, *47*, 2649-2660.

(8) Shearer, J.; Long, L. M. *Inorg.Chem.* **2006**, *45*, 2358-2360.

(9) Neupane, K. P.; Shearer, J. *Inorg. Chem.* **2006**, *45*, 10552-10566.

(10) Buckingham, D. A.; Marzilli, L. G.; Sargeson, A. M. *J. Am. Chem. Soc.* **1967**, *89*, 5133-5138.

(11) Keyes, W. E.; Caputo, R. E.; Willett, R. D.; Legg, J. I. *J. Am. Chem. Soc.* **1976**, *98*, 6939-6945.

(12) Smith, G. G.; Khatib, A.; Reddy, G. S. *J. Am. Chem. Soc.* **1983**, *105*, 295-297.

(13) Stadtherr, L. G.; Angelici, R. J. *Inorg. Chem.* **1975**, *14*, 925-930.

(14) Pasini, A.; Casella, L. *J. Inorg. Nucl. Chem.* **1974**, *36*, 2133-2144.

(15) Jilek, A.; Kreil, G. *Monatshefte fur Chemie* **2008**, *139*, 1-5.

(16) Bobde, V.; Beri, S.; Rawale, S.; Satyanarayana, C. V. V.; Durani, S. *Tetrahedron* **1995**, *51*, 3077-3086.

(17) Kreil, G. *Annu. Rev. Biochem.* **1997**, *66*, 337-345.

(18) Heck, S. *et al. Science* **1994**, *266*, 1065-1068.

(19) Nakagawa, S. H.; Hua, Q.-x.; Hu, S.-Q.; Jia, W.; Wang, S.; Katsoyannis, P. G.; Weiss, M. A. *J. Biol. Chem.* **2006**, *281*, 22386-22396.

(20) Jilek, A.; Molay, C.; Tippelt, C.; Grassi, J.; Mignogna, G.; Müllegger, J.; Sander, C.; Fehrer, C.; Barra, D.; Kreil, G. *Proc. Natl. Acad. Sci.* **2005**, *102*, 4235-.

(21) Bansal, P. S.; Torres, A. M.; Crossett, B.; Wong, K. K. Y.; Koh, J. M. S.; Geraghty, D. P.; Vandenberg, J. I.; Kuchel, P. W. *J. Biol. Chem.* **2008**, *283*, 8969-8975.

(22) Fujii, N. *Biol. Pharm. Bull.* **2005**, *28*, 1585-1589.

(23) Fujii, N.; Satoh, K.; Harada, K.; Ishibashi, Y. *J. Biochem (Tokyo)* **1994**, *116*, 663-669.

(24) Fujii, N.; Ishibashi, Y.; Satoh, K.; Fujino, M.; Harada, K. *Biochim. Biophys. Acta* **1994**, *1204*, 157-163.

(25) Roher, A. E.; Lowenson, J. D.; Clarke, S.; Wolkow, C.; Want, R.; Cotter, R. J.; Reardon, I. M.; Zurcher-Neely, H. A.; Heinrikson, R.; Ball, M. J.; Greenberg, B. D. *J. Biol. Chem.* **1993**, *268*, 3072-3083.

(26) Kubo, T.; Nishimura, S.; Kumagae, Y.; Kaneko, I. *J. Neurosci. Res.* **2002**, *70*, 474-483.

(27) Nauser, T.; Schöneich, C. *J. Am. Chem. Soc.* **2003**, *125*, 2042-2043.

(28) Mozziconacci, O.; Williams, T. D.; Kerwin, B. A.; Schöneich, C. *J. Phys. Chem. B* **2008**, *112*, 15921-15932.

(29) Neese, F.; Version 2.8 ed.; University of Bonn: **2009**.

(30) Sinnecker, S. R., A.; Klamt, A.; Diedenhofen, M; Neese, F. *J. Phys. Chem. A* **2006**, *110*, 2235-2245.

(31) Becke, A. D. *J. Chem. Phys.* **1986**, *84*, 4524-4529.

(32) Perdew, J. P. *Phys. Rev. B.* **1986**, *33*, 8822-8824.

(33) Schaefer, A.; Horn, H.; Ahlrichs, R. *J. Chem. Phys.* **1992**, *97*, 2571-2577.

(34) Schaefer, A.; Huber, C.; Ahlrichs, R. *J. Chem. Phys.* **1994**, *100*, 5829-5835.

(35) Neese, F. *J. Comput. Chem.* **2003**, *2003*, 1740-1747.

(36) Becke, A. D. *J. Chem. Phys.* **1993**, *98*, 1372-1377.

(37) Becke, A. D. *J. Chem. Phys.* **1993**, *98*, 5648-5652.

(38) Lee, C.; Yang, W.; Parr, R. G. *Phys. Rev. B.* **1988**, *37*, 785-789.

(39) Crapo, J. D.; McCord, J. M.; Fridovich, I. *Methods Enzymol.* **1978**, *53*, 382-393.

(40) Tietze, D.; Breitzke, H.; Imhof, D.; Koeth, E.; Weston, J.; Buntkowsky, G. *Chem.--Eur. J.* **2009**, *15*, 517-523.

(41) Bruschi, M.; De Gioia, L.; Zampella, G.; Reiher, M.; Fantucci, P.; Stein, M. *J. Biol. Inorg. Chem.* **2004**, *9*, 873-884.

(42) Amouri, H.; Gruselle, M. *Chirality and Entantiomers. In Chirality in Transition Metal Chemistry: Molecules, Supramolecular Assemblies, and Materials*; Wiley, 2009.

Chapter 4: Site-specific chiral inversion of NCC within longer peptides upon nickel incorporation

The metal abstraction peptide (MAP) is a tripeptide with the sequence NCC that is capable of reacting with a metal ion to form a metal-peptide complex,[1,2] in which the metal is coordinated in *cis* 2N:2S square planar geometry. In NCC, the sulfur ligands derive from the cysteine side chains, one amino nitrogen ligand is from the N-terminus, and one amido nitrogen ligand is from the peptide backbone.[1] Our previous studies on the tripeptide complex revealed that it is a functional mimic of nickel superoxide dismutase (Ni-SOD) and that site-specific chiral inversion of the first (Asn) and third (Cys) residues is vital to this observed activity.[2] While metal is incorporated with the peptide composed of all L amino acids, over a period of hours to days, the LLL-NCC is converted to DLD-NCC. This chiral inversion is critical for the superoxide dismutase activity, as conversion from the LLL to DLD form moves the asparagine side chain out of the way, allowing the substrate access to the unoccupied axial site of the metal center. Cyanide, a structural mimic of superoxide, was used to confirm that a fifth ligand can only coordinate to the metal center in the chirally inverted, or DLD, form. Additionally, electrochemical studies demonstrated that the expected midpoint potential is only observed after chiral inversion occurs, and SOD activity of the complexes increases with chiral inversion.[2]

The structural change that occurs in the tripeptide complex is both site and structurally specific. When the tripeptide sequence is incorporated into a longer sequence, such as a pentapeptide, 8mer, or even a whole protein, metal is incorporated in a similar fashion, where the cysteinyl sulfur and backbone nitrogen ligands coordinate the metal. Although the same nitrogens bind, the first nitrogen is embedded in a peptide bond, converting it to an amide, rather

than being the amino terminal nitrogen group. As has been demonstrated in Ni-SOD and its maquettes, this change in binding moiety alters the redox potential and SOD activity.[3]

Chiral inversion in proteins and peptides is rare; all naturally occurring, biosynthetic peptides and proteins that contain D amino acids are first generated entirely from L amino acids, and the inversion occurs as a post-translational modification. Racemases catalyze the site-specific inversion of amino acids.[4] D amino acids can form in mammalian proteins that are found in aged tissues, particularly racemization-prone aspartic acid residues.[4,5] These spontaneous chiral inversions follow a mechanism involving cyclization and hydrolysis reactions, and the environment of the protein helps initiate and drive the conversion.[5] Metal-amino acid chelates can undergo base-catalyzed racemization at the α-carbon, but conditions for inversion are harsh, requiring several hours at elevated temperature (>90 °C) and basic pH (>9).[6-10] In contrast to these racemization mechanisms, complete conversion of L amino acids to D amino acids within proteins has been reported to proceed via a free radical reaction, where cysteine residues are involved in the single electron transfer event.[11] In these unidirectional reactions, a cysteinyl radical is generated by UV light and subsequently abstracts hydrogen from a surrounding amino acid, leading to epimerization.[11-14]

Interestingly, no chiral inversion has been observed in Ni-SOD[15-17] or reported for peptide maquettes that contain the metal binding sequences that mimic the activity of Ni-SOD.[3,18,19] In peptide mimics of Ni-SOD, it has been shown, however, that proline may undergo an isomerization reaction. In native Ni-SOD, the Leu4-Pro5 bond is *cis*, but in some of the peptide mimics of the enzyme, it is *trans*.[15,16,20,21] This may allow the carbonyl group within this bond to act as a fifth ligand and force the substrate to approach from the opposite side compared to the native enzyme. This may explain why His1 is not necessary for catalysis in some of the maquettes;[20] however, the issue is not resolved because studies on a forced *cis*-maquette exhibit

similar SOD activity to the *trans* form, suggesting proline isomerization is not likely influential in the activity of these sytems.[21]

While the accessibility of the active site to substrate certainly impacts activity, Pro isomerization does not provide a point of direct comparison of the inner sphere effects on Ni chemistry. The difference in amine/amide coordination versus *bis*-amide coordination in peptide sequences impacts the reactivity of the metal center. Shearer and coworkers have performed studies on maquettes of Ni-SOD, which binds nickel(II) utilizing the N-terminus, a backbone nitrogen, and two cysteine side chains. In these studies, where the maquette was acetylated to generate a *bis*-amide (versus not acetylated, with mixed amine/amide coordination), the redox potential and SOD activity of the complex changed.[3] Studies on *bis*-amide vs amine/amide coordination in the maquette system suggest a difference in behavior of NCC (mixed amine/amide) and NCC within a longer sequence (*bis*-amide) may occur due to a similar factor. If the electronic properties vary slightly, the electron transfer reaction that is required for chiral inversion may also be impacted. Converting the amine/amide to *bis*-amide coordination versus may not only impact SOD activity, but also chiral inversion, potentially altering the position or timescale of metal incorporation. Here we compare the differences in reactivity of the NCC tripeptide alone versus NCC embedded in a longer sequence, with respect to chiral inversion and superoxide dismutase activity, to investigate the influence of *bis*-amide 2N:2S coordination versus a mixed amine/amide 2N:2S coordination.

4.1. Experimental

4.1.1. Generation of metal-peptide complexes: The peptides GGNCC, GGGCC, GNNCC, and GNGCC, as well as GGNCC with D-cysteine in the fifth position (XXLLD-GGNCC), GGNCC

with D-asparagine in the third position and D-cysteine (XXDLD-GGNCC) in the fifth position, and GGNCC with D-cysteine in the fourth position (XXLDL-GGNCC) were purchased from Genscript Corporation (Piscatway, NJ, USA). The longer sequences GGGCCGGK and GGNCCGGK, where the sequence is in the middle of a peptide sequence rather than at a terminus, were also purchased. Nickel-pentapeptide complexes were generated in either 50 mM potassium phosphate at pH 7.4 or in 50 mM sodium borate at pH 10 by adding one equivalent of $NiSO_4$, while 8mer peptide-complexes were generated by incubation with nickel-charged immobilized metal affinity chromatography resin, as previously described.[1,2]

4.1.2. Expression and purification of Ni-PRL-1: Ni-PRL was expressed and purified as described previously.[22,23] Briefly, the gene for PRL-1 encoded in a pET-30 Xa/LIC expression vector was transformed into BL21(DE3)*E. coli* cells and grown at 37 °C in minimal media supplemented with trace metals in an orbital shaker at 250 rpm. Expression was induced with 1 mM IPTG at an OD_{600} of 0.6 to 0.8 and harvested by centrifugation after 3 hours. Cells were lysed with a French pressure cell and centrifuged for 1 hour at 21,000 x g. The soluble protein was purified using Ni-IMAC chromatography, upon which metal was incorporated into the NCC tripeptide sequence. Protein was eluted with imidazole, the His tag was cleaved with Factor Xa, and a size exclusion chromatography step was performed to obtain the pure nickel-bound protein. Protein concentration was determined from the absorbance at 280 nm (ε_{280}= 19,420 L mol^{-1} cm^{-1}).

4.1.3. CD and absorption studies: Ni-peptide samples were placed in a cuvette with a 1-cm path length and scanned from 800-300 nm using both absorption and CD spectroscopy. Samples were scanned immediately after generation and then subsequently monitored at various time points.

Background scans of buffer alone were subtracted from each scan. Spectra for Ni-PRL-1 were also collected immediately after purification. Absorption studies were performed on an Agilent 8453 UV/Visible spectrophotometer. Circular dichroism analysis was performed on a J-815 (Jasco Corporation) spectrapolorimeter.

4.1.4. Deconvolution of CD and absorption data: Deconvolution of CD and absorption data was performed using Igor Pro (Wavemetrics). Iterative Gaussian deconvolutions were performed with a constant peak width of 1650 cm^{-1}. Absorption band energies were kept within 10% of the corresponding CD bands due to the broad nature of the absorption spectrum.

4.1.5. ESI-MS: Samples of Ni-GGGCC, Ni-GGNCC, Ni-GNNCC, and Ni-GNGCC were diluted 100x in a 1:1 mixture of methanol/water and analyzed on an LCT Premier (Waters Corporation) operating in negative ion mode, as described previously.[1,2]

4.1.6. Electrochemistry: Electrochemical data were collected as previously described.[1] 3-mL samples of 3 mM Ni-GGNCC and 3 mM GGGCC were prepared in 50 mM potassium phosphate at pH 7.4. After incorporation, pH was raised to 10 to observe more intense signal. CV data were collected with a CH1812C Electrochemical Analyzer potentiostat (CH Instruments) with a three-electrode setup (platinum working electrode, Bioanalytical Systems, Inc.; Pt auxiliary electrode; Ag/AgCl reference electrode) in a glass CV cell. Potential was applied from zero to 1.2 V with a scan rate of 0.2 V per second, and current was measured.

4.1.7. Coordination of cyanide and IR analysis: Samples of Ni-GGGCC and Ni-GGNCC were prepared at a concentration of 3 mM in 50 mM potassium phosphate at pH 7.4. One equivalent of potassium cyanide was added to each of the samples. Samples were flash frozen and lyophilized. IR analysis was performed to observe the cyanide peak in each sample. IR spectra were acquired from dry powder samples on a Perkin Elmer Spectrum 100 FT-IR spectrometer equipped with a universal ATR (Attenuated Total Reflection) sampling accessory. The spectrum of solid potassium cyanide was used to compare the shift of $\nu(C\equiv N)$ vibration from the free to the nickel-coordinated state.

4.1.8. Ni-SOD xanthine/xanthine oxidase coupled assay: Ni-SOD activity was determined as reported previously,[1] except Ni-peptides were generated *in situ* using one equivalent of $NiSO_4$. SOD activity of Ni-GGGCC, Ni-GGNCC, Ni-GNNCC, and Ni-GNGCC was determined using the standard xanthine/xanthine oxidase method developed by Crapo and coworkers.[24] All reagents were generated in 50 mM potassium phosphate, 100 μM EDTA reaction buffer at pH 7.8 except for Ni-NCC, which was generated in 50 mM potassium phosphate, pH 7.4. In this assay, 600 μM cytochrome c from bovine heart (Sigma), 300 μM xanthine (Sigma) and enough xanthine oxidase from buttermilk (Sigma) to cause a change in absorbance at 550 nm of 0.02 – 0.04 AU per minute were added to a final volume of 300 μL with reaction buffer. The change in absorbance at 550 nm was monitored on a Cary 100 UV-Visible spectrophotometer (Varian).

4.1.9. MCD: Samples containing 3 mM Ni-GGNCC were prepared in 50 mM phosphate at pH 7.4. An equal volume of glycerol was added, yielding a 50% glycerol solution containing 1.5 mM Ni-GGNCC. The sample was placed in an MCD cell and flash frozen. Spectra were

collected by A. Glass on a J-815 (Jasco Corporation) interfaced with an Oxford Spectromag 4000 at +7 and -7 Tesla, and the difference was found via subtraction in order to remove any CD signal. Spectra were collected at 20, 8, and 4.5 K, and analyzed to identify any changes in the spectra that indicate paramagnetic character. The feasibility of correlating these low temperature data with the structure of Ni-NCC at room temperature is demonstrated by the lack of apparent changes in the corresponding CD spectra collected at 298 and 4.5 K.

4.2. Results

4.2.1. Preparation and spectroscopic characterization of Ni-peptides and Ni-PRL-1

The NCC tripeptide sequence was incorporated into a series of four pentapeptides (GGNCC, GGGCC, GNNCC, and GNGCC), two 8mers (GGGCCGGK and GGNCCGGK), and also characterized within the full-length phosphatase in which it was discovered (PRL-1). As previously reported,[1,2] metal incorporation in the appropriate geometry occurs via metal transfer from a weaker chelating moiety. While immobilized metal affinity chromatography resin has been an ideal choice for obtaining pure compounds for examination following the metallation reaction, for studies requiring immediate spectroscopic analysis, a solution transfer is preferential. Although $NiCl_2$ fails to generate the desired complex, $NiSO_4$ enables metal incorporation and provides the same spectral features without the need for a solid support. The peptides were analyzed with CD spectroscopy to validate the ligands involved in the metal coordination. While the spectral features were slightly different than those previously reported for the Ni-NCC tripeptide, this is to be expected, as the nitrogen ligand from the N-terminus in the tripeptide is replaced by an amide in the longer peptides. The four pentapeptides have identical spectral profiles, with only differences in intensity (Figure 4.1). Absorbance and CD

spectra were deconvoluted and features were compared to those of the tripeptide NCC (Figure 4.2 and Table 4.1).[1]

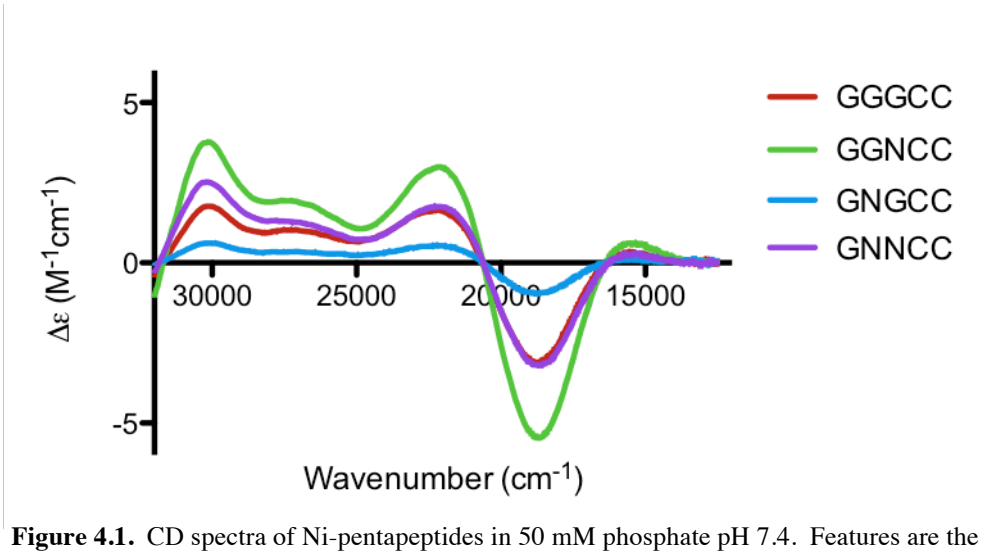

Figure 4.1. CD spectra of Ni-pentapeptides in 50 mM phosphate pH 7.4. Features are the same with different peptides, though intensity differences are present.

Table 4.1. Energies of spectral bands in Ni-GNNCC.

Ni-GNNCC			
CD		**Absorption**	
Energy (cm^{-1})	**Δε (M^{-1} cm^{-1})**	**Energy (cm^{-1})**	**ε (M^{-1} cm^{-1})**
16413	0.8	16 400	36
19216	-3	19 100	90
22500	1.74	23 600	250
27 400	1.1	26800	220
30 500	2.2	30500	600
33 526	-3.25	32900	2200

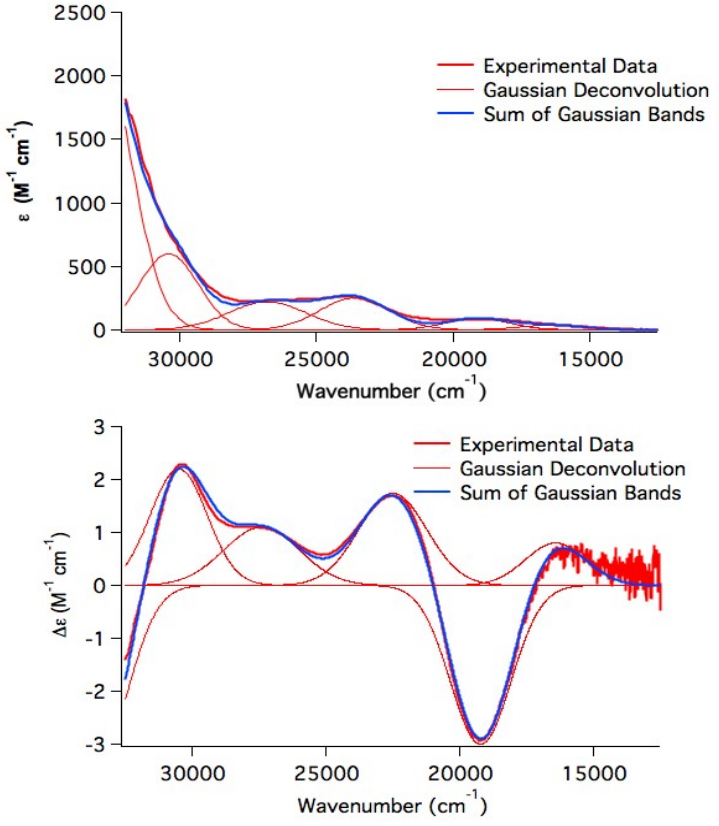

Figure 4.2. Deconvolution of Ni-GNNCC CD and absorption spectra.

The tripeptide (NCC) sequence was also placed in the middle of the 8mers: GG**GCC**GGK and GG**NCC**GGK. The spectral features are similar to that of the pentapeptides, showing that embedding NCC in a longer sequence does not further change the coordination, indicating the metal is bound in the same *cis* 2N:2S square planar arrangement as observed with NCC (Figure 4.3). Differences in intensity are observed, likely due to differences in metal incorporation efficiency. ESI-MS operating in negative ion mode shows 1:1 ratio of peptide to metal (for Ni-GGNCC, m/z = 506.22, calculated = 506.02). These data further indicate that the coordination is the same here as in the nickel tripeptide complex we reported previously (Figure 4.4). The peptide GG**NCH**GGK was also used to show that the absence of one of the cysteine ligands provides different coordination. No CD signal was observed with this peptide after metal incorporation was attempted under the same conditions used for the other 8mers, suggesting this

histidine-containing peptide may be retained on the chelation resin (data not shown). MS data indicate the metal did not insert into the modified sequence, suggesting the incorporation mechanism depends on the presence of the second Cys. Mutation of the analogous Cys in PRL-1 (C171) also prevents metal binding (unpublished data).

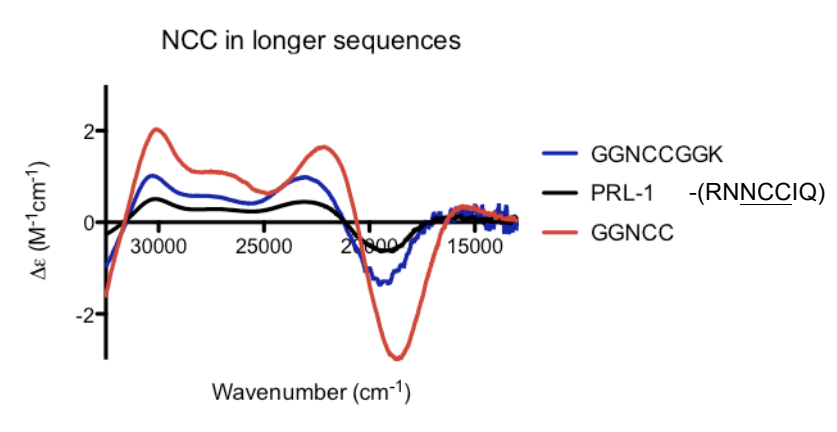

Figure 4.3. CD of GGNCC, GGNCCGGK, and PRL-1, which contains the NCC sequence. All samples were scanned 24 hours after metal incorporation to match the time frame under which PRL-1 data were collected.

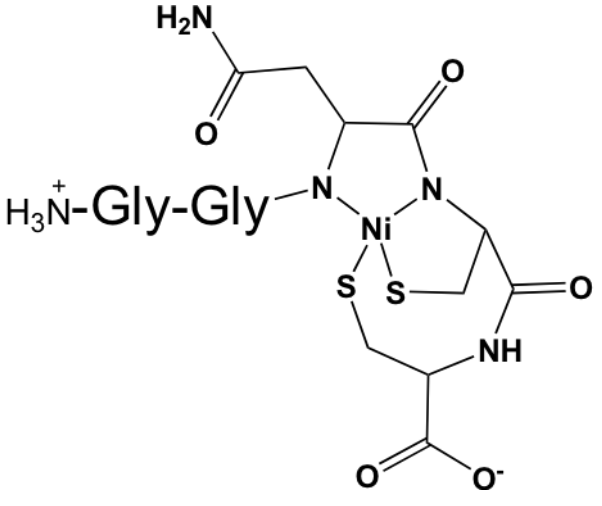

Figure 4.4. Proposed coordination of Ni-GGNCC.

In the case of the Ni-NCC tripeptide complex, the nickel ion is primarily Ni^{II};[1] however, the change from amine/amide coordination that is present in the tripeptide to the *bis*-amide coordination that is present in the pentapeptide may stabilize a Ni^{III} state and cause more of a $Ni^{II/III}$ mixture to be present. To test for the presence of Ni^{III}, MCD data was collected on the Ni-GGNCC sample. MCD data show no temperature dependence of the spectra at field, which suggests that no paramagnetic component is present (data not shown).

For the pentapeptide system, minor buffer-dependent differences in the spectral features are apparent at approximately 25 000 cm^{-1} (Figure 4.5), suggesting a possible interaction with one or both of the anionic buffer species with the complex. The choice of buffer has limited effect on reactivity of the complex after metal is incorporated. Following the insertion reaction, no spectral changes occur over time except loss of intensity (Figure 4.6). This lack of change over time suggests that chiral inversion either does not occur or it is concomitant with metal incorporation, so a change in CD signal is not observed.

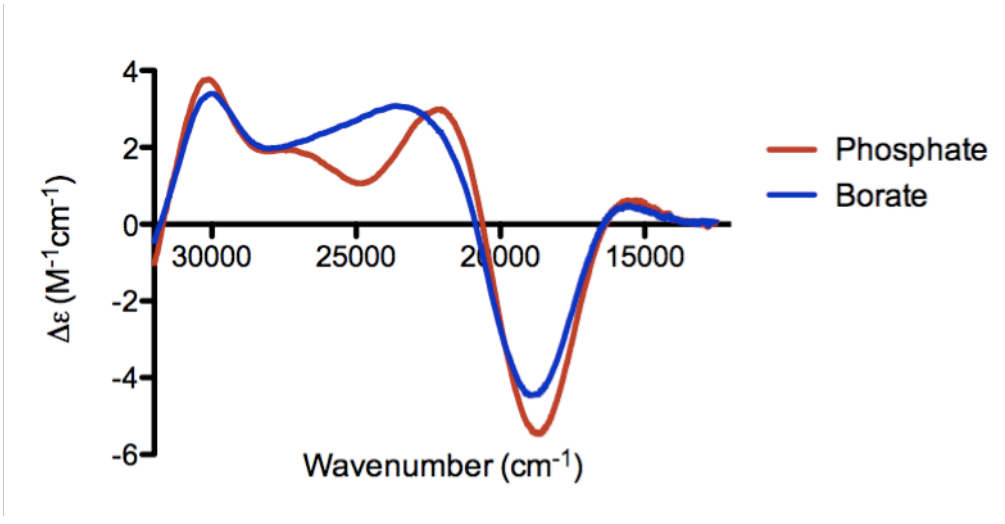

Figure 4.5. CD of Ni-GGNCC, showing buffer dependent features. Ni-GGNCC in 50 mM potassium phosphate is shown in red, while Ni-GGNCC in 50 mM sodium borate is shown in blue. Spectra were collected immediately after initiating the reaction.

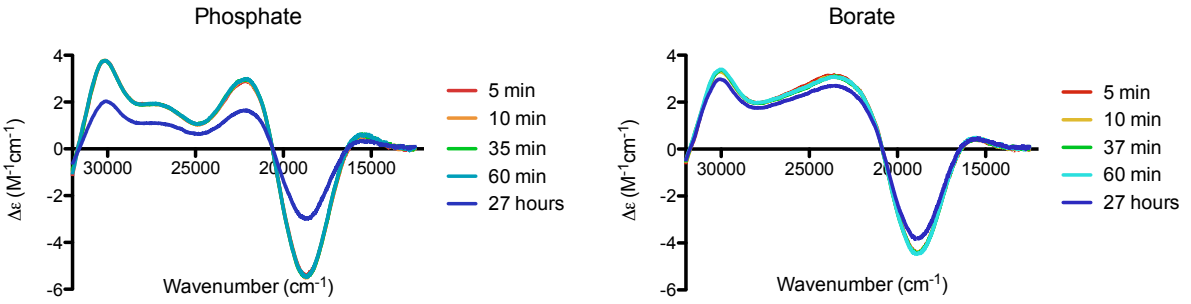

Figure 4.6. Aging does not change the spectral features of Ni-GGNCC within a given buffer system.

4.2.2. Reactivity of pentapeptides: SOD activity, coordination of fifth ligand, and electrochemistry

With the NCC tripeptide, a measure of chiral inversion is the ability to bind of the complex to coordinate a fifth ligand, to have a measurable midpoint potential, and exhibit SOD activity. To probe these three measures of reactivity of the pentapeptide immediately after generation, the xanthine/xanthine oxidase assay was performed, coordination of CN^- was monitored with CD and IR, and electrochemical studies were performed using cyclic voltammetry (CV). All of these studies were done on freshly generated samples to determine if activity, and therefore chiral inversion, occurs just after metal incorporation.

The pentapeptides have reactivity similar to the aged NCC tripeptide (IC_{50} = 4.1 x 10^{-5} M),[1,2] which corresponds to the activity of the chirally inverted form. The longer peptides with an asparagine adjacent to the N-terminal side of the motif have slightly lower activity, (6.1 x 10^{-5} M for GNNCC), while the longer peptides with a glycine adjacent to the N-terminal end of the motif have slightly higher activity (1.0 x 10^{-5} M for GGNCC), but it is still within the same order of magnitude.

Cyclic voltammetry was used to measure the midpoint potential of the pentapeptides. The GGGCC and GGNCC peptides have similar potentials (0.78 to 0.8 V vs Ag/AgCl at pH 10). These are slightly higher than those reported for the NCC tripeptide complex aged in phosphate buffer (0.71 mV vs Ag/AgCl).[1] Interestingly, the pentapeptide signal can be measured immediately after generation, whereas the tripeptide generated in phosphate buffer does not have a measurable potential until it has aged. The result suggests that chiral inversion may occur upon generation of the pentapeptide-metal complex.

To determine if CN^- has access to binding the metal, the pentapeptide complexes Ni-GGNCC and Ni-GGGCC were generated, and CD was measured of each complex immediately before and after the addition of cyanide (Figure 4.7). The vibration of CN^- is shifted to correspond to Ni-bound CN^- (Table 4.2), as was observed previously with the tripeptide complex, suggesting that CN^- is able to coordinate to the nickel-pentapeptide complex immediately after generation. This suggests axial access is available immediately and structural rearrangement occurs concomitant with metal incorporation.

Table 4.2. Coordination of CN^- to different nickel species, showing that CN^- coordinates to the pentapeptide immediately after generation, whereas with the tripeptide, chiral inversion must occur before a fifth ligand can bind. NCC and GGNCC samples were examined in phosphate at pH 7.4.

Species	**ν(C≡N) (cm^{-1})**
KCN	2076
$K_2[Ni(CN)_4]$[25]	2123
Ni(CN)-(mSOD)[25]	2108
Ni-NCC + CN^- (fresh)[2]	N/A
Ni-NCC + CN^- (aged—chirally inverted)[2]	2107
Ni-GGNCC + CN^- (fresh)	2113

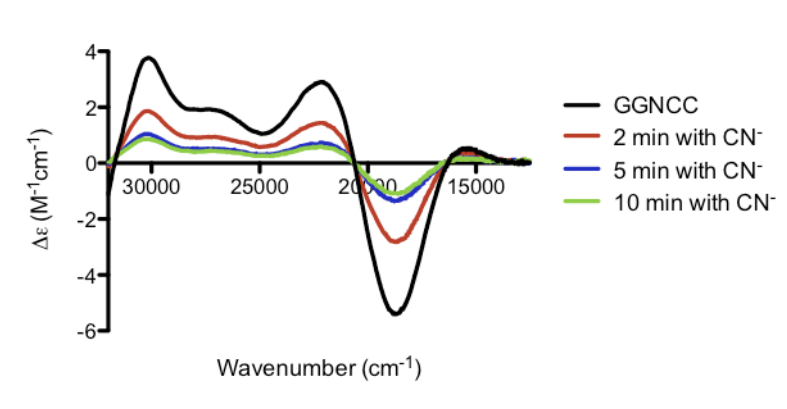

Figure 4.7. CD spectra of GGNCC in 50 mM potassium phosphate buffer scanned immediately after generation and at time points after the addition of 1 equivalent of cyanide.

4.2.3. Characterization of Ni-pentapeptide complexes synthesized to contain D *amino acids*

In the NCC tripeptide, chiral inversion occurs at the first and third positions, where nickel incorporated into LLL-NCC converts it to the DLD-NCC isoform over the course of hours. The inversion of the asparagine Cα reorients its side chain away from the space above the plane, allowing coordination of a fifth ligand or substrate and thereby promoting activity.[2] Based on the SOD activity of and CN^- binding by the Ni-pentapeptide complexes immediately after generation, we hypothesized that chiral inversion within the NCC sequence is accelerated by the *bis*-amide coordination compared to the amine/amide complex. In order to further support the occurrence of chiral inversion in the pentapeptide and validate the proposed position(s), the pentapeptide XXDLD-GGNCC was examined and the nickel complex was generated. CD spectra of the D-containing sequence were collected and compared to data from the all L isoform (Figure 4.8). Interestingly, the XXDLD- and XXLLL-GGNCC nickel complexes have spectra that are nearly mirror images of one another (Figure 4.8). This indicates that the positions that undergo chiral inversion are not the same in the amine/amide and *bis*-amide complexes. Moreover, the XXDLD form cannot be responsible for SOD activity in the pentapeptide complex.

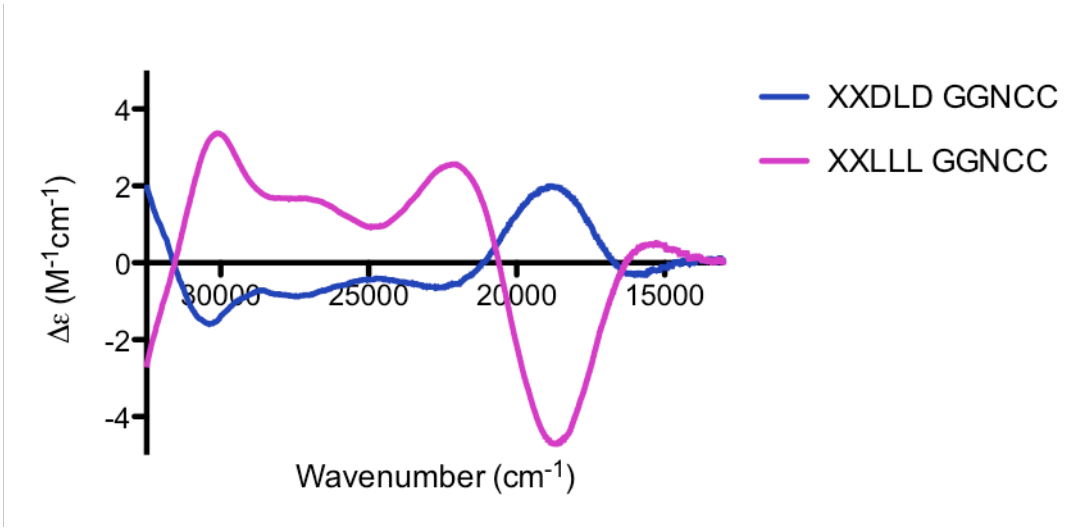

Figure 4.8. Comparison of CD profiles of purchased all L and XXDLD-GGNCC. The two complexes have exact mirror imaged signs.

The peptides XXLDL-GGNCC and XXLLD-GGNCC were metallated and compared to the all L form, as well (Figure 4.9). The spectra of the peptides with D-cysteine (XXLLD and XXDLD) are different from that observed with the all L form of GGNCC, further indicating the site of chiral inversion differs between the pentapeptides and the tripeptide. Although the XXLDL-GGNCC is not an exact match, with different intensity ratios of the peaks at 27 500 and 22 500 cm^{-1}, it is sufficiently similar to suggest Cys4 inverts to the D form.

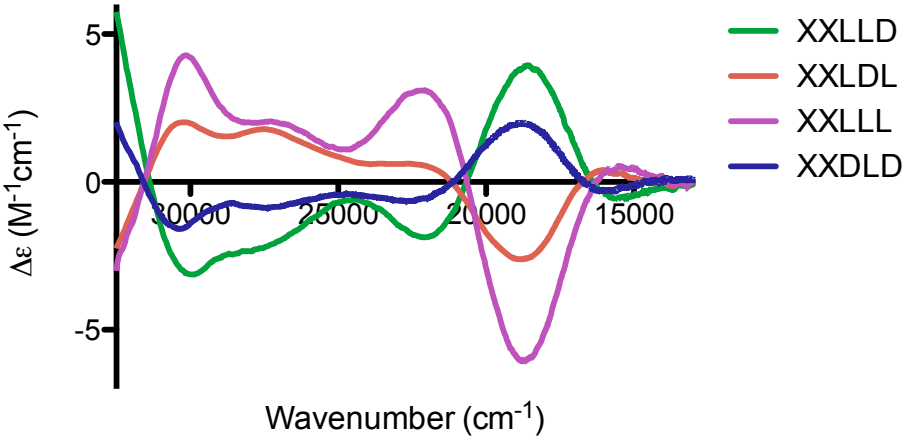

Figure 4.9. CD profiles of several chiral forms of GGNCC in phosphate buffer.

4.3. Discussion

The sequence NCC is capable of coordinating nickel in a 2N:2S geometry, where the sulfur ligands come from the cysteine side chains, one amino nitrogen ligand from the N-terminus, and one amido nitrogen ligand from the peptide backbone. While metal is incorporated with the peptide composed of all L amino acids, the LLL-NCC is converted to DLD-NCC within hours. After this site-specific chiral inversion, the Ni-tripeptide complex is a functional mimic of the enzyme superoxide dismutase. This chiral inversion is critical for the superoxide dismutase activity, as conversion from the LLL to DLD form moves the asparagine side chain out of the way and allows the substrate to have access to the unoccupied axial site of the metal center.

The tripeptide sequence may also be incorporated into a longer sequence. Here, we examined the coordination of nickel into the NCC sequence within a series of pentapeptides (GGNCC, GGGCC, GNNCC, and GNGCC). ESI-MS confirms monomeric incorporation of nickel into each sequence, and MCD studies reveal that the nickel is a diamagnetic nickel(II) species, as is the case in the tripeptide. The CD spectral features differ from those of the tripeptide, which is expected because the nitrogen ligand from the N-terminus in the tripeptide is converted to an amide in the pentapeptides. These data together indicate that the ligating moieties are the same; the same two cysteinyl sulfur and backbone nitrogen ligands are utilized, but the extension at the N-terminus changes the nitrogen coordination from mixed amine/amide to *bis*-amide. The similarity of the four pentapeptides, with and without asparagine present in position 3, confirms that the asparagine side chain is not directly involved in metal coordination and nitrogen ligation is due solely to the backbone amides. As is the case in the tripeptide system, minor buffer-dependent differences in the spectral features are apparent at approximately 25 000 cm^{-1}. This suggests a possible interaction with one or both of the buffer species with the

complex. The buffer, however, has limited effect on reactivity of the complex after metal is incorporated, as no changes occur over time except loss of intensity. Axial coordination of square planar complexes has been reported to alter band intensities in some cases without altering the absorption spectrum.[26] In the case of the tripeptide, chiral inversion is slower in the presence of phosphate buffer than in borate buffer, but no changes occur over time in either system with the pentapeptide. This lack of change over time suggests that chiral inversion either does not happen or it is associated with metal incorporation, such that a change in CD signal is not observed.

The Ni-NCC tripeptide complex is not able to bind a fifth ligand, have a measurable redox potential, or exhibit SOD activity until site-specific chiral inversion has occurred. In contrast, even immediately after generation, the pentapeptides containing the NCC sequence exhibit all of these features, suggesting conversion to an arrangement with open access to the axial position or that the asparagine is oriented differently than in LLL-Ni-NCC. Interestingly, the longer peptides that have an additional asparagine on the N-terminal side of the NCC sequence (GNGCC and GNNCC) have slightly lower activity, suggesting the presence of this side chain may slightly impair accessibility to the metal center and therefore reactivity.

In the tripeptide, LLL-NCC converts to the DLD-NCC isoform over the course of hours. The inversion of the asparagine's Cα reorients its side chain away from the space above the plane, allowing coordination of a fifth ligand or substrate, thereby promoting activity.[2] Based on the reactivity of the Ni-pentapeptide complexes immediately after generation, it was hypothesized that chiral inversion within the NCC sequence happens quickly, upon metal incorporation. In the pentapeptides, XXDLD and what starts as XXLLL-GGNCC, nickel complexes

have spectra that closely mirror one another, indicating that the XXDLD is not the isoform necessary for SOD activity of the pentapeptide complex.

Because the complex formed from XXLLL-GGNCC closely resembles the mirror image of XXDLD, this led to the conclusion that inversion is likely occurring at the central cysteine position in the pentapeptides, generating XXLDL-GGNCC. This parallels the tripeptide, where DLD-NCC and LDL-NCC have CD spectra that are exact mirror images of one another. The XXLDL-GGNCC control was found not to be an exact match to the complex generated from XXLLL-GGNCC, as the ratios of the peak intensities at 27 500 and 22 500 cm^{-1} differ. This similarity suggests Cys4 indeed undergoes an inversion to the D form.

Pentapeptides that contain an inverted Cys5 have primarily negative features, with a positive feature at 18 500 cm^{-1}, while peptides with an inverted Cys4 are the mirror image of this. This suggests that both cysteines do not invert and that only the cysteine at position 4 undergoes racemization. The inversion of Asn3 has only a minor impact on the profile, as the spectra of XXDLD and XXLLD are highly similar. Our previous work showed that DLD- and LLD-NCC have only minor spectral differences as well. It is likely that chiral inversion occurs at Cys4, but inversion at Asn3 may also occur, because the complex generated from the all L form also closely resembles the mirror image of the XXLLD form. Thus, it can be deduced that either inversion in one position to XXLDL or in two positions to XXDDL occurs. The peptide XXDDL was not examined, and it is possible that either or both chiral species form. Regardless, the data indicate that GGNCC undergoes chiral inversion and at a different position than in the tripeptide. DFT calculations, chiral chromatography, or perhaps the characterization of additional peptides will be necessary to confirm the possible inversion of Asn3.

The extension of the sequence from NCC to GGNCC causes several inherent differences in the two peptides. First, the N-terminal amine that participates in binding in the tripeptide is an amide in the pentapeptide. Second, the addition of extra residues can change the dynamics of the peptide and access to the metal center. Either of these may be responsible for the chiral inversion occurring at a different position. Inversion of the central cysteine in XXNCC allows access to the open axial site, as does inversion of the first and third positions in NCC. In the pentapeptide, the central Cys would then extend above the plane rather than below the plane as it does in the tripeptide. This is a possibility, because the inversion in chirality appears to occur on the very rapid timescale of metal incorporation. This, however, would suggest a difference in the mechanism of chiral inversion between the amine/amide and *bis*-amide systems.

The differences in *bis*-amide versus amine/amide coordination may alter both the rate of inversion and the difference in position at which chiral inversion occurs. Studies on peptide maquettes of Ni-SOD have shown that the difference in amine/amide coordination versus *bis*-amide coordination in peptide sequences can change the reactivity of the metal center, with respect to both redox potential and SOD activity.[3] We confirm this by the changes observed in the redox potential for the *bis*-amide GGNCC (0.8 V vs Ag/AgCl) versus the mixed amine/amide NCC (0.72 V vs Ag/AgCl). These studies comparing *bis*-amide and amine/amide coordination in other systems suggests the difference in behavior of NCC (mixed amine/amide) and XXNCC (*bis*-amide) may be due to a similar factor. The *bis*-amide species likely facilitates faster chiral inversion and in a different position, on the timescale of metal incorporation, compared to the mixed amine/amide species. Further understanding of the differences between these two systems may provide additional insight into how inner sphere effects control nickel reactivity.

4.4. References

(1) Krause, M. E.; Glass, A. M.; Jackson, T. A.; Laurence, J. S. *Inorg. Chem.* **2010**, *49*, 362-364.

(2) Krause, M. E.; Glass, A. M.; Jackson, T. A.; Laurence, J. S. *Inorg. Chem.* **2011**, *50*, 2479-2487.

(3) Neupane, K. P.; Shearer, J. *Inorg. Chem.* **2006**, *45*, 10552-10566.

(4) Jilek, A.; Kreil, G. *Monatshefte fur Chemie* **2008**, *139*, 1-5.

(5) Fujii, N. *Biol. Pharm. Bull.* **2005**, *28*, 1585-1589.

(6) Buckingham, D. A.; Marzilli, L. G.; Sargeson, A. M. *J. Am. Chem. Soc.* **1967**, *89*, 5133-5138.

(7) Keyes, W. E.; Caputo, R. E.; Willett, R. D.; Legg, J. I. *J. Am. Chem. Soc.* **1976**, *98*, 6939-6945.

(8) Smith, G. G.; Khatib, A.; Reddy, G. S. *J. Am. Chem. Soc.* **1983**, *105*, 295-297.

(9) Stadtherr, L. G.; Angelici, R. J. *Inorg. Chem.* **1975**, *14*, 925-930.

(10) Pasini, A.; Casella, L. J. *Inorg. Nucl. Chem.* **1974**, *36*, 2133-2144.

(11) Nauser, T.; Schöneich, C. *J. Am. Chem. Soc.* **2003**, *125*, 2042-2043.

(12) Mozziconacci, O.; Williams, T. D.; Kerwin, B. A.; Schöneich, C. *J. Phys. Chem. B* **2008**, *112*, 15921-15932.

(13) Schöneich, C. *Chem. Res. Toxicol.* **2008**, 21, 1175-1179.

(14) Mozziconacci, O.; Sharov, V.; Williams, T. D.; Kerwin, B. A.; Schöneich, C. *J. Phys. Chem. B* **2008**, 112, 9250-9257.

(15) Wuerges, J.; Lee, J.-W.; Yim, Y.-I.; Yim, H.-S.; Kang, S.-O.; Carugo, K. D. *Proc. Natl. Acad. Sci.* U.S.A. **2004**, 101, 8569-8574.

(16) Barondeau, D. P.; Kassmann, C. J.; Bruns, C. K.; Tainer, J. A.; Getzoff, E. D. *Biochemistry* **2004**, *43*, 8038-8047.

(17) Herbst, R. W.; Guce, A.; Bryngelson, P. A.; Higgins, K. A.; Ryan, K. C.; Cabelli, D. E.; Garman, S. C.; Maroney, M. J. *Biochemistry* **2009**, *48*, 3354-3369.

(18) Shearer, J.; Long, L. M. *Inorg. Chem.* **2006**, *45*, 2358-2360.

(19) Neupane, K. P.; Gearty, K.; Francis, A.; Shearer, J. *J. Am. Chem. Soc.* **2007**, *129*, 14605-14618.

(20) Schmidt, M.; Zahn, S.; Carella, M.; Ohlenschlaeger, O.; Goerlach, M.; Kothe, E.; Weston, J. *ChemBioChem* **2008**, *9*, 2135-2146.

(21) Tietze, D.; Tischler, M.; Voigt, S.; Imhof, D.; Ohlenschlaeger, O.; Goerlach, M.; Buntkowsky, G. *Chem.--Eur. J.* **2010**, *16*, 7572-7578.

(22) Skinner, A. L.; Vartia, A. A.; Williams, T. D.; Laurence, J. S. *Biochemistry* **2009**, *48*, 4262-4272.

(23) Laurence, J. S.; Hallenga, K.; Stauffacher, C. V. *Journal of Biomolecular NMR* **2004**, *29*, 417-418.

(24) Crapo, J. D.; McCord, J. M.; Fridovich, I. *Methods Enzymol.* **1978**, *53*, 382-393.

(25) Tietze, D.; Breitzke, H.; Imhof, D.; Koeth, E.; Weston, J.; Buntkowsky, G. *Chem.--Eur. J.* **2009**, *15*, 517-523.

(26) Murray, C. K.; Margerum, D. W. *Inorg. Chem.* **1982**, *21*, 3501-3506.

Chapter 5. Conclusions

The metal abstraction peptide (MAP) is a metal-binding tripeptide, described here with the sequence asparagine-cysteine-cysteine (NCC). The MAP was discovered serendipitously through IMAC purification of a phosphatase studied in the Laurence lab. Phosphatase of regenerating liver (PRL-1) is a protein tyrosine phosphatase, falling into a class of proteins that do not bind metal. Purification of this protein with nickel immobilized metal affinity chromatography (IMAC) resulted in elution of a protein with a reddish-brown color that could not be removed even after extensive dialysis with EDTA, with extensive heating of the protein, or through denaturation with 7 M guanidine-HCl. ICP-MS verified that nickel was present, suggesting the presence of a high affinity metal binding site. Tryptic digests indicated metal binding occurred near the C-terminus of the protein, and the use of site-directed mutagenesis and control peptides confirmed that the metal-binding sequence involved the three contiguous residues asparagine-cysteine-cysteine (NCC).

The unique, high affinity binding of metal within MAP and its versatility to be easily encoded into proteins of interest leads to the possibility of many potential biotechnological and pharmaceutical applications, but in order to utilize this sequence as a metal-binding tag, it is important to understand the structure and reactivity of this novel system. In order to accomplish this, extensive characterization of the nickel-bound form of the tag was performed. Studies on the nickel-bound form of the tripeptide, Ni-NCC, reveal that the peptide binds Ni^{II} with a 2N:2S, square planar geometry. One of the novelties of this system, however, is the method of incorporation. Metal incorporation into the desired geometry is accomplished by incubation with a weakly chelated nickel ion, where metal is transferred from the weak chelator to the peptide to generate a metal-tripeptide complex. This reaction, termed transmetallation, is necessary for

generation of the desired 2N:2S, square planar Ni^{II} complex; the simple addition of metal in the absence of a chelator fails to provide the desired complex, providing an extrinsic method of selectivity.

After characterizing the structure of Ni-NCC, similarities to the active site of the enzyme nickel superoxide dismutase (Ni-SOD) were realized, and closer comparison revealed that Ni-NCC is a structural mimic of this enzyme. Ni-NCC and Ni-SOD both have 2N:2S coordination, utilizing a backbone amide, the N-terminal amine, and two cysteine side chains as ligands. Additionally, Ni-NCC acts as a functional mimic of Ni-SOD, catalyzing the breakdown of superoxide. While peptide mimics of Ni-SOD have been explored in the past, the MAP complex differs in that it is not derived from the sequence of the parent enzyme yet acts as a functional mimic of the enzyme. While Ni-NCC is much less efficient than Ni-SOD, it shows activity and maintains a redox potential in the appropriate range to disproportionate superoxide. Unlike Ni-SOD, however, and unlike any metal-peptide complex known, Ni-NCC undergoes a chiral rearrangement over time under ambient conditions. Changes in the sign of the CD signal over time suggested the possibility of site-specific chiral inversion, and mass spectrometry and studies on peptides synthesized to contain D amino acids indicate chiral inversion occurs at two of the alpha carbon atoms in the tripeptide, leading to a DLD-NCC complex. This chiral inversion is unique, and to our knowledge, this is the first example of site-specific chiral inversion of amino acids that depends on metal binding.

Because of the potential applications of the MAP tag and its use as part of longer peptide/protein sequences, understanding the behavior of this sequence in the context of a longer protein is important. Additionally, understanding the peptide as part of a larger structure aids in the understanding of the primary coordination and the impact changes in this coordination can cause. While NCC embedded in longer sequences utilizes the same ligands as the tripeptide

itself, the extension of the sequence changes the nitrogen from an amine ligand due to N-terminal coordination to an amide. This forces the two nitrogen ligands to both be amides, leading to a *bis*-amide 2N:2S coordination of the metal. The reactivity of NCC embedded in a longer sequence is similar to that of Ni-NCC. The redox potential is altered somewhat, as expected when changing from mixed amine/amide to *bis*-amide coordination, but it is still appropriate to perform superoxide disproportionation. While the CD profile of the nickel-tripeptide complex inverts slowly over time, no change is observed for the pentapeptide; however, the immediate ability of the pentapeptide to have the same reactivity as the tripeptide suggests it is already inverted in some form, allowing access to an axial, substrate binding position on the nickel center. This suggests that in the case of the pentapeptide, chiral inversion occurs upon metal incorporation. Interestingly, through the use of control D-containing peptides, it was observed that chiral inversion occurs in a different position; in GGNCC, Cys4 inverts to a D-chirality.

It is proposed that the *bis*-amide coordination of the pentapeptide changes the electron flow within the complex and causes the chiral inversion to occur in a different position. With the inversion of the central cysteine rather than the asparagine and terminal cysteine, the opposite face of the plane is likely open for reactivity. The differences in this system are an excellent example of how a minor change in the structure, forcing amide coordination instead of amine, can change the properties of a nickel-coordination sphere enough to cause differences in the reactivity, which in this case, then causes further, more significant structural differences.

5.1. Novelty of the metal abstraction peptide

Though proteins with cysteine residues have been reported to bind metal,[1-3] the geometry and chemistry of the Ni-NCC motif is unique. Shortly after publication of our first paper in

Inorganic Chemistry describing the NCC sequence, moderate characterization of another CC containing peptide from the parent protein HspA was published. As described above, HspA from *Helicobacter pylori* has a histidine- and cysteine-rich tail at its C terminus, which allows it to bind two nickel ions, one of which is specifically at a Cys-Cys sequence.[2] Confirming our study, the authors propose a 2N:2S coordination, utilizing two cysteinyl side chains and two backbone amides. Although their suggested structure is different than ours, less characterization has been performed and it is possible they have generated a similar metal-peptide structure.[4] Metallothionein is a small protein where approximately 30% of the residues in the sequence are cysteine. This protein serves to coordinate soft, often toxic, metal ions.[5] The sequences used to sequester metal in this protein include Cys-Cys, Cys-X-Cys, and Cys-X-Y-Cys, but many divalent cations can bind to this protein, and in a review paper, nickel coordination to this Cys-Cys sequence was not described.[6] No protein besides MAP that has been reported to bind nickel using adjacent cysteine residues has been shown to have any catalytic activity, and very little characterization of these complexes has been performed prior to our analysis of the MAP complex.

5.2. Future directions

Future directions of the nickel project are mechanistic in nature. While site-specific chiral inversion has been observed in the first and third positions of the NCC tripeptide, the mechanism for this inversion remains to be determined. Studies on the mechanism have already been initiated by our collaborators and will provide additional insight into the Ni-NCC system. Further, the difference in position of the chiral inversion in NCC in a longer sequence is very much of interest. While it is likely that the difference in coordination between mixed

amine/amide in the tripeptide and *bis*-amide in the longer sequences drives the differences in reactivity with respect to chiral inversion, further characterization of this mechanism would be useful in understanding the overall reactivity of this system. Interestingly, in the case of the tripeptide, the inversion in borate occurs immediately, while in phosphate, it occurs slowly over the course of hours-days. We suggested previously that borate might stabilize a Ni^{III} species and cause the inversion to happen quickly; similarly, the presence of the *bis*-amide coordination may also stabilize Ni^{III}, allowing quick chiral inversion to occur. The difference in position is likely due to this coordination difference as well as the presence of additional residues on the N-terminal end of the sequence.

The work performed on the nickel complexes of these peptides has opened the door to additional studies on different metals with numerous biotechnological and medical applications. The MAP will be placed inline with therapeutic proteins or peptides that have the potential to be used as targeting agents. Platinum, for example, may be used as an anti-cancer therapeutic. Our work with nickel has determined the ligands important for metal binding, found the conditions that are useful for metal incorporation, as well as has probed basic principles of stability, structure, and reactivity. While these will differ for each metal employed, basic principles and assays to monitor each of these variables have been established and will be useful in the advancement of the MAP tag as a technology.

5.3. References

(1) Kaluarachichi, H.; Sutherland, D. E. K.; Young, A.; Pickering, I. J.; Stillman, M. J.; Zamble, D. B. *JACS*. **2009**, *131,* 18439-18500..

(2) Rowinska-Zyrek, M.; Witkowska, D.; Valensin, D.; Kamysz, W.; Kozlowski, H. *Dalton Trans*. **2010**, *39*, 5814-5826.

(3) Heaton, D. N.; George, G. N.; Garrison, G.; Winge, D. R. *Biochemistry* **2001**, *40*, 743-451.

(4) Kopera, E.; Krezel, A.; Protas, A. M.; Belczyk, A.; Bonna, A.; Wyslouch-Cieszynska, A.; Poznanski, J.; Bal, W. *Inorg. Chem*. **2010**, *49*, 6636-6645.

(5) Lippard, S. J.; Berg, J. M. *Principles of Bioinorganic Chemistry*; University Science Books: Mill Valley, CA, 1994.

(6) Coyle, P.; Philcox, J. C.; Carey, L. C.; Rofe, A. M. *Cell Mol Life Sci* **2002**, *59*, 627-647.